Molecular Assembly of Electron Transferring Flavoprotein Complexes

Thesis submitted for the degree of
Doctor of Philosophy
at the University of Leicester

by

Matthew Ronald Benjamin Jones BSc (Bristol)
Department of Biochemistry
University of Leicester

July 2002

ProQuest LLC
789 East Eisenhower Parkway
P.O. Box 1346
Ann Arbor, MI 48106-1346

ABSTRACT

The spectroscopic, kinetic and structural properties of electron transferring flavoprotein (ETF) from *Methylophilus methylotrophus* (sp. W_3A_1) have been investigated. Recombinant ETF has been expressed and purified, and its spectroscopic properties compared with those of native ETF by UV/visible spectrophotometry, fluorescence spectroscopy, circular dichroism spectroscopy and HPLC. The kinetics of electron transfer between W_3A_1 ETF and its physiological redox partner, trimethylamine dehydrogenase (TMADH), have been investigated in the presence and absence of glycerol to determine the effects of hydrodynamics on the electron transfer rate. It was found that the kinetics of electron transfer are unaffected by the concentrations of glycerol used in these analyses. Small angle X-ray solution scattering has been used to generate low resolution, model-independent molecular envelope structures for *M. methylotrophus* ETF, human ETF and *Paracoccus denitrificans* ETF. These analyses have indicated that all forms of ETF sample a range of conformations in solution. These studies suggest that an "induced fit" mechanism accounts for assembly of the TMADH-ETF electron transfer complex. Fluorescence and absorption spectroscopy studies of the TMADH-ETF complex have indicated that a series of conformational changes occur during complex assembly, and that electron transfer within mutant TMADH-ETF complexes can occur while the complex is in one or more metastable states. Furthermore, these studies have indicated that ETF undergoes a stable conformational change (termed structural imprinting) when it interacts transiently with TMADH. The imprinted form of ETF exhibits an enhanced rate of electron transfer to the artificial electron acceptor ferricenium. These studies show that the properties of electron transfer proteins can be affected lastingly by transient interaction with their physiological redox partners. This may have significant implications for our understanding of biological electron transfer reactions *in vivo*.

PREFACE

The work described in this thesis was conducted by the author in the Department of Biochemistry at the University of Leicester mainly during the period between September of 1998 and July of 2002.

The work described in this thesis is original unless otherwise acknowledged in the text or by references.

None of the work described in this thesis has been submitted for another degree at this or any other University.

Matthew RB Jones, 25th July 2002.

ACKNOWLEDGEMENTS

I would like to thank my supervisor Professor Nigel S Scrutton for introducing me to the strange and wonderful world of redox enzymology and for his advice, professionalism and boundless enthusiasm for the wonders of modern bioscience.

I would like to thank Dr J Günter Grossmann at the CCLRC Laboratory, Daresbury, for the benefit of his assistance and expertise during the collection and analysis of the small angle X-ray scattering data. Special thanks go to Dr Andras Málnási-Csizmadia and to Professor Clive R Bagshaw at Leicester University for their help and advice during the fluorescence spectroscopy work.

Many thanks go to members of Lab 124 both past and present, particularly Jaswir, without whom my PhD would not even have begun, much less been completed.

On a more personal level, I would like to thank my parents, Raymond Clive Jones and Marie Louisa Jones. It is to them that I dedicate this PhD.

Finally, extra special thanks go to Zbyszek Kominek, for keeping me sane for the first 18 months of my PhD, and to Vasiliki Tzibazi, for driving me mad for the rest of it.

ABBREVIATIONS

In addition to the standard abbreviations for chemical elements, amino acids and nucleotides, the following abbreviations have been used throughout this thesis, in some cases without prior definition:

ADP	Adenosine diphosphate
AMP	Adenosine monophosphate
CC	Cytochrome *c*
CCP	Cytochrome *c* peroxidase
CD	Circular dichroism spectroscopy
DCPIP	2,6-dichlorophenolindophenol
DE52	Diethylaminoethyl cellulose
DMA	Dimethylamine
DMI	1,2-dimethylimidazole
DNA	Deoxyribonucleic acid
DTT	Dithoithreitol
EDTA	Ethylenediaminetetra-acetic acid
eT	Electron transfer
ETF	Electron transferring flavoprotein
ETF_{ox}	Oxidised ETF
ETF_{sq}	Semiquinone ETF
ETF-QO	Electron transferring flavoprotein ubiquinone oxidoreductase
FAD	Flavin adenine dinucleotide
FMN	Flavin mononucleotide
FTIR	Fourier Transform Infrared Spectroscopy
GAPDH	Glyceraldehyde-3-phosphate dehydrogenase
HPLC	High performance liquid chromatography
IPTG	Isopropyl-β-D-thiogalactopyranoside
MADH	Methylamine dehydrogenase
MCAD	Medium chain acyl Co-A dehydrogenase
MIP	Molecularly imprinted polymer
MMO	Methane monooxygenase

NMR	Nuclear magnetic resonance
OD595	Optical density at 595 nm
PAGE	Polyacrylamide gel electrophoresis
PMS	Phenazine methosulphate
PMSF	Phenylmethylsulphonyl flouride
PRK	Phosphoribulokinase
SAXS	Small angle X-ray scattering
SDS	Sodium dodecyl sulphate
TEMED	N, N, N',N' - tetramethylethylenediamine
TMA	Trimethylamine
TMAC	Trimethylammonium chloride
TMADH	Trimethylamine dehydrogenase
Tris	2-amino-2-hydroxymethylpropane-1,3-diol
TTQ	Tryptophan tryptophylquinone
UV	Ultraviolet

Mutant enzymes are represented using the one-letter code for the wild-type amino acid, the number of the amino acid in the primary sequence, and the one-letter code for the amino acid in the mutant protein, *e.g.* Y442G denotes tyrosine 442 mutated to glycine.

CONTENTS

CHAPTER 2
MATERIALS AND METHODS

CHAPTER 3
PURIFICATION OF TMADH AND ETF - PRELIMINARY CHARACTERISATION OF RECOMBINANT W_3A_1 ETF

CHAPTER 4
ANALYSIS OF ELECTRON TRANSFERRING FLAVOPROTEIN USING SMALL ANGLE X-RAY SCATTERING

CHAPTER 5
SPECTROSCOPIC ANALYSIS OF THE DYNAMIC INTERACTION BETWEEN ETF AND TMADH

CHAPTER 1
INTRODUCTION

1.1 Biological Electron Transfer

Electron transfer reactions are some of the most ubiquitous and fundamental reactions in biological systems. They play a vital role in many physiological reactions, such as respiration and photosynthesis, nitrogen fixation, steroid synthesis and the metabolism of xenobiotic compounds. For example, the transfer of electrons from ferrocytochrome *c* to cytochrome *c* oxidase drives the pumping of protons across the mitochondrial inner membrane during respiration (Stryer, 1995). Also, the transfer of electrons from adrenodoxin to cytochrome P450 drives the catalytic cycle of cytochrome P450 during the synthesis of cholesterol (Coon *et al.*, 1992).

During protein-mediated electron transfer, reducing equivalents flow down a potential energy gradient between redox centres, which act as localised potential energy wells. Directionality of the flow of reducing equivalents is achieved by sequential transfer of electrons along a series of redox centres of increasing midpoint potential. Many examples of protein-mediated electron transfer occur between multiple redox centres housed within the same protein molecule, *e.g.* the photosynthetic reaction centre of *Rhodopseudomonas viridis* (Deisenhofer & Michel, 1989). Interprotein electron transfer reactions involve shuttling of electrons between redox centres housed in separate macromolecular electron carriers. For example, transfer of electrons occurs between haem groups housed within cytochrome *c* and cytochrome *c* peroxidase (Pelletier & Kraut, 1992). Typically, the orbital overlap between the electron donor and the electron acceptor is weak (redox centres are normally separated by distances of 10 - 20 Å), but nonetheless interprotein electron transfer reactions occur at extremely fast rates and exhibit a very high degree of specificity.

1.1.1 Theory of Protein-Mediated Electron Transfer

The basic equation for describing rates of electron transfer (k_{eT}) is "Fermi's Golden Rule" (Eq. 1.1);

$$k_{eT} = \frac{2\pi}{\hbar} H_{AB}^2 (FC) \qquad \text{(Eq. 1.1)}$$

where h = Planck's constant, $\hbar = h/2\pi$ and FC is the Franck Condon factor (see below). Basically, this equation is composed of two parts; k_{eT} = (electronic factor)^2(nuclear factor). The electronic factor, *i.e.* that the electronic coupling matrix element (H_{AB}) represents the electronic coupling between the wave functions of the reactant(s) and the product(s), and can only be understood in quantum mechanical terms. However, the nuclear factor (*i.e.* the Franck Condon factor, FC) can be understood in classical terms provided that the frequency of the nuclear motions are not too high in relation to temperature (Marcus & Sutin, 1985).

1.1.2 The Nuclear Factor in Determining k_{eT}

The Franck Condon principle states that transfer of electrons between redox centres (*i.e.* the movement of charge within a chemical system) is accompanied by a nuclear reorganisational event due to changes in the equilibrium positions of the polar groups in the system. The energy terms that comprise the Franck Condon factor can be illustrated using nuclear potential energy curves (Marcus & Sutin, 1985; Gray & Winkler, 1996). These are represented graphically in Figure 1.1. The nuclear potential energy of the reactant(s) and the surrounding medium can be summarised as a single harmonic oscillator potential. The potential energy of the product(s) can be described in a similar way, but the lowest point on the product potential energy curve (*i.e.* the equilibrium position of the nuclei in the product system) is displaced on the nuclear coordinate axis and lies at a lower potential energy than that of the reactant system. The difference in potential energy between the equilibrium positions of the reactants and the products is ΔG^o, the driving force for the electron transfer reaction. Because electrons are extremely light particles in comparison to atomic nuclei, movement of electrons cannot drive nuclear reorganisation. Therefore, electron transfer can only occur when the nuclear coordinates of the reactant(s) and product(s) are identical (*i.e.* at the intersection of the potential energy curves of the two systems). The energy required to shift the nuclear coordinates of the reactant(s) to this intersection point (*i.e.* the transition state) is the

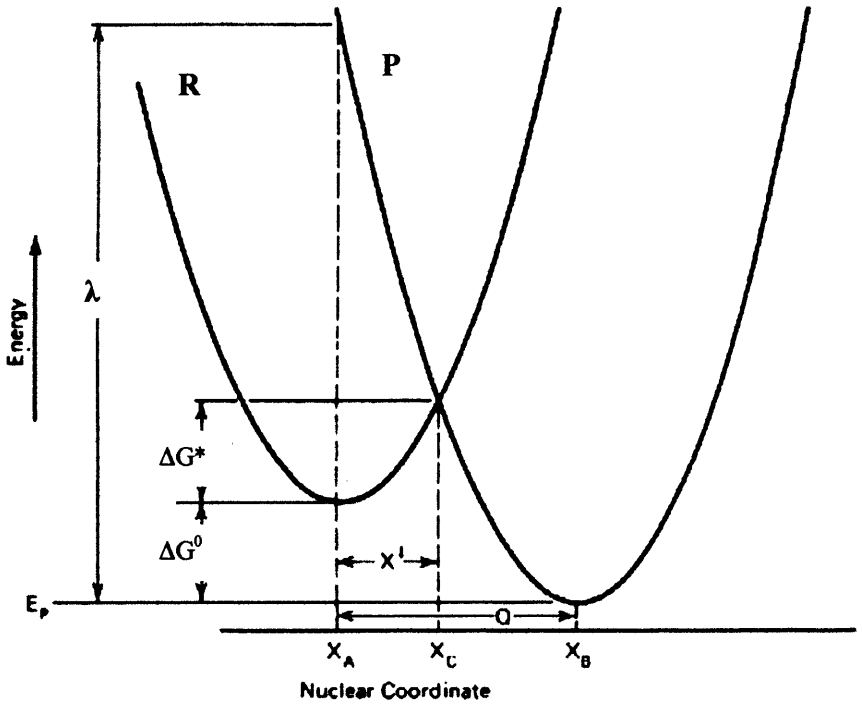

Figure 1.1
Nuclear potential energy curves to illustrate the energy terms comprising the nuclear factor of protein electron transfer (after Gray & Winkler, 1996). In this scheme, the R curve and the P curve represent the nuclear potential energies of the reactant system and the product system, respectively. ΔG^0 = the Gibbs free energy change, ΔG^* = the activation energy, and λ = the reorganisational energy.

activation free energy, ΔG^*. However, as the electronic coupling between redox centres in biological systems is so weak, there is a very low probability that electron transfer will occur at the transition state, and typically the reactant(s) potential energy will oscillate beyond the potential energy intersection with the product(s) many times before electron transfer will occur. The third energy term is the nuclear reorganisational energy (λ), which is defined as the energy required to shift the nuclear coordinates of the reactant(s) at equilibrium to a geometry identical to that of the product(s) at equilibrium, but without electron transfer taking place. The equation relating the activation free energy (ΔG^*) to the free energy change (ΔG^o) and the reorganisational energy (λ) is;

$$\Delta G^* = \frac{(\lambda + \Delta G^0)^2}{4\lambda} \qquad \text{(Eq. 1.2)}$$

This equation is known as the "Marcus energy gap law". The form of the equation is such that where $-\Delta G^o < \lambda$, ΔG^* decreases as $-\Delta G^o$ increases, and hence the reaction rate increases as a function of $-\Delta G^o$; this is known as the normal region. The normal region continues until $-\Delta G^o = \lambda$, at which point $\Delta G^* = 0$; this is known as the activationless region, and in this case the reaction rate is at a maximum. As $-\Delta G^o$ increases beyond this point ($-\Delta G^o > \lambda$), ΔG^* increases once again and the reaction rate falls, giving rise to the inverted region. When the vibrational energies of the nuclear motions ($\hbar\omega$) are small in comparison to the Boltzman thermal energy of the system ($k_B T$) it is possible to describe the Franck Condon factor classically. The "golden rule" equation hence takes the form;

$$k_{eT} = \frac{4\pi^2 H_{AB}^2}{h(4\pi\lambda RT)^{1/2}} e^{-(\Delta G^0 + \lambda)^2 / 4\lambda RT} \qquad \text{(Eq. 1.3)}$$

1.1.3 The Electronic Factor in Determining k_{eT}

The electronic coupling matrix element (H_{AB}) is a measure of the electronic coupling between the wavefunctions of the product(s) and the reactant(s). Where there is extensive orbital overlap between redox centres (*i.e.* when H_{AB} is very high) and once the potential energy intersection between R and P states is reached, the transferring electron oscillates between reactant and product, resulting in a "splitting" of the reactant and product potential energy curves (by a value of $2H_{AB}$) and a smooth transition of the system from reactant to product. In this case, the electron transfer reaction is said to be "adiabatic", and the reaction can be defined in terms of the thermodynamic parameters $\Delta H^{\ddagger}$ and $\Delta S^{\ddagger}$. However, as previously stated, in biological systems orbital overlap between redox centres is weak, and the probability of electron transfer at the potential energy intersection is low. Therefore, there is no splitting of the R and P potential energy terms, and the reaction is said to be "non-adiabatic". In this case, the electron tunnels from donor to acceptor through the intervening protein medium. The relationship between H_{AB} and the electron tunneling pathway distance (r) is described by Gamow's tunneling equation;

$$H_r^2 = H_0^2 e^{-\beta r} \qquad \text{(Eq. 1.4)}$$

where H_0 = electronic coupling at van der Waals separation and β is the electronic decay factor. The value of β depends on the medium through which the electron must tunnel, and varies from zero (for electrons tunneling through a fully conjugated pathway) to 2.8 $Å^{-1}$ (for electrons tunneling through a vacuum). The rate of electron transfer is related to the electron tunneling pathway distance (r) by the following equation;

$$k_{eT} = k_0 e^{-\beta(r-r_0)} e^{-(\Delta G^0+\lambda)^2/4\lambda RT} \qquad \text{(Eq. 1.5)}$$

Experimental investigation of electron transfer in proteins has suggested an intermediate value (β = 1.4 ± 0.2 $Å^{-1}$) for electron tunneling through a typically packed

protein matrix (Moser *et al.*, 1992). However, this does not specifically address inhomogeneities in polypeptide structure between redox centres in specific electron transfer complexes. It is likely that any such inhomogeneities will have evolved in order to influence electron tunneling rates to the physiological advantage of the system. Recently, Dutton and co-workers (Page *et al.*, 1999) formulated an empirical expression to account for variations of β in exergonic electron tunneling rates;

$$\log_{10}k_{eT} = 13.0 - (1.2\text{-}0.8\rho)(R - 3.6) - 3.1(\Delta G + \lambda)^2/\lambda \qquad \text{(Eq. 1.6)}$$

This expression includes a term for the packing density (ρ) of protein atoms in the volume between redox centres. One may define ρ as the fraction of the volume between redox centres that is within the united van der Waals radius of intervening the atoms. Thus far, this equation has proven to be the most accurate in predicting rates of physiological electron transfer.

1.1.4 Kinetic Complexity

In biological electron transfer reactions, reaction steps other than the actual electron transfer event (non-eT reaction steps) sometimes define the rate at which the overall electron transfer reaction occurs. The kinetic complexity model for electron transfer postulates that formation of the active electron transfer complex may be dependent upon non-eT reaction steps (Davidson, 1996). Clearly, if such reaction steps are rate-limiting then the observed reaction rate (k_{obs}) will not be representative of the rate of electron transfer (k_{eT}), and the reaction will not be susceptible to analysis by Marcus electron transfer theory. Such reactions are said to be "gated" electron transfer reactions. For gated electron transfer reactions, solvent conditions such as viscosity, ionic strength and pH can alter the observed electron transfer rate by affecting the non-eT reaction steps that are a prerequisite to electron transfer within the complex. Reaction steps that may define the observed electron transfer rate in "gated" electron transfer reactions include ligand binding, protonation/deprotonation and changes in protein conformation. For example, kinetic studies of the electron transfer reaction between aminoquinol methylamine dehydrogenase and amicyanin have revealed that electron transfer rates are

gated by a proton transfer step in this complex (Bishop & Davidson, 1995). Furthermore, kinetic studies using laser flash photolysis have confirmed that electron transfer reactions between zinc(II) cytochrome *c* and two of its redox partners, ferricytochrome b_5 and plastocyanin, are gated by a conformational rearrangement process (Qin and Kostic, 1994). In this case, it has been postulated that small-scale conformational changes (not to be confused with the Franck Condon nuclear reorganisation event described previously) in one or more of the components of the electron transfer complex are required for the formation of the active complex. Also, studies of the methanol dehydrogenase-cytochrome c_{551i} electron transfer complex have indicated that conformational changes within the complex contribute to the observed rates of electron transfer (Harris *et al.*, 1994).

1.2 The Study of Interprotein Electron Transfer

1.2.1 Methods for the Study of Interprotein Electron Transfer

In order that we might have a more complete understanding of the physical and chemical processes that occur in interprotein electron transfer complexes it is desirable to have model systems that may be characterised in terms of their physical and chemical interactions. Ideally, the constituent proteins of such model systems should be easy to purify in large quantities, they should be sufficiently robust to withstand physical and chemical manipulation, and they should be readily susceptible to chemical and/or genetic modification. Interactions between components of electron transfer complexes have been studied by structural, spectroscopic, kinetic and modelling techniques, and a complementary approach involving several of these techniques is usually desirable. X-ray crystallography has been used to obtain static structural information for physiological electron transfer complexes, such as the cytochrome *c* peroxidase-cytochrome *c* complex (Pelletier & Kraut, 1992) and the methylamine dehydrogenase-amicyanin-cytochrome c_{551i} complex (Chen *et al.*, 1994). Kinetic experiments using laser flash photolysis have been used to establish that rates of protein mediated electron transfer reactions can be gated by small-scale configurational fluctuations (Qin & Kostic, 1994). More recently, X-ray scattering, a low-resolution structural technique, has been used to probe large-scale conformational changes that occur during the assembly of the methane monooxygenase

electron transfer complex (Gallagher *et al.*, 1999). Brownian dynamics simulations of protein-protein association have also been used to investigate the diffusional, electrostatic and conformational factors involved in complex assembly for a variety of protein systems (Gabdoulline & Wade, 2001).

1.2.2 The Cytochrome *c* Peroxidase – Cytochrome *c* System

Cytochrome *c* peroxidase (CCP) is a monomeric, 31 kDa haemoprotein found in yeast mitochondria, and is a member of a superfamily of plant, bacterial and fungal peroxidases (Bosshard *et al*, 1991; Welinder *et al.*, 1992). CCP catalyses the two-electron reduction of hydrogen peroxide to water by ferrous cytochrome *c* (CC) in the following reaction (Yonetani, 1976);

$$2Fe^{2+}CC + H_2O_2 + 2H^+ \rightarrow 2Fe^{3+}CC + H_2O$$

During this reaction, CCP undergoes a two electron oxidation by peroxide to form an intermediate, termed compound I, which contains two oxidising equivalents, one on the haem in the form of a ferryl iron species [Fe^{4+}=O] and another as a cation free radical on the Trp-191 side chain (Sivaraja *et al.*, 1989; Huyett *et al.*, 1995). Compound I is subsequently re-reduced by two sequential electron transfer reactions from reduced (ferrous) CC. Kinetic analyses have shown that reduction of the Trp-191 radical occurs prior to reduction of the haem (Hahm *et al.*, 1992, 1993, 1994; Pappa *et al.*, 1996).

The cytochrome *c* peroxidase–cytochrome *c* electron transfer complex is one of the most studied and best understood model systems for interprotein electron transfer. The proteins fulfil the criteria outlined above for an ideal model system, and detailed molecular structures are available for both of the individual proteins (Takano and Dickerson, 1981; Ochi *et al.*, 1983; 1990; Louie and Brayer, 1990; Finzel *et al.*, 1984; Wang *et al.*, 1990). Many different techniques have been utilised in an attempt to characterise the interactions of these two proteins, the most influential of which will be discussed below.

A computer model for the molecular interaction between CCP and CC was developed (Poulos & Kraut, 1980). The model postulated that the interacting surface

between the two proteins comprised four salt bridges between the ring of positively charged residues surrounding the haem of CC and a patch of negatively charged residues on the surface of CCP. The distance between the haem of CCP and the haem of CC was calculated as 25 Å. The model was calculated with the intention of maximising the interacting surface between the two proteins while minimising the distance between redox centres, but it is nonetheless a static interpretation of the complex. Northrup *et al.* (1988) used Brownian dynamics simulations to probe the possible interactions between CCP and CC. In these simulations, it was determined that there are three sites on the surface of CCP where the criteria for docking with CC are met. The electrostatic potential energy of the interaction between CCP and CC was calculated for a range of relative molecular orientations, and it was found that the electrostatic potential energy minima corresponded to the docking sites on the surface of CCP. These electrostatic potential energy minima for interaction were located adjacent to Asp-34, Asp-148 and Asp-217 of CCP. An analysis of the ionic contacts in over 200 potential complexes (formed at these three putative sites) concluded that no single complex structure was significantly more favourable than the others. More recently, Brownian dynamics simulations have been used to calculate theoretical rates of protein-protein association for a range of reacting proteins, including CC and CCP (Gabdoulline & Wade, 2001). Theoretical association rates were calculated with respect to diffusional encounter and electrostatic translational and orientational steering between the two proteins. The most favourable structure for each complex was derived from computation of Boltzmann factors of the protein interaction energies. The results of these simulations indicated that the theoretical association rate for the most energetically favourable CC/CCP complex is sufficiently high to accommodate a two-step electron transfer mechanism, in which the proteins first associate with the aid of electrostatic steering, and electron transfer then takes place via a short-range step. This supports the hypothesis that electron transfer takes place in a stable, specific electron transfer complex and is not the product of transient, non-specific associations.

In 1992 the structure for a complex formed by yeast CCP and CC was determined at 2.3 Å resolution (Pelletier & Kraut, 1992); this is one of a very few structures available for a soluble, transiently-formed physiological electron transfer complex, and its

determination allowed a direct comparison with the theoretical models for the complex. The crystal structure of the CCP:CC complex from yeast is shown in Figure 1.2. In contrast to the computer model developed by Poulos & Kraut (1980), the crystal structure of the complex revealed that the predominant forces that stabilise the complex are hydrophobic and van der Waals interactions. The closest approach distance at the interface of the two molecules is a weak intermolecular hydrogen bond (3.3 Å) between Glu-290 of CCP and Asn-70 of CC. However, there was significant overlap between the intermolecular interaction surfaces suggested by computer modeling and that observed from the crystal structure, and there was a good agreement between the haem–haem distance calculated from the model and that calculated from the crystal structure (25 Å and 26 Å respectively). The crystal structure suggests that the electron transfer pathway between CCP and CC may consist of a short chain of residues, Trp-191, Gly-192, Ala-193 and Ala-194, in CCP. The indole ring of Trp-191 (the site of the cationic radical intermediate) is in van der Waals contact with the haem of CCP. Pelletier & Kraut also solved the crystal structure for a complex between CCP and horse CC. In this structure, horse CC is shown in complex with CCP in an orientation very similar to that of the yeast CC/CCP complex. The authors considered this as evidence of a unique binding site for CC on the surface of CCP, which is in direct contradiction to the results of the Brownian dynamics simulations.

More recently, crystallographic evidence has suggested that CCP might undergo a conformational change during electron transfer. Crystals structures have been determined for mutant (F202G) and wild-type CCP saturated with an exogenous ligand (Cao *et al.*, 1998). The structure of F202G CCP saturated with 1,2-dimethylimidazole (DMI) shows displacement of a five amino acid loop (Pro-190 to Asn-195) which exposes Trp-191 to the protein surface. Similarly, from the structure of wild-type CCP saturated with 2-amino-5-methylthiazolium iodide (2a5mt) it was calculated that the fractional occupancies of the "closed" (no displacement) and "open" (Pro-190 to Asn-195 displaced as in the F202G structure) conformers were approximately 0.8 and 0.2 respectively. Using the above data in conjunction with solution kinetic data from the ligand binding reaction it was calculated that in the absence of ligand approximately 4% of the wild-type protein will exist in the open-loop conformer at any given time.

Figure 1.2
A stereo α-carbon representation of the CCP:cc complex structure from yeast (Taken from Pelletier & Kraut, 1992). The exposed methyl group (CBC) on the cytochrome *c* haem and the two residues on CCP (Ala^{193} and Ala^{194}) that serve as a docking site for CBC are labeled.

However, as the half-life of loop opening was found to be vastly in excess of 100 s, it remains unclear whether or not this particular conformational change plays any significant role in propagating the electron transfer reaction. It should also be noted that we do not, as yet, possess any detailed structural information on the oxidised form (complex I) of CCP, and hence we cannot say with any degree of certainty whether or not the oxidation state of the enzyme affects its conformation.

Kinetic analyses have also been utilised to elucidate the mechanism of the CCP/CC interaction. Laser-flash photolysis has been used to investigate the effects of configurational gating on the rate of electron transfer from CC to CCP (Mei *et al.*, 1999). Laser excitation of a rubipyridine-bound derivative of CC (Ru-39-CC) in complex with CCP results in extremely rapid electron transfer from the rubipyridine component to the haem of CC, and hence enabled measurement of electron transfer rates from the haem of CC to Trp-191 of CCP. The rate constant of the interprotein electron transfer step was measured as $2 \times 10^6\ s^{-1}$. This rate was independent of both temperature and viscosity of the medium, and hence it was concluded that the reaction was not gated by configurational fluctuations within the complex and that the measured rate constant for the interprotein electron transfer step represented the intrinsic electron transfer rate. Zhou and Hoffman (1993, 1994) used CC zinc-substituted haem to investigate the steady-state electron transfer reaction from the ferric haem of CCP to zinc-CC, thus circumventing the normal physiological reaction involving the Trp-191 radical. Their studies have shown that CCP possesses two CC binding sites, one of which has a much higher affinity for CC than the other and is presumed to be the site suggested by the crystal structure of the complex. Binding of CC at the low affinity site is increased at low ionic strength. Fluorescence quenching studies (Kornblatt & English, 1987) and potentiometric studies (Mauk *et al.*, 1994) both support the contention that CCP can bind two molecules of CC. Subsequently, Hoffman and coworkers attempted to examine the electron transfer reaction at the low affinity binding site by using redox inert copper-substituted CC as a competitive inhibitor (Zhou *et al.*, 1995). The results of these experiments seem to suggest that the electron transfer rate is approximately 1000-fold greater than that observed at the high affinity site. However, this conclusion has met with significant disagreement. In Miller *et al.* (1996), a bulky sulfhydryl reagent, 3-(N-

maleimidylpropionyl)-biocytin (MPB) was introduced at residue 193, inside the high affinity binding site of CCP. The effect of this modification was to reduce the transient and steady-state electron transfer rates 20-100 fold. However, the low rate of catalysis of the modified enzyme was constant irrespective of ionic strength, which seemed to indicate that the low affinity complex formed between CCP and CC at low ionic strength is not electron transfer reactive. Following on from this result, Miller (1996) proposed a complete mechanism for the steady-state oxidation of CC by CCP. It was suggested that, at low ionic strength, the rate of catalysis at the high affinity binding site is limited by the rate of dissociation of CC, and that binding of CC to the low affinity site increases the rate of CC dissociation at the high affinity site. This "substrate assisted displacement" was consistent with the NMR studies of Yi *et al.* (1994). The location of the low affinity binding site on the surface of CCP was elucidated by site-directed mutagenesis (Leesch *et al.*, 2000). The second binding site was found to be focussed around residues 146-150 of CCP, which is the region where the haem of CCP is closest to the surface of the protein and which corresponds exactly to one of the electrostatic potential energy minima found in the Brownian dynamics studies of Northrup *et al.* (1988). As well as locating the second binding domain, Leesch *et al.* (2000) use their kinetic data to calculate kinetic and thermodynamic parameters for the binding of CC to CCP. In their interpretation of the results, they incorporate the negative cooperativity proposed by Miller (1996) into their kinetic scheme; binding of CC to one site on CCP decreases the affinity of the other site for CC approximately four-fold. However, they also conclude that the low affinity binding site is catalytically active and that it possesses a reactivity constant 10-fold greater than that of the high affinity binding site.

In conclusion, although kinetic analyses have helped to confirm the existence of a second CC binding domain on CCP and to highlight its importance in the catalytic process, there is still much disagreement concerning the precise role of the second binding domain. Despite a wealth of structural, computational and kinetic data we still do not have a complete mechanism for the steady-state electron transfer reaction between CC and CCP. However, recent developments, such as the purification of a highly deuterated recombinant CCP for use in NMR studies (Savenkova *et al.*, 2001) will undoubtedly continue to lead us towards a more complete understanding of the system.

1.2.3. The Methylamine Dehydrogenase – Amicyanin – Cytochrome c_{551i} System

Methylamine dehydrogenase (MADH) is an enzyme present in the soluble electron transfer pathways of several Gram-negative bacteria, where it enables these organisms to use methylamine as a source of carbon (McIntire *et al.*, 1991; Davidson, 1993). MADH from *Paracoccus denitrificans* is a 125 kDa heterotetramer with two sets of identical subunits. Each of the smaller subunits contains a tryptophan tryptophylquinone (TTQ) cofactor. MADH catalyses the oxidative deamination of methylamine to formaldehyde and water. The two electrons derived from the substrate are passed sequentially to amicyanin, a type I blue copper protein (Husain & Davidson, 1985). *In vitro* studies have indicated that electrons are subsequently passed from amicyanin to cytochrome c_{551i} (Husain & Davidson, 1986). The terminal electron acceptor in the electron transfer pathway is a membrane bound oxidase (Davidson, 1993).

The methylamine dehydrogenase–amicyanin–cytochrome c_{551i} system represents one of the best structurally characterised electron transfer complexes. The structures of MADH in isolation, of MADH in complex with amicyanin, and of the complex between MADH, amicyanin and cytochrome c_{551i} have all been solved by X-ray crystallography (Chen *et al.*, 1992. 1994). The crystal structure of the complex between MADH, amicyanin and cytochrome c_{551i} is shown in Figure 1.3. The orientation of MADH with respect to amicyanin is identical in both the binary and the ternary complex. The crystal structure shows a concave region between the heavy (H) and light (L) subunits of MADH interacting with a convex region of amicyanin. The interacting surface between MADH and amicyanin is largely hydrophobic, and comprises 25 residues from MADH (8 residues from the H subunit and 17 from the L subunit) and 20 residues from amicyanin which form an interacting surface of approximately 750 $Å^2$. In addition, the interface between MADH and amicyanin is stabilised by one strong salt bridge and one weak salt bridge, and three solvent molecules are present at the interface between the two proteins. The interface between amicyanin and cytochrome c_{551i} is smaller (approximately 430 $Å^2$) and more hydrophilic than that between MADH and amicyanin. Amicyanin and cytochrome c_{551i} interact via one salt bridge, four hydrogen bonds, one Glu-Asp interaction and two solvent molecules.

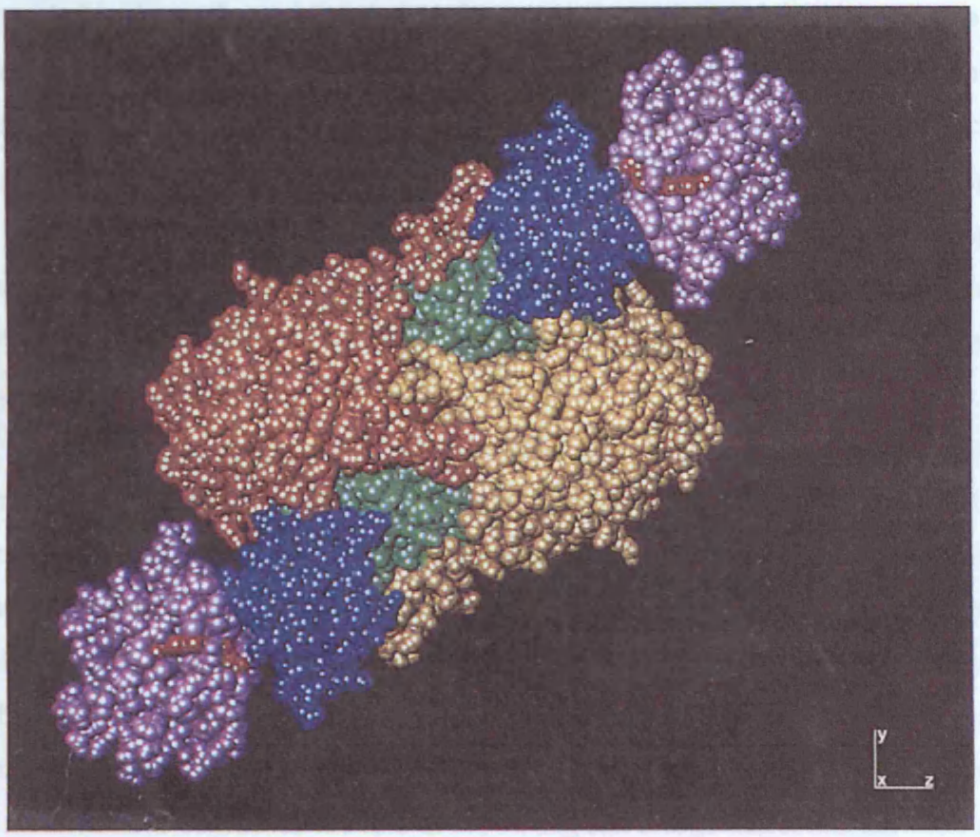

Figure 1.3
The crystal structure of the ternary complex formed between methylamine dehydrogenase, amicyanin and cytochrome c_{551i} (Taken from Chen *et al.*, 1994). This space-filling model depicts the $(HLAC)_2$ octamer. The colour scheme is as follows: yellow and brown for the two H subunits, green for the L subunit, blue for amicyanin, purple for cytochrome, and red for TTQ and for the haem group of the cytochrome, which appears partially exposed.

It has been demonstrated that the ternary complex is kinetically active in its crystalline state (Merli *et al.*, 1996). MADH can be oxidised by methylamine, and electrons are transferred from MADH to amicyanin and from amicyanin to cytochrome c_{551i}. This observation supports the contention that the structure of the ternary complex in the crystalline state is an accurate representation of the structure of the ternary complex in solution. Also, cross-linking studies have indicated that amicyanin contacts both MADH subunits and that the complex is stabilised by hydrophobic interactions (Kumar & Davidson, 1990).

Site-directed mutagenesis has also been used to probe the binding interaction between MADH and amicyanin. Mutation of Phe-97 of amicyanin to Glu severely disrupts binding, establishing the importance of hydrophobic interactions involving this residue (Davidson *et al.*, 1997). Also, mutation of Arg-99 and Lys-68, the two residues on the surface of amicyanin which respectively form the strong and weak salt bridges with MADH, affect the dissociation constant and the ionic strength dependence of complex formation. More recently, mutational studies where both MADH and amicyanin are mutated have confirmed the role of the strong salt bridge that forms between Arg-99 of amicyanin and αAsp-180 of MADH in stabilising the complex (Zhu *et al.*, 2000). These studies have also enabled the formulation of a sequential model for the interaction of the two proteins that is consistent with thermodynamic and structural data. According to this model, an initial hydrophobic interaction between the two proteins is followed by a repositioning of Arg-99 and αAsp-180 to form the strong salt bridge that stabilises the complex.

The PATHWAYS II program has been used as a guide to predict the electron transfer pathways from MADH to amicyanin and from amicyanin to cytochrome c_{551i} (Chen *et al.*, 1994). The program predicted two prominent paths from the TTQ of MADH to the copper cofactor of amicyanin, one involving Trp-108 of TQQ and another involving two main chain residues of the L subunit. Calculation of the relative efficiencies of these two pathways indicated that in the latter the coupling is about three-fold more efficient than in the former, but this depends critically on the presence of a solvent molecule which may not be present in solution. Similarly, the program predicted two prominent paths from the copper of amicyanin to the iron of cytochrome c_{551i}, one

involving Cys-92 of amicyanin and another involving Met-98. Both pathways were predicted to be of equal efficiency, but recent modifications in the Pathways algorithm to include contributions from the anisotropy of metal-ligand coupling result in the prediction that pathways via Cys-92 should be at least 100-fold more strongly coupled than the pathways via any of the other copper ligands (Davidson *et al.*, 2000). However, experimental studies involving site-directed mutagenesis of cytochrome c_{551i} along the pathway involving Cys-92 have failed to confirm this prediction, leading to speculation about the usefulness of the Pathways algorithm in predicting electron transfer pathways for ET reactions of metalloproteins.

The molecular event that is responsible for gating the electron transfer reaction from MADH to amicyanin is the transfer of a solvent exchangeable proton (Bishop & Davidson, 1995). The rate of the proton transfer reaction is influenced by pH and by the concentration of monovalent cations (Bishop & Davidson, 1997). Prior kinetic studies have revealed that MADH binds monovalent cations, which results in an increase in the observed rate of electron transfer between MADH and amicyanin (Gorren *et al.*, 1995). X-ray crystallography has been used to identify two putative monovalent cation-binding sites on the surface of MADH (Labesse *et al.*, 1998); a proximal site which is stabilized by several oxygen ligands, and a distal site which requires cation-π interactions involving residue αPhe-55. Studies involving site-directed mutagenesis have revealed that cation binding to the proximal site is responsible for the enhancement of the rate of gated electron transfer, and cation binding to the distal site is responsible for spectral perturbations in MADH (Sun & Davidson, 2001).

Interestingly, there is substantial kinetic evidence to indicate that cytochrome c_{551i} cannot accept electrons from free amicyanin, and that cytochrome c_{551i} can only accept electrons from amicyanin in the presence of MADH (Husain & Davidson, 1986; Gray *et al.*, 1986; Davidson & Jones 1995, 1996). Potentiometric analysis revealed that binding of MADH to amicyanin decreases the redox potential of the copper cofactor of amicyanin by 73 mV, which facilitates the otherwise thermodynamically unfavourable transfer of electrons to cytochrome c_{551i} (Gray *et al.*, 1988). Structural, mutagenesis and potentiometric studies have revealed the molecular basis for this complex dependent effect (Zhu *et al.*, 1998). In free solution, the midpoint potential (E_m) of amicyanin is

strongly dependent on pH. This pH dependence correlates with a single protonated ligand of the copper cofactor, His-95, which possesses a pK_a of 7.5. Protonation of His-95 is associated with a conformational change of this residue. When amicyanin is bound to MADH the conformational "flipping" of His-95 is stearically hindered, which shifts the pK_a of amicyanin to a much lower value. This eliminates the dependence of the E_m on pH over physiologic ranges and hence facilitates electron transfer to cytochrome c_{551i}. Although it is still not clear why the system should have evolved in this manner, these findings are significant because they demonstrate the means by which complex formation may alter the redox properties of the interacting proteins.

1.2.4 The TMADH/ETF system

There is still a significant lack of detailed structural information for many physiologically relevant electron transfer pathways because many electron transfer systems involve membrane-bound proteins and complexes, which are not amenable to conventional structural analyses. Therefore, although many advances have been made in the study of interprotein electron transfer, such studies are still dominated by a relatively small number of well-characterised systems. The limitations imposed upon the study of interprotein electron transfer create a requirement for the study of novel model systems for interprotein electron transfer. Discovery and investigation of such systems will hopefully eventuate in a broader, more holistic understanding of the molecular basis of interprotein electron transfer reactions and of the macromolecular processes involved in the assembly of electron transfer complexes. The TMADH-ETF complex from *Methylophilus methylotrophus* (sp. W_3A_1) is ideal for such investigations. The genes encoding both proteins have been cloned and sequenced, and the catalytically active proteins have been expressed (Boyd *et al.*, 1992; Chen & Swenson, 1994). Both proteins are soluble, stable, and can be readily purified from both native and recombinant sources (Steenkamp & Mallinson, 1976; Steenkamp & Gallup, 1978; Scrutton *et al*, 1994; Chen & Swenson, 1994). The crystal structures for native and recombinant TMADH have been solved (Lim *et al.*, 1986; Trickey *et al.*, 2000). Although attempts to obtain a crystal structure for free ETF have been unsuccessful (White *et al.*, 1994), the TMADH-ETF complex has been crystallised and a structure for the complex is awaited (Scrutton,

NS – personal communication). The kinetics of electron transfer within the TMADH-ETF have been the subject of extensive analysis (Huang *et al*, 1995; Wilson *et al*, 1995; Wilson *et al*, 1996; Wilson *et al*, 1997b; Basran *et al*, 2000). The macromolecular assembly of the TMADH-ETF complex has been investigated using analytical ultracentrifugation techniques (Wilson *et al.*, 1997a) and molecular modelling (Chohan *et al.*, 1998). In the two subsequent sections a more detailed examination of these proteins and of their interaction is presented.

1.3 TMADH

1.3.1 Structure and Function of TMADH

The enzyme trimethylamine dehydrogenase (TMADH) is an iron-sulphur flavoprotein that catalyses the oxidative demethylation of trimethylamine to form dimethylamine and formaldehyde (Steenkamp & Mallinson, 1976);

$$(CH_3)_3N + H_2O \rightarrow (CH_3)_2NH + CH_2O + 2H^+ + 2e^-$$

The enzyme is found in methylotrophic bacteria where it enables the organism to subsist on trimethylamine as the sole carbon source. TMADH is a homodimer, and each subunit has a molecular mass of 83 kDa (Lim *et al.*, 1986). Each subunit consists of three domains; a large, medium and small domain, which are composed of four segments of the amino acid chain. Segment 1 (380 residues) corresponds to the large N-terminal domain, segments 2 and 4 (115 and 50 residues, respectively) comprise the medium domain and segment 3 (55 residues) forms the small domain. Each TMADH subunit contains three cofactors; a flavin mononucleotide (FMN), a 4Fe-4S centre, and a molecule of ADP. The large domain of TMADH is an 8-stranded parallel α/β barrel, which forms the active site of the enzyme and contains the covalently bound (6-*S*-cysteinyl) FMN and the 4Fe-4S centre, which are located in close proximity to each other (the distance between the isoalloxazine ring of the FMN and the 4Fe-4S centre is approximately 6 Å). The medium and small domains both consist of 5 - stranded parallel β sheets surrounded by α helices and anti-parallel β sheets. The medium domain contains a molecule of ADP, but this is not thought to posses any catalytic or regulatory activity; the enzyme is not sensitive to

ADP concentration, and the tightly bound ADP cofactor does not exchange with radio-labeled ADP in solution (Scrutton, 1994).

Following binding of substrate to TMADH, the two electrons derived from the demethylation reaction initially reduce the covalently bound FMN in the active site (the reductive half-reaction). The two electrons are then sequentially transferred to the 4Fe-4S centre (intraprotein electron transfer). Subsequently, interprotein eT occurs when TMADH binds to its physiological electron acceptor, electron transferring flavoprotein (ETF), and one electron is passed from the 4Fe-4S centre of TMADH to the flavin in ETF (the oxidative half-reaction). *In vivo*, substrate reduction of one subunit of TMADH reduces it to the 2-electron level (though 3-electron reduction of TMADH is possible using dithionite as a reducing agent). The distribution of the two electrons can be either a) fully reduced (dihydroquinone) FMN and oxidised 4Fe-4S centre, or b) semiquinone FMN and reduced 4Fe-4S centre.

1.3.2 Reaction Kinetics of TMADH

Much work has been carried out to unravel the kinetics of the reductive half-reaction of TMADH (Steenkamp & Mallinson, 1976; Steenkamp & Beinert, 1982a,b; Rohlfs & Hille, 1991, 1994; Rohlfs *et al.*, 1995; Huang & Hille, 1995; Huang *et al.*, 1996; Falzon & Davidson 1996a,b; Jang *et al.*, 1999). Analyses of the reduction of TMADH using the non-physiological substrate diethylmethylamine (DEMA) have enabled the determination of a complete mechanism for the reduction of the FMN cofactor and the 4Fe-4S centre (Rohlfs & Hille, 1994). Substrate reduction of TMADH has also been investigated using stopped-flow kinetic spectroscopy (Steenkamp & Beinert, 1982a,b). These analyses revealed that reduction of the FMN cofactor is extremely rapid ($t_{1/2}$ < 2ms), and that the intramolecular electron transfer step (electron transfer between the FMN cofactor and the 4Fe-4S centre on TMADH) is the rate limiting step in the reductive half reaction (k_{lim} = 100 s^{-1}). It was also observed that rates of intramolecular electron transfer are dependent on the concentration of substrate. It was suggested that substrate binding might alter the redox potentials of the flavin and/or the 4Fe-4S centre, thus rendering intramolecular electron transfer less favourable. Subsequent analyses revealed that the intramolecular electron transfer step exhibited

multiphasic behaviour (Falzon & Davidson, 1996a,b). At low substrate concentrations transients were fast and monophasic, but as the concentration of substrate was increased the transients became biphasic, and an increasing proportion of the amplitude was contributed to by the slow phase. At very high substrate concentrations slow, monophasic transients were observed. It was suggested that there may be a second, inhibitory binding site for TMA on TMADH. However, there is no structural evidence for a second TMA binding site, and more recent kinetic evidence has suggested that discrete inhibitory substrate-binding site is not required to account for the effects of excess substrate inhibition (Jang *et al.*, 1999). Finally, the steady-state reaction of trimethylamine dehydrogenase (TMADH) with the artificial electron acceptor ferricenium hexafluorophosphate (Fc) has been studied by stopped-flow spectroscopy, with particular reference to the mechanism of inhibition by TMA (Roberts *et al.*, 1999). It was established that substrate inhibition is attributable to partitioning between redox cycles in TMADH. In the steady state reaction of TMADH with TMA the enzyme undergoes two alternate redox cycles, termed the 0/2 and 1/3 cycles on the basis of the number of reducing equivalents present in the oxidized/reduced enzyme encountered in each cycle. Partitioning between these redox cycles is dependent on both TMA and electron acceptor concentration.

Rational engineering of the active site of TMADH has succeeded is selectively altering the specificity of TMADH in favour of the non-physiological substrate dimethylamine (DMA) (Basran *et al.*, 1997). A triple mutant of TMADH was generated (Y60Q-S74T-W105F) which exhibited increased specificity for DMA relative to TMA (k_{lim}/K_d quotients for reaction with the triple mutant were 7.42 $s^{-1}M^{-1}$ and 1.85 $s^{-1}M^{-1}$, respectively). The change in specificity was attributed to substantially reduced rates of flavin reduction with trimethylamine and poor binding of the substrate to the active site.

There has also been a considerable body of work concerning the oxidative half-reaction of TMADH. However, before discussing the oxidative half-reaction of TMADH in any detail it is first necessary to introduce its physiological electron acceptor, ETF, and the family of proteins to which it belongs.

1.4 Electron Transferring Flavoprotein

1.4.1 The ETF Superfamily

Electron transferring flavoproteins (ETFs) function as physiological electron carriers between degradative enzymes in bacteria and mitochondria and their respective membrane-bound electron transfer pathways (Thorpe, 1991). ETFs have been isolated from bacterial (*Methylophilus methylotrophus* (sp. W_3A_1), *Megasphaera elsdenii* and *Paracoccus denitrificans*) and mammalian (human, pig and rat) sources. Mammalian ETF has a very broad specificity, and is known to accept electrons from at least nine primary flavoprotein dehydrogenases. These include the four straight-chain-specific fatty acyl-CoA dehydrogenases (short, medium, long and very-long chain acyl-CoA dehydrogenase), as well as several dehydrogenases involved in amino acid and choline catabolism (Roberts *et al.*, 1996). Reducing equivalents from these dehydrogenases are transferred to ETF, and are then transferred sequentially to ETF-ubiquinone oxidoreductase (ETF-QO) and finally to ubiquinol-cytochrome *c* oxidoreductase, complex III (Ruzicka & Beinert, 1977). In contrast, ETF from *M. methylotrophus* is highly specific in terms of its electron donor. Thus far, the only electron donor for *M. methylotrophus* ETF that has been identified is TMADH (Steenkamp & Gallup, 1978; Davidson *et al.*, 1986). *M. methylotrophus* ETF cannot be reduced by other dehydrogenases from *M. methylotrophus*, such as methylamine dehydrogenase or methanol dehydrogenase, or by dehydrogenases from other organisms.

All ETFs are heterodimeric. The molecular masses of the two subunits range from 31-42 kDa for the large (α) subunit and 25-38 kDa for the small (β) subunit. All ETFs contain one non-covalently bound flavin adenine dinucleotide (FAD) redox centre with the exception of the *M. elsdenii* protein, which contains two equivalents of FAD (Whitfield & Mayhew, 1974). ETFs from human, pig, *P. denitrificans* and *M. methylotrophus* also contain one equivalent of AMP, which is thought to play a role in protein folding. It has been shown that AMP facilitates the reconstruction of holo-ETF from the guanidine-denatured protein (Griffin *et al.*, 1997; Swenson & Chen, 1996).

The genes encoding ETFs have been cloned and sequenced from several different sources; human (Finocchiaro *et al.*, 1988), rat (Shinzawa *et al.*, 1988), *P. denitrificans* (Bedzyk *et al.*, 1993) and *M. methylotrophus* (Chen & Swenson, 1994), and three of these

(human, rat and *M. methylotrophus*) have been expressed as the active protein. Of the ETFs for which sequences have been reported, human and *P. denitrificans* ETF share the highest degree of similarity (about 54%), whereas ETF from *M. methylotrophus* is only moderately conserved (about 30% identity with both human and *P. denitrificans*). Between all ETFs for which the amino acid sequence is known, one of the most highly conserved regions of polypeptide sequence is a region near the C-terminus of the large subunit (Chen & Swenson, 1994). This polypeptide sequence contains a highly conserved *GXGXXG* motif and an acidic residue at its C-terminus, and represents a consensus sequence for FAD binding.

The crystal structures for human and *P. denitrificans* ETF have been solved at 2.1 Å and 2.6 Å resolution, respectively (Roberts *et al.*, 1996; Roberts *et al.*, 1999). The overall fold for both human and *P. denitrificans* forms of ETF is identical. The structure of human and *P. denitrificans* ETF consists of three distinct domains. Domains I and II comprise the N- and C-terminal regions of the α subunit, respectively, while domain III consists entirely of the β subunit. The FAD cofactor resides in a cleft between the C-terminal half of the α subunit (domain II) and the β subunit (domain III), while the AMP molecule is associated solely with the β subunit.

A molecular model has been generated for the complex formed between human ETF and one of its physiological electron donors, medium chain acyl-CoA dehydrogenase (MCAD) (Roberts *et al.*, 1996). This was achieved by manual inspection of the two structures, followed by rigid body energy minimization using the X–PLOR package. The model depicts a surface area of interaction between the two molecules of approximately 3400 $Å^2$, and a flavin-flavin distance of approximately 19.5 Å. However, the authors suggest that conformational flexibility in one or both proteins may decrease the distance between the two flavins in the soluble complex by as much as 3-4 Å.

There are only two notable structural differences between human and *P. denitrificans* ETF. Firstly, in human ETF the polypeptide chain between residues 90 and 96 of the β subunit is folded into an α-helix, whereas in the *P. denitrificans* protein this sequence is in the form of a random coil. Secondly, when the structures of human and *P. denitrificans* ETF were superimposed it was found that domain I of human ETF is twisted by approximately 4° when compared to the orientation of domain I in *P. denitrificans*

ETF. This difference in gross molecular structure is probably not related to donor and/or acceptor specificity, as the only region of these proteins which is known to influence reactions with primary dehydrogenases and ETF-QO is domain III, the N terminal region of the β subunit (Herrick *et al.*, 1994). On the basis of this observation it was suggested that these ETF proteins may be flexible in free solution, and that this flexibility may play a role in electron transfer reactions (Roberts *et al.*, 1999).

1.4.2 ETF from *M. methylotrophus*

ETF from *M. methylotrophus* (sp. W_3A_1) is a highly specific electron carrier that accepts electrons only from TMADH, and consists of two subunits with molecular masses of 34 kDa and 29 kDa (Chen & Swenson, 1994). In addition to its FAD cofactor, the protein also contains a tightly bound molecule of AMP associated with its β subunit (DuPleiss *et al.*, 1994). Although the function of this AMP molecule has not been determined, there is evidence to suggest that it is involved in the folding of the holoenzyme (Swenson & Chen, 1996; Griffin *et al.*, 1997). The genes encoding the subunits of W_3A_1 ETF have been cloned and sequenced, and the active protein has been expressed in *E. coli* (Chen & Swenson, 1994), but thus far a crystal structure for the protein has not been obtained, though extensive trials have been carried out (White *et al*, 1994). Both native and recombinant forms of W_3A_1 ETF are purified predominantly in the semiquinone (one electron-reduced) form (Steenkamp & Gallup, 1978; Chen & Swenson, 1994). W_3A_1 ETF has one of the most highly positive redox potentials (+ 0.154 Volts) of any known flavoprotein (Byron *et al.*, 1989; Talfournier *et al.*, 2001). This is consistent with its need to accept electrons from the 4Fe-4S redox centre of TMADH, which has a redox potential of + 0.102 Volts. With its FAD cofactor in its oxidised state, W_3A_1 ETF can accept one electron from TMADH and dissociate from its redox partner with the FAD reduced to the semiquinone level. Semiquinone ETF does not act as an electron acceptor for TMADH in steady state reactions, and further reduction of isolated W_3A_1 ETF to its dihydroquinone state can only be accomplished electrochemically (Byron *et al.*, 1989). However, it was recently discovered that ETF can be reduced fully to its dihydroquinone form, both enzymatically (by substrate reduction) and chemically (by dithionite reduction) when it forms a complex with

TMADH (Jang *et al*, 2000). It was estimated that binding of ETF to TMADH shifts the redox potential of the FAD_{sq}/FAD_{hq} couple of ETF from – 0.197 Volts to about 0 Volts. Such a large change in redox potential is indicative of a substantial change in the environment of the flavin, which in turn suggests that ETF may undergo a large-scale conformational change when it binds to TMADH.

1.4.3 Electron Transfer between TMADH and ETF

The kinetics of electron transfer between TMADH and W_3A_1 ETF have been studied by stopped-flow spectroscopy (Huang *et al.*, 1995). These analyses used both native TMADH and TMADH that had been covalently modified to inactivate one or the other of its two redox centres. TMADH was treated with phenylhydrazine (which results in the addition of a phenyl moiety at the C-4a position of the flavin) to render its FMN cofactor redox inactive, and reduced with dithionite to load one electron onto the 4Fe-4S centre. Similarly, TMADH was treated with ferricenium hexafluorophosphate to render its 4Fe-4S centre inactive, and reduced with trimethylamine to transfer reducing equivalents onto the FMN cofactor. Analysis of the reaction rates between oxidised ETF and all three forms of reduced TMADH revealed that electrons are transferred from TMADH to ETF solely through the 4Fe-4S centre of TMADH. The results also yielded a value for the dissociation constant (K_d) for electron transfer from TMADH to ETF of 10 μM. The kinetics of this reaction are not affected by high salt concentrations, indicating that electrostatic forces do not influence the association or dissociation of the TMADH/ETF complex. The kinetics of electron transfer between substrate reduced TMADH and the inorganic electron acceptor ferricenium hexafluorophosphate have also been studied by stopped flow spectroscopy (Wilson *et al.*, 1995). These analyses, together with the previously determined crystallographic coordinates of TMADH, led to the suggestion of a putative electron tunneling pathway from the 4Fe-4S centre of TMADH to the FAD of ETF, which involves Tyr 442 of TMADH. This in turn led to the proposal of a putative ETF binding pocket on the surface of the enzyme; a large concave surface with approximate dimensions of 1,200 $Å^2$. Subsequent work investigated further the role of Tyr 442 in the electron transfer pathway by investigating the electron transfer reaction between ETF and either wild type or mutant TMADH (Wilson *et al.*, 1997).

Mutation of Tyr 442 to either Phe or Leu resulted in modest reductions in the observed rates of electron transfer from TMADH to ETF (1.4-fold and 2.2-fold respectively). However, mutation of Tyr 442 to Gly resulted in a substantial decrease in the electron transfer rate (approx. 30-fold), and in an increased dissociation constant for the complex. There are several postulates to explain these observations; a) Tyr 442 may be located on the electron tunneling pathway between the 4Fe-4S centre of TMADH and the FAD of ETF, and hence mutation of this residue may decrease the extent of electronic coupling between electron donor and acceptor. b) Tyr 442 may be directly involved in stabilising the interaction between TMADH and ETF. c) Mutation of Tyr 442 to Gly may cause a change in the local protein structure in the putative binding pocket on the surface of TMADH, and hence indirectly affect the interaction between the two proteins. Evidence for the latter hypothesis includes the fact that Tyr-442 is known to be located within an α helix in the surface cavity of TMADH, and therefore mutation of this residue to Gly may destabilise the helix and alter the local protein structure. Examination of the crystal structure of TMADH suggested a possible electron transfer pathway to ETF involving Val 344. This residue is next to Cys-345, one of the cysteinyl ligands of the 4Fe-4S centre, and therefore Val 344 may provide a direct route for the transfer of electrons to the isoalloxazine ring of ETF.

However, recent results investigating the reactions of TMADH mutated at position 344 have indicated that this residue is not located on the electron transfer pathway from TMADH to ETF (Basran *et al.*, 2000). Mutation of Val 344 to Ala, Cys, Gly, Ile or Tyr did not result in substantial changes in the rates of electron transfer from TMADH to ETF, although these mutations did result in changes in the electron transfer rate between TMADH and the inorganic electron acceptor ferricenium. One conclusion of this study was that, once again, Tyr 442 might be involved in coupling of TMADH to ETF and/or in transfer of electrons from the 4Fe-4S centre to the FAD. Also, this study revealed that the rate of electron transfer from wild-type TMADH to ETF increases linearly as a function of ETF concentration, with a second order rate constant of 1.44 x 10^6 M^{-1} s^{-1}. However, mutants altered at position 442 display a hyperbolic dependence on the concentration of ETF. Limiting rate constants (k_{lim}) for electron transfer in the mutant complexes range from approximately 50 s^{-1} (for the Y442F mutant) down to 6 s^{-1} (for the

Y442G mutant). This saturation behaviour with respect to ETF concentration was also observed in previous kinetic analyses of the Y442F, Y442L and Y442G TMADH mutants (Wilson *et al.*, 1997). The linear relationship between the observed rates of electron transfer in the wild-type complex and the concentration of ETF suggest that complex formation is rate limiting, and that the intrinsic rate of electron transfer (and any conformational reorganisation within the complex) following complex formation is rapid. The appearance of saturation kinetic behaviour for mutants altered at residue 442 might be the result of a reduction of the intrinsic electron transfer rate constant (k_{eT}). However, it is perhaps more likely (given the relatively slow limiting rates of electron transfer for the mutant complexes) that this behaviour represents a reduction of the rate constant for the structural reorganisation of TMADH and/or ETF to form the active electron transfer complex.

1.4.4 Domain Motion in W_3A_1 ETF - The Model

As previously stated, there is no crystal structure currently available for W_3A_1 ETF. However, the genes encoding the two subunits of W_3A_1 ETF have been cloned, sequenced and expressed (Chen & Swenson, 1994), and the structure of human ETF (which shares 31% sequence identity with W_3A_1 ETF) has been determined at 2.1 Å resolution (Roberts *et al.*, 1996). Using these data, together with the information regarding the ETF binding site on the concave surface of TMADH and the proposed role of Tyr 442 / Val 344 in the electron transfer pathway as described by Wilson *et al* (1997), a model has been built of the proposed molecular structure of W_3A_1 ETF, both in free solution and in complex with TMADH (Chohan *et al.*, 1998). The first step in this procedure was homology modeling of W_3A_1 ETF using the structure of human ETF as a template. According to this model, the two subunits of W_3A_1 ETF, α (residues 1 - 321) and β (residues 322 - 585), comprise three domains; domain I (the N-terminal region of the α subunit), domain II (the C-terminus of the α subunit and a small C-terminal region of the β subunit) and domain III (the majority of the β subunit). The molecule is thought to be Y – shaped, with domains I and III forming a shallow "bowl" in which domain II rests. The isoalloxazine ring of FAD interacts solely with domain II (Figure 1.4). The second stage of the modeling procedure was to dock ETF onto the crystal structure of

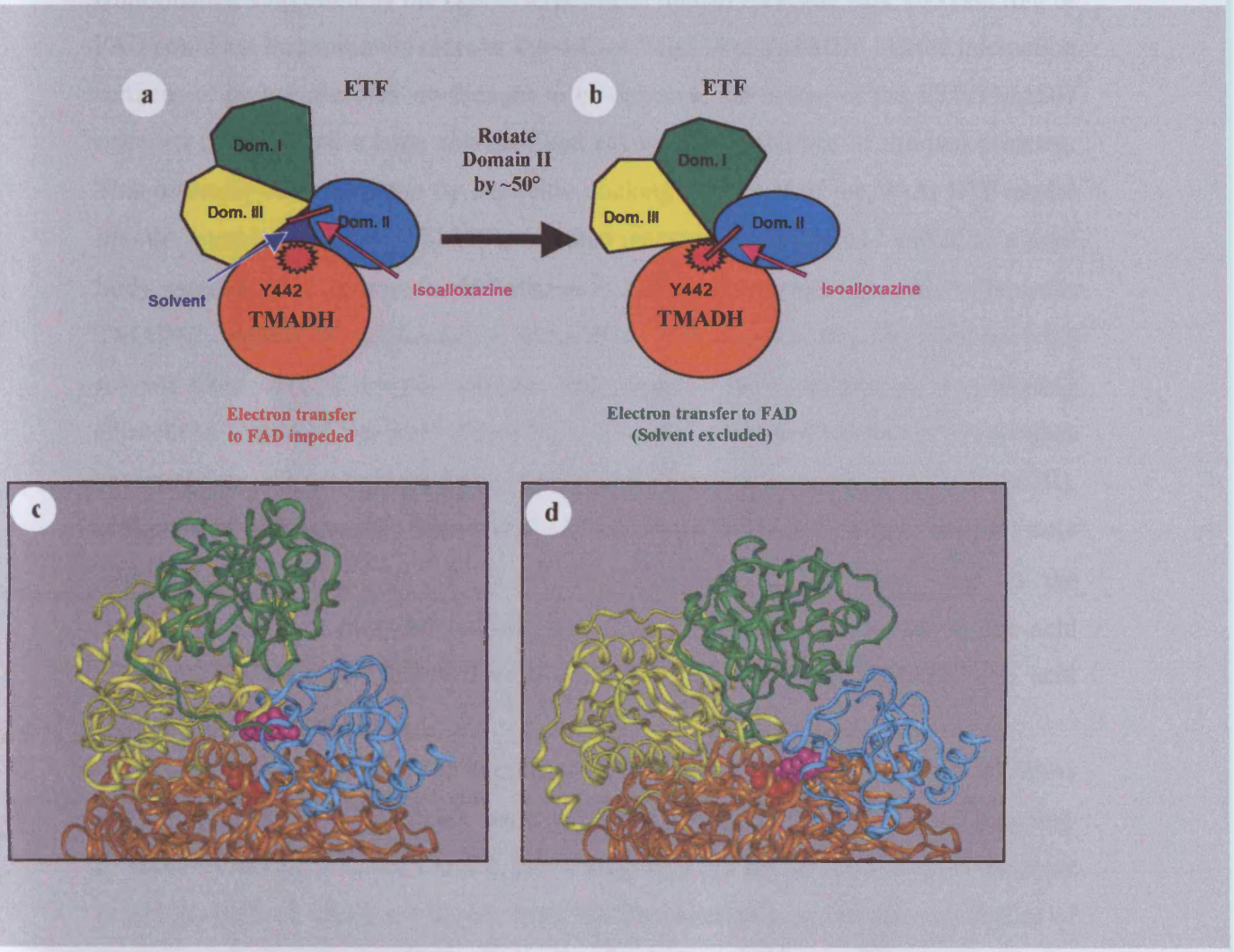

Figure 1.4
Model of domain motion in W_3A_1 ETF. In the eT inactive complex with TMADH (panel A) the isoalloxazine ring of ETF is not adjacent to the residues thought to be on the electron transfer pathway between TMADH and ETF, and there is a large solvent filled cavity at the interface of the two proteins. Rotation of domain two by 50 degrees relative to domains one and three eliminates these difficulties (panel B). Panels C and D are a molecular graphics representation of the scheme shown in panels A and B respectively.

TMADH. This proved problematic, however, because when W_3A_1 ETF is modeled in the conformation suggested by the crystal structure of human ETF, the isoalloxazine ring of FAD could not be positioned close to Tyr-442 or Val-344 of TMADH. As the interacting surfaces of both molecules are thought to be concave, the model of the ETF/TMADH complex incorporated a large solvent-filled cavity at the interface of the two proteins. This difficulty was overcome by explicitly docking domain II of the W_3A_1 ETF model into the crystal structure of TMADH, and then repositioning domains I and III as a rigid body, rotating these domains by 50° relative to domain II, to remove stearic overlap with TMADH. Altering the conformation of the W_3A_1 ETF model in this way eliminates the solvent filled cavity from the complex and positions the isoalloxazine ring directly adjacent to Tyr-442 / Val-344. Thus, W_3A_1 ETF was purported to exist in two distinct conformations; eT inactive (in free solution) and eT active (in complex with TMADH), as illustrated in Figure 1.4. The model of "eT active" W_3A_1 ETF shows the molecule with domain II rotated by 50° in the direction of domain I, which exposes the isoalloxazine ring of the FAD cofactor and suggests a patch of about ten amino acid sidechains on domain I interacting with a corresponding patch of ten amino acid sidechains on domain II.

There is further evidence to support the conformational flexibility model for W_3A_1 ETF. Firstly, W_3A_1 ETF contains two putative "hinge" regions; a poly-glycine sequence (^{193}GGG^{195}) linking domains I and II, and a long loop (15 amino acids) linking domains II and III, both of which are absent from the corresponding amino acid sequences of human and *P. denitrificans* ETF. Secondly, electrochemical evidence suggests that the conformation of ETF in solution might play a role in stabilising the semiquinone form of the protein, and hence in the function of ETF as an electron chaperone (Byron *et al.*, 1989). This is consistent with the requirement of the highly electropositive W_3A_1 ETF to transfer reducing equivalents to membrane-bound cytochromes. The model of W_3A_1 ETF suggests that domain III shields the isoalloxazine ring from oxidation in the eT inactive conformation, but in the eT active form this protection is lost. The proposed molecular structure of W_3A_1 ETF in the FAD binding cavity suggested that the guanidinium group of Arg-237, which is located over the *si* face of the flavin isoalloxazine ring, may play a role in the stabilization of the semiquinone form of the

protein. In subsequent studies, site directed mutagenesis was used to change Arg-237 to Ala (Talfournier *et al.*, 2001). In contrast to the wild type protein, it was found that the R237A mutant of W_3A_1 ETF was purified predominantly in the fully oxidised form. The midpoint redox potentials of the FAD cofactor were determined by anaerobic redox titration. It was found that mutation of Arg-237 to Ala markedly destabilises the semiquinone form of W_3A_1 ETF, resulting in redox potentials for the FAD_{ox}/FAD_{sq} and FAD_{sq}/FAD_{hq} couples of - 0.31 Volts and - 0.43 Volts, respectively. This mutant of W_3A_1 ETF was also readily susceptible to full reduction to the dihydroquinone form, indicating that the kinetic block to full reduction seen in wild type ETF is substantially removed in R237A ETF. These results confirm the role of Arg-237 in stabilising the semiquinone form of W_3A_1 ETF and provide further evidence in support of the molecular model of the protein.

1.5 Aims of this Thesis

The aims of the research described in this thesis were to investigate the physical, structural and dynamic parameters that govern complex assembly and electron transfer reactions in W_3A_1 ETF. This was achieved using a combined spectroscopic, structural and kinetic approach. The work involved analysis of wild-type W_3A_1 ETF with respect to reactions with its physiological redox partner, TMADH, and with inorganic electron acceptors. The work also involved the use of novel structural techniques to elucidate the characteristics of soluble ETF. Analyses were extended to include ETFs from sources other than *M. methylotrophus*.

The more general goal of the work was to develop the TMADH-ETF system as a model for the study of interprotein electron transfer, and to expand the body of knowledge and understanding concerning the mechanism of electron transfer in biologically relevant systems.

CHAPTER 2

MATERIALS AND METHODS

2.1 Materials

2.1.1 Chemicals and Reagents

All chemicals used were of AnalaR grade or of equivalent purity, with the exception of methanol and acetic acid used for polyacrylamide gel electrophoresis (PAGE) staining, which were of laboratory grade. "Timentin" (15:1 w/w ticarcillin sodium:potassium cavulanate) was from Beecham Research Laboratories. Trimethylamine hydrochloride (TMA), phenylmethylsulphonyl fluoride (PMSF), flavin mononucleotide (FMN), 2-mercaptoethanol, bromophenol blue, Coomassie brilliant blue, N,N,N,'N'-tetramethylethylenediamine (TEMED), tris (hydroxymethyl) aminomethane (tris), sodium azide and ampicillin were from Sigma Chemical Company. Ammonium persulphate, potassium ferricyanide and sodium dodecyl sulphate (SDS) were from BDH Chemicals. Sodium dithionite was from Virginia Chemicals, and phenylhydrazine was from Eastman Kodak. Ferricenium hexafluorophosphate was synthesised (by N S Scrutton) as described in Lehman *et al* (1990). The *DC* Protein Assay Kit was supplied by Bio-Rad, the QuikChange™ Site-Directed Mutagenesis Kit was supplied by Stratagene, the T7 Sequencing™ Kit was supplied by Pharmacia Biotech, the Wizard™ *Plus* Maxiprep DNA Purification System was supplied by Promega, and the Recovery™ Plasmid and Cosmid Prep Kit was supplied by Hybaid. Glass distilled, deionised water was used throughout.

2.1.2 Bacterial Strains and Media

Methylophilus methylotrophus (sp. W_3A_1) was a gift from Professor F. Scott Mathews (Dept. of Biochemistry, Washington University School of Medicine, St Louis, Missouri, U.S.A.). *Escherichia coli* strain TG1 [K12, (r_k^-, m_k^-, r_b^-, m_b^-), Δ (*lac-pro*), *sup* E, *thi*, *hsd* D5/F' *tra* D36, *pro* A^+ B^+, *lac* I^q, *lac* Z ΔM15] was purchased from Stratagene. *Escherichia coli* strain B ER2566 [$F^-\lambda^-$ *fhuA2[lon] omp T lacZ::T7 genel gal*

sulA11 Δ(mcrC-mrr) 144::is10 R(mcr-73::miniTn10)2 R(zgb-210::Tn10)1 (TetS) endA1 [dcm]] was purchased from New England Biolabs.

M. methylotrophus was grown in the minimal medium described by Colby and Zatman (1973), which consisted of (per litre) 1.2 g K_2HPO_4, 0.62 g KH_2PO_4, 0.05 g $CaCl_2.6H_2O$, 0.2 g $MgSO_4.7H_2O$, 0.1 g NaCl, 1.0 mg $FeCl_3.6HO$, 0.5 μg $(NH4)_2SO_4$, 5.0 μg $CuSO_4.5H_2O$, 10 μg $MnSO_4.5H_2O$, 10 μg Na_2MoO_4, 10 μg H_3BO_3, 70 μg $ZnSO_4.7H_2O$, and 5 μg $CoCl_2.6H_2O$. The pH of the medium was adjusted to pH 7.0 with HCl, and a filter sterilised stock solution of TMA was added to the medium to a final concentration of 0.3% (w/v).

E. coli strains TG1 and B ER2566 were grown in 2xYT medium, which consisted of (per litre) 16 g tryptone, 10 g yeast extract and 5 g NaCl. Solid medium was produced by the addition of 1.5% (w/v) bactoagar to the liquid medium. Transformed bacteria were grown on plates supplemented with 50 μg/ml ampicillin, and in 2xYT medium supplemented with 50 μg/ml "timentin" (the stock solutions of ampicillin and "timentin" were filter sterilised before use). Glycerol stocks were made by adding 1.0 ml of bacterial culture to 0.5 ml of sterile glycerol, and stored at -70 °C. All media were autoclaved before use.

2.1.3. Restriction/DNA Modification Enzymes and Plasmid DNA

Restriction enzymes *Sap* I and *Dpn* I were purchased from New England Biolabs Inc., and *Eco* RI, *Kpn* I and *Nco* I were purchased from Amersham Life Science. Cloned *Pfu* DNA polymerase was from Stratagene. DNAseI was from BDH Biomedical Inc. T4 DNA ligase was from Amersham Life Science. The expression plasmid pKK-GEM was previously constructed (by J Basran) as described by Chen and Swenson (1996). The expression plasmid pTYB11 was purchased from New England Biolabs.

2.1.4. Chromatographic Media and Membranes

Pre-swollen diethylaminoethyl cellulose (DE52) anion exchange resin was purchased from Whatman Biosystems Ltd. Phenyl Sepharose high performance hydrophobic interaction resin was from Pharmacia, and Hydroxyapatite Bio-Gel HT was

from Bio-Rad. Ultrafiltration membranes and centricons were from The Amicon Corporation, and dialysis membranes were from Medicell International Ltd. Chitin beads (50 - 100μm) were purchased from New England Biolabs. Sephacryl 2000HR was purchased from Pharmacia.

2.2 Recombinant DNA Techniques

2.2.1 Mini-Preparation of Plasmid DNA

For plasmid DNA isolation, a single transformed colony of *E. coli* was picked from an agar plate and used to inoculate 5 ml of 2xYT medium containing 50 μg/ml timentin. Cultures were grown overnight at 30 °C with vigorous shaking. Preparation of the plasmid DNA from these cultures was carried out with the Hybaid Recovery Plasmid and Cosmid Prep Kit, using the supplied reagents and following the manufacturer's instructions throughout, with the exception that the volume of cells microcentrifuged in the initial stage of the preparation was 5 ml, and the cell pellet obtained from this centrifugation step was resuspended in 100 μl of Cell Resuspension Buffer. Plasmid DNA was eluted with 50 μl of sterile distilled water. The concentration of plasmid DNA obtained by this method was determined by measuring the absorbance at 260 nm (1 μg/ml of DNA has an absorbance of 0.03 at 260 nm).

2.2.2. Large-Scale Preparation of Plasmid DNA

As before, a single transformed bacterial colony was selected to inoculate 5 ml of 2xYT medium containing 50 μg/ml timentin, and grown overnight at 37 °C with shaking. This culture was used to inoculate 200 ml of 2xYT medium containing 50 μg/ml timentin, and grown at 25 °C for 36-48 hours with shaking. Preparation of the plasmid DNA was carried out using the Wizard™ *Plus* Maxiprep DNA Purification System, using the supplied reagents and following the manufacturer's instructions throughout. Plasmid DNA was eluted with 1.5 ml of sterile distilled water and the concentration was determined by measuring the absorbance at 260 nm.

2.2.3. Production of Transformation Competent Cells

One loop of cells taken from a frozen stock of TG1 (or B ER2566) cells was used to inoculate 5 ml of 2xYT medium and grown overnight at 37 °C. This culture was used to inoculate 200 ml of 2xYT medium containing 20 mM $MgSO_4$, and grown at 37 °C until the optical density at 600 nm was 0.48-0.5. Cells were chilled on ice for 5 min and then centrifuged (in pre-chilled centrifuge tubes) at 5,000g for 5 min at 4 °C. Following this step, all operations were performed on ice to avoid loss of competence. Cells were resuspended in 100 ml of Transformation Buffer I (30 mM K acetate, 100 mM $RbCl_2$, 10 mM $CaCl_2$, 50 mM $MnCl_2$, 15% (v/v) glycerol, adjusted to pH 5.8 with dilute acetic acid and sterilised by filtration), left on ice for 5 min and centrifuged at 5,000g for 5 min at 4 °C. The cells were resuspended in 10 ml of Transformation Buffer II (10 mM MOPS, 75 mM $CaCl_2$, 10 mM $RbCl_2$, 15% (v/v) glycerol, adjusted to pH 6.5 with 1 M NaOH and sterilised by filtration) and left on ice for 15 min. The cells were then aliquoted into Eppendorf tubes precooled in dry ice, snap frozen in dry ice and stored at -80 °C.

2.2.4. Transformation of Competent Cells

50 µl of competent TG1 cells (or 150 µl of competent B ER2566 cells) were thawed at room temperature and incubated on ice for 10 min. Plasmid DNA (approximately 50 ng in 10 µl) was added to the cell suspension, and the cells left on ice for 30 minutes. The cells were then heat shocked at 42 °C for 90 seconds exactly, and returned to ice for 2 min. 250 µl of 2xYT medium was added to the cells, which were then incubated at 37 °C for 1 hour with gentle shaking. These cultures were spread on 2xYT agar plates supplemented with 50 µg/ml ampicillin. The plates were inverted and incubated at 37 °C overnight.

2.2.5. Agarose Gel Electrophoresis

Agarose gels containing 0.8% (w/v) agarose and 0.6 µg/ml ethidium bromide (EtBR) were made up in 1xTAE buffer (40 mM Tris-acetate, 2mM EDTA) and cast in 11 cm x 12 cm trays, and electrophoresis was performed in 1xTAE buffer. Aliquots of sample DNA (10 µl) had added to them 2 µl of 6x loading buffer (10 mM Tris-HCl at pH

7.5, 50 mM EDTA, 10% (w/v) glycerol, 0.25% (v/v) bromophenol blue) prior to being loaded onto the gel. The DNA markers used were a 1 kilobase (kb) ladder (with marker sizes ranging from 0.5 kb to 10 kb) purchased form MBI Fermentas. Gels were run at 130 V for 90 min and visualised by ultraviolet illumination.

2.2.6. Design of Primers for Site Directed Mutagenesis

Design of mutagenic primers took into account codon usage in *M. methylotrophus*, as described in Boyd *et al.* (1992) (i.e. the most frequently used codons for the amino acids tyrosine, lysine, serine and alanine were used in the mutagenic oligonucleotide sequence). At least 10 base pairs were included on either side of the mutation site to ensure effective annealing. Also, primers were examined to ensure the absence of palindromic sequences and a lack of restriction sites for the *Dpn* I restriction enzyme. Mutagenic primers were synthesised in the Protein and Nucleic Acid Chemistry Laboratory at Leicester University. The sequence (5'-3') of the mutagenic primer is given below, with the mutant codon highlighted in bold:

For the αR237A mutant:

5' CTT TGC TGC TCA **GCT** CCG ATT GCG GAT 3'

2.2.7. Site Directed Mutagenesis

Site directed mutagenesis was carried out (by J Basran) on the ETF α-subunit gene cloned into the pKK-GEM expression plasmid. Mutations were generated using the QuikChange™ Site-Directed Mutagenesis Kit sold by Stratagene, and the manufacturer's instructions were followed throughout, with the only amendment being the addition of a ligation step to the manufacturer's protocol. After being subjected to digestion with *Dpn* I, 20 µl of the mutagenised DNA was added to 5 µl of 10x ligation buffer and 24 µl of sterile distilled water, and 1 µl of T4 DNA ligase was added to start the reaction. The reaction mixture was then incubated at 16 °C overnight, and the remainder of the protocol was carried out according to the manufacturer's instructions.

2.3 Methods for Protein Analysis

2.3.1 SDS Polyacrylamide Gel Electrophoresis

SDS polyacrylamide gel electrophoresis (SDS PAGE) was carried out according to the method described by Leammli (1970) using 12 % acrylamide gels in a slab gel system. The compositions of the gels were as follows: for the 12 % separating gel, 4.8 ml 30 % acrylamide, 3.0 ml of 1.5 M Tris-HCl buffer at pH 8.8, 4.04 ml water, 100 µl of 10 % (w/v) SDS, 50 µl of 10 % (v/v) ammonium persulphate and 10 µl TEMED; for the stacking gel, 1.33 ml 30 % acrylamide, 1.25 ml of 1.5 M Tris-HCl buffer at pH 6.8, 7.26 ml water, 100 µl of 10 % SDS, 50 µl of 10 % ammonium persulphate, and 10 µl TEMED. Protein samples (typically 5-50 µg) were added to an equal volume of "loading buffer" (0.77 g DTT, 10 ml of 10 % SDS, 1.25 ml of 1.25 M Tris-HCl at pH 6.8, 5 ml glycerol and 0.5 % bromophemol blue in ethanol diluted to 50 ml with water) and incubated at 100 °C for 5 min before being loaded onto the gel. Gels were run at a constant current of 40 mA until the dye reached the base of the gel (approximately one hour). The composition of the running buffer used was 57.6 g glycine, 110 g tris, and 20 g SDS diluted to a final volume of two litres with water. Gels were stained using Coomassie Brilliant Blue R250 (0.25 % in a 5:1:5 v/v solution of methanol: acetic acid: water) for 30 min and destained in a 5:1:5 solution of methanol: acetic acid: water.

2.3.2 Purification of TMADH and ETF from *M. methylotrophus* (W_3A_1)

Small-scale seed cultures were prepared by inoculating three one-litre flasks of Colby & Zatman medium with approximately 3 ml of a suspension of W_3A_1 (stored as glycerol stocks at -80 °C). These were grown for 48 hours at 30 °C with vigorous shaking. These seed cultures were used to inoculate three 20 litre tanks of Colby & Zatman medium. The tanks were aerated by connecting perforated plastic tubing to bench top air lines and suspending them in the medium. These cultures were grown at room temperature until the optical density at 595 nm reached 0.7 or above (approximately three days). Bacteria were harvested by centrifugation for 15 min at 5,000 rpm and 4 °C. Cells were resuspended in 50 mM potassium phosphate buffer, pH 7.5, and lysed by passing them through a French pressure cell at 80,000 psi internal pressure. To the resultant extract, $MgCl_2$ was added to a final concentration of 15 mM, a small spatula

(approx. 1 mg) of DNAse was added and the extract was incubated at 4 °C for 10 min. The extract was then clarified by centrifugation in a Sorvall SS-34 rotor (15,000 rpm, 45 min, 4 °C). The supernatant was brought to 50 % saturation with $(NH_4)_2SO_4$ by slow addition of the solid salt with gentle stirring for 10 min, and the extract was centrifuged in a Sorvall GSA rotor (10,000 rpm, 30 min, 4 °C) to remove unwanted precipitated proteins. Both TMADH and ETF were then precipitated by bringing the supernatant to 80 % saturation with $(NH_4)_2SO_4$ and the precipitated proteins harvested by centrifugation in a GSA rotor (10,000 rpm, 30 min, 4 °C). The pellet was resuspended in 50 ml 20 mM potassium phosphate buffer, pH 7.5, (Buffer A) and dialysed against 2 x 4l of the same buffer for 16 hours to remove the salt.

The dialysed extract containing TMADH and ETF was applied to a DE-52 ion exchange column (4 x 15 cm) which had been equilibrated with buffer A. The column was washed extensively (i.e. more than 5 column volumes were passed through it) to elute weakly bound proteins. Both TMADH and ETF were eluted from the column with a linear increasing salt gradient formed from 500 ml of buffer A and 500 ml of buffer A containing 0.5 M NaCl. The column was run at a flow rate of approx. 200 ml/hour and 8 ml fractions were collected. TMADH eluted at about 0.18 M NaCl and ETF at about 0.25 M NaCl. Fractions were identified by their characteristic colour; TMADH fractions were brown, and ETF fractions were deep yellow.

Fractions containing TMADH were pooled and solid $(NH_4)_2SO_4$ was added to 50 % saturation. The resulting mixture was centrifuged in a GSA rotor (10,000 rpm, 20 min, 4 °C) to remove any precipitated proteins, and was then applied to a phenyl Sepharose HP hydrophobic interaction column (1.5 x 10 cm), equilibrated with buffer A containing $(NH_4)_2SO_4$ to 50 % saturation. The column was washed extensively and TMADH was eluted using a descending linear gradient of $(NH_4)_2SO_4$ from 50 % saturation to 0 % saturation contained in buffer A; the total gradient volume was 600 ml. Fractions of 4 ml were collected and those containing TMADH were pooled and dialysed against buffer A (2 x 4l) for 16 hours. The enzyme was judged homogeneous by SDS PAGE and was stored at -20 °C in the presence of 20 % (v/v) ethylene glycol.

The ETF fractions were pooled and dialysed against 20 mM potassium phosphate buffer, pH 7.2 (Buffer B) (2 x 4l) for 16 hours to remove the NaCl. The protein was applied to a hydroxyapatite Bio-Gel HT (1.5 x 10 cm) column equilibrated with buffer B. ETF was eluted using 50 mM potassium phosphate buffer, pH 7.2. Fractions of 4 ml were collected, and those containing ETF were pooled. The enzyme was judged near-homogeneous by SDS PAGE and was stored at -80 °C in the presence of 20 % (v/v) ethylene glycol.

2.3.3 Purification of Recombinant ETF

Single colonies of transformed TG1 cells were used to inoculate 5 ml cultures of 2xYT medium supplemented with 50 μg/ml timentin. These cultures were grown at 30 °C for 16 hours with vigorous shaking, and samples from each culture were analysed by SDS PAGE. Cultures containing ETF were used to inoculate 200 ml of 2xYT medium supplemented with 50 μg/ml timentin, and grown at 25 °C for 48 hours with vigorous shaking. This culture was used to inoculate 10 litres of 2xYT medium supplemented with 50 μg/ml timentin, and grown at 25 °C for 72 hours with vigorous shaking. Bacteria were harvested by centrifugation 15 min at 5G and 4 °C. Cells were resuspended in a minimum volume of buffer B, and lysed by passing them through a French pressure cell at 80,000 psi internal pressure. To the resultant extract, $MgCl_2$ was added to a final concentration of 15 mM, a small spatula (approx. 1 mg) of DNAse was added and the extract was incubated at 4 °C for 10 min. The extract was then clarified by centrifugation in a Sorvall SS-34 rotor (15,000 rpm, 45 min, 4 °C). The supernatant was brought to 50 % saturation with $(NH_4)_2SO_4$ by slow addition of the solid salt with gentle stirring for 10 min, and the extract was centrifuged in a Sorvall GSA rotor (10,000 rpm, 30 min, 4 °C) to remove unwanted precipitated proteins. ETF was then precipitated by bringing the supernatant to 80 % saturation with $(NH_4)_2SO_4$ and the precipitated protein harvested by centrifugation in a GSA rotor (10,000 rpm, 30 min, 4 °C). The pellet was resuspended in 20 ml Buffer B and dialysed against 2 x 4l of the same buffer for 16 hours to remove the salt.

The dialysed extract containing recombinant ETF was applied to a DE-52 ion exchange column (4 x 15 cm) which had been equilibrated with buffer B. The column was washed extensively (i.e. more than 5 column volumes) to elute weakly bound proteins. ETF was eluted from the column with a linear increasing salt gradient formed from 500 ml of buffer B and 500 ml of buffer A containing 0.5 M NaCl. The column was run at a flow rate of approx. 200 ml/hour and 8 ml fractions were collected. ETF eluted at approximately 0.25 M NaCl. Fractions containing ETF were identified by their characteristic deep yellow colour.

The ETF fractions were pooled and dialysed against buffer B (2 x 4l) for 16 hours to remove the NaCl. The protein was applied to a second DE-52 column (1.5 x 10 cm) equilibrated with buffer B. ETF was eluted using a linear increasing salt gradient formed from 200 ml of buffer B and 200 ml of buffer A containing 0.5 M NaCl. Fractions of 4 ml were collected, and those containing ETF were pooled. For SAXS, the protein was loaded onto a 1 x 50 ml Sephacryl 200 HR column, and protein eluted in 2 ml fractions. The enzyme was judged homogeneous by SDS PAGE and was stored at -80 °C in the presence of 20 % (v/v) ethylene glycol.

2.3.4 Purification of Mutant TMADH Proteins

Single colonies of TG1 cells (transformed with expression plasmid pSV2tmdveg encoding the mutant enzyme) were used to inoculate 5 ml cultures of 2xYT medium supplemented with 50 μg/ml timentin. These cultures were grown at 37 °C for 16 hours with vigorous shaking, and samples from each culture were analysed by SDS PAGE. Cultures containing TMADH were used to inoculate 200 ml of 2xYT medium supplemented with 50 μg/ml timentin, and grown at 37 °C for 24 hours with vigorous shaking. This culture was used to inoculate 10 litres of 2xYT medium supplemented with 50 μg/ml timentin, 0.1 g/l riboflavin and 0.2 g/l ferrous sulphate, and grown at 37 °C for 36 hours with vigorous shaking. Bacteria were harvested by centrifugation 15 min at 5000 g and 4 °C. Cells were resuspended in a minimum volume of buffer A, and lysed by passing them through a French pressure cell at 80,000 psi internal pressure. To the resultant extract, $MgCl_2$ was added to a final concentration of 15 mM, a small spatula of DNAse was added and the extract was incubated at 4 °C for 10 min. The extract was

then clarified by centrifugation in a Sorval SS-34 rotor (15,000 rpm, 45 min, 4 °C), and approximately 10 mg of FMN was added. The supernatant was brought to 50 % saturation with $(NH_4)_2SO_4$ by slow addition of the solid salt with gentle stirring for 10 min, and the extract was centrifuged in a Sorval GSA rotor (10,000 rpm, 30 min, 4 °C) to remove unwanted precipitated proteins. TMADH was then precipitated by bringing the supernatant to 80 % saturation with $(NH_4)_2SO_4$ and the precipitated protein harvested by centrifugation in a GSA rotor (10,000 rpm, 30 min, 4 °C). The pellet was resuspended in 20 Buffer A and dialysed against 2 x 4l of the same buffer for 16 hours to remove the salt.

The dialysed extract containing mutant TMADH was applied to a DE-52 ion exchange column (4 x 15 cm) which had been equilibrated with buffer A. The column was washed extensively (i.e. more than 5 column volumes were passed through it) to elute weakly bound proteins. TMADH was eluted from the column with a linear increasing salt gradient formed from 500 ml of buffer B and 500 ml of buffer A containing 0.5 M NaCl. The column was run at a flow rate of approx. 200 ml/hour and 8 ml fractions were collected. TMADH eluted at about 0.18 M NaCl. TMADH fractions were identified by their characteristic brown colour.

Fractions containing TMADH were pooled and solid $(NH_4)_2SO_4$ was added to 50 % saturation. The resulting mixture was centrifuged in a GSA rotor (10,000 rpm, 20 min, 4 °C) to remove any precipitated proteins, and was then applied to a phenyl Sepharose HP hydrophobic interaction column (1.5 x 10 cm), equilibrated with buffer A containing $(NH_4)_2SO_4$ to 50 % saturation. The column was washed extensively and TMADH was eluted using a descending linear gradient of $(NH_4)_2SO_4$ from 50 % saturation to 0 % saturation contained in buffer A; the total gradient volume was 600 ml. Fractions of 4 ml were collected and those containing TMADH were pooled and dialysed against buffer A (2 x 4l) for 16 hours. The enzyme was judged homogeneous by SDS PAGE and was stored at -20 °C in the presence of 20 % (v/v) ethylene glycol.

All recombinant forms of TMADH studied are under-flavinylated (Scrutton *et al.*, 1994; Packman *et al.*, 1995; Mewies *et al.*, 1996). The flavin content of the mutant

enzymes was determined using the spectrophotometric method described by Scrutton *et al.* (1994).

2.3.5 Analytical Gel Filtration

Separation of proteins from homogeneous reaction mixtures was achieved by gel filtration chromatography, using a Superose™ 6 HR 10/30 column with a bed volume of 24 ml. The column was equilibrated with 50 mM potassium phosphate buffer, pH 7.0, at 4 °C, and a flow rate of 0.3 ml per minute was used. No more than 240 µl of sample (*i.e.* 1 % of the column bed volume) was loaded onto the column at any one time. Elution of protein fractions was monitored at 280 nm with a spectrophotometric unit, and eluate fractions of 0.5 ml were collected. The column was calibrated using proteins with molecular masses of 13,700 kDa (Ribonulease A), 25,000 kDa (Chymotrypsinogen A), 43,000 kDa (Ovalbumin), and 67,000 kDa (Albumin), and Blue Dextran 2000.

2.3.6 Determination of Protein Concentration

Concentration of pure TMADH was calculated using an extinction coefficient of 27,300 $M^{-1}cm^{-1}$ at 442 nm (Kasprzak *et al.*, 1983), which indicates the concentration of TMADH subunits (i.e. active sites). Concentration of mutant forms of TMADH was determined using an extinction coefficient of 20,000 $M^{-1}cm^{-1}$ at 280 nm (E.K.Wilson, PhD thesis).

Native ETF purifies as a mixture of oxidised and (predominantly) semiquinone enzyme (Steenkamp & Gallup, 1978) and is stable to air oxidation in this form. The enzyme was fully oxidised by treatment with potassium ferricyanide, and excess oxidant was removed using a Sephadex G-25 gel filtration column equilibrated in the appropriate buffer. The concentration of the oxidised enzyme was determined using an extinction coefficient of 11,300 $M^{-1}cm^{-1}$ at 438 nm (Steenkamp & Gallup, 1978). The concentration of oxidised recombinant ETF was determined by the same method. All spectrophotometric measurements were made using a Hewlet-Packard 8452A single beam diode array spectrophotometer.

For HPLC, the concentration of ETF (native and recombinant) was determined using the *DC* Protein Assay Kit purchased from Bio-Rad, following the manufacturer's

instructions throughout. Bovine serum albumin was used as the standard protein; the concentrations of the standards used were 0.171 mg/ml, 0.343 mg/ml, 0.685 mg/ml and 1.37 mg/ml, made up in 50 mM potassium phosphate buffer, pH 6.8. A calibration curve was plotted over this range.

2.3.7 Fluorimetric Analyses

All spectrofluorimetric analyses were performed using an SLM Instruments 48000 spectrofluorimeter attached to a 450W Xe lamp (except for lifetime measurements, where a 200W Hg-Xe lamp was used). All analyses were carried out at 20 °C in 50 mM potassium phosphate buffer, pH 7.0, in quartz cuvettes with a light path of 5 mm. Static emission spectra were measured from 460 nm to 700 nm, exciting at 450 nm. Static excitation spectra were measured from 300 nm to 520 nm, measuring emission at 530 nm. All static spectra were measured at a protein concentration of 10 μM. Kinetic measurements of ETF fluorescence were carried out using an excitation wavelength of 450 nm and measuring emission at 530 nm. The concentration of ETF used in all kinetic experiments was 5 μM, and the concentration of TMADH varied from 0.25 μM to 15 μM. To minimize the effects of photobleaching on the observed fluorescence signal, measurements were taken at timed intervals commensurate with the time scale of the experiment, and the sample was only exposed to the excitation beam for a maximum of 10 seconds per measurement.

Glan-Thompson polarisers were used for anisotropy measurements, both to polarize the excitation light and to polarize the emitted light at both emission photomultipliers. For lifetime measurements, a 200W Hg-Xe lamp and an excitation wavelength of 436 nm (corresponding to a peak in the arc lamp emission intensity) were used. Modulation frequencies were generated using an SLM PTS 500 frequency synthesizer. Nanosecond fluorescence lifetimes were calculated from frequency modulation data.

2.3.8 HPLC

Reverse phase high performance liquid chromatography (HPLC) was performed on a Waters Spherisorb S5 OD52 reverse phase column, with a flow rate of 0.2 ml/min.

All samples were boiled for 5 min prior to column application. The column was equilibrated with a solution consisting of 80 % 50 mM potassium phosphate buffer, pH 6.5 (Buffer C) and 20 % methanol, and samples were eluted using an ascending linear gradient of methanol from 20 % to 100 % in buffer C. Elution of the cofactors was monitored at 436 nm with a diode array unit.

2.3.9 Circular Dichroism Spectropolarimetry

Circular dichroism (CD) spectra were measured using a Jasco J-715 spectrapolarimeter. Samples were held in a cylindrical quartz cuvette with a path length of 10 mm. All spectra were measured at 20 °C in 50 mM potassium phosphate buffer, pH 7.0, and a protein concentration of 3 μM was used.

2.3.10 Difference Spectroscopy

Difference spectroscopy was performed using a Hellma quartz Suprasil Precision Cell, which is a split-cell cuvette containing two compartments, each with a light path of 4.375 mm (total light path including divider was 1 cm). The contents of the separate compartments in the cuvette were mixed by inversion, and spectrophotometric analysis of the contents was made before and after mixing to obtain a difference spectrum.

2.3.11 Preparation of Anaerobic Samples

Anaerobic buffers were prepared by placing them in a sealed glass vessel covered with a rubber septa (which had a syringe needle piercing it to release the pressure) and bubbling oxygen-free argon through the buffer for at least 30 min. Protein samples were made anaerobic by eluting them through a Bio-Rad 10 DG gel filtration column under anaerobic conditions (< 10 ppm in N_2) in a glove box supplied by Belle Technology. Anaerobic dithionite solutions were prepared by adding solid sodium dithionite directly to anaerobic buffer and mixing under anaerobic conditions, as before.

2.3.12 Phenylhydrazine Inactivation of TMADH

Inactivation of the isoalloxazine ring of TMADH was achieved by incubating 25 μM TMADH (contained in 50 mM sodium pyrophosphate, pH 7.7) with 2 mM

phenylhydrazine, 70 μM DCPIP and 1 mM PMS for 3 hours at 30 °C for three hours. The mixture was subjected to gel filtration (using a Bio-Rad 10 DG gel filtration column) to remove phenylhydrazine, and the inactivated TMADH was dialysed against 50 mM phosphate buffer, pH 7 (2 x 2L). The concentration of phenylhydrazine inactivated TMADH was determined using an extinction coefficient of 202,000 $M^{-1}cm^{-1}$ at 280 nm (Wilson *et al.*, 1997).

2.3.13 Rapid Kinetic Analysis

Single wavelength rapid reaction kinetic experiments were carried out using an Applied Photophysics stopped-flow apparatus (SF.17MV), and data were collected and analysed using an Acorn A5000 computer and Spectrakinetics software (Applied Photophysics). Monophasic transients (single exponential) were fitted to equation 2.1;

$$A_t = A_0 e^{-kt} + b \qquad \text{(Eq. 2.1)}$$

where A_t is the absorbance at time t, A_0 is the initial absorbance and b is a floating end point to account for a non-zero baseline. Biphasic transients (double exponential) were fitted to equation 2.2;

$$A_t = C_1(1 - e^{-k_{fast}t}) + C_2(1 - e^{-k_{slow}t}) + b \qquad \text{(Eq. 2.2)}$$

Stopped flow transients were fitted to single or double exponential expression depending on the experiment (see Chapter 3 for details). When working with sodium dithionite as a reactant, all stopped flow work was performed under anaerobic conditions (< 10 ppm in N_2) in a glove box supplied by Belle Technology.

2.3.14 X-ray scattering data collection

Oxidised W_3A_1 ETF for X-ray scattering studies was obtained by treatment with potassium ferricyanide, followed by rapid gel filtration (Sephadex 25) to remove excess oxidant. Oxidised protein was used immediately in scattering experiments after gel

filtration and dilution (for concentration dependent scattering experiments). UV/Vis absorption spectra were recorded before and after X-ray exposure for samples in both oxidation states to ensure that no X-ray dependent redox change occurred. This also allowed the concentration of ETF samples to be determined using the absorption at 438 nm. SAXS experiments were performed with protein concentrations between 0.3 and 15 mg/ml. X-ray solution scattering data were collected in two sessions with the low-angle scattering camera on station 2.1 (Towns-Andrews *et al.*, 1994) at the Synchotron Radiation Source, Daresbury, U.K. using a position-sensitive multiwire proportional counter (Lewis, 1994). At the sample-to-detector distance of 2.4 m and the X-ray wavelength of $\lambda = 1.54$ Å, a momentum transfer interval of 0.002 Å $^{-1}$ = s = 0.050 Å $^{-1}$ was covered. The modulus of the momentum transfer is defined as $s = 2\sin\Theta/\lambda$, where 2Θ is the scattering angle. The s-range was calibrated using an oriented specimen of wet rat tail collagen (based on a diffraction spacing of 670 Å). Samples were contained in a brass cell holding a teflon ring sandwiched by two mica windows that defines the sample volume of 120 µl and a thickness of 1.5 mm. The brass cell was maintained at 4 °C during data acquisition. Buffer and sample were measured in alteration, each in a frame of 60 s (amounting to a total measuring time of up to 30 min depending on sample concentration and changes monitored on-line during experiments).

2.3.15 Interpretation of X-ray scattering data

Reduction and analysis of scattering data was performed as described in Grossmann *et al* (1998). Radius of gyration R_g, forward scattering intensity I^o and the intraparticle distance distribution function $p(r)$ were calculated from the experimental scattering data using the indirect Fourier Transform method as implemented in the program GNOM (Semenyuk and Svergun, 1991). Relative I^o/c values (c = sample concentration) give the relative molecular weight of the protein samples when referenced against a suitable standard (bovine serum albumin was used with a known molecular mass of 66 kDa). The maximum linear dimension D_{max} of the particle can be evaluated owing to the characteristic of $p(r)$. The volume V of the particle can be calculated from the Porod invariant (Porod, 1951) and a correction factor taking into account the limited experimental scattering range (Feigin and Svergun, 1987). The multipole expansion

method proposed by Stuhrmann (1970) and developed by Svergun et al. (1997) was used to obtain the molecular shape of W_3A_1 ETF. The smoothed scattering profile of reduced W_3A_1 ETF was fitted *ab initio* by the scattering from an envelope function starting from an ellipsoidal initial approximation (consistent with the experimental R_g and D_{max} values). The molecular shape was characterized with spherical harmonics using 19 free parameters (4^{th} order harmonics), which is acceptable given the minor differences compared to the shape obtained for 3^{rd} order harmonics (10 free parameters) and considering the information content in the data used.

2.3.16 Generation of Simulated X-ray Scattering Profiles

In order to take advantage of the already existing structural knowledge for these three-domain proteins, scattering data simulations were carried out using previously determined crystal structures and atomic models for the structures of *M. methylotrophus* ETF, Human ETF and *P. denitrificans* ETF. For W_3A_1 ETF, simulations were performed using molecular models of ETF in free solution and in the conformation expected when in complex with TMADH (Chohan *et al*, 1998). For Human and *P. denitrificans* ETF, simulations were performed using the crystal structures for the two proteins (Roberts *et al*, 1996 & 1999) and molecular models of these proteins in which domain II was rotated by 25 and 50 degrees relative to domains I and III. Parameters and scattering curves were computed from the model coordinates using the program CRYSOL (Svergun *et al.*, 1995), which also considers the hydration shell of the solvated protein.

CHAPTER 3

PURIFICATION OF TMADH AND ETF - PRELIMINARY CHARACTERISATION OF RECOMBINANT W_3A_1 ETF

3.1 Introduction

The availability of large quantities of pure protein is a prerequisite to any study of the interactions of those proteins *in vitro*. This chapter describes the protocols used for the purification of TMADH and ETF from both native and recombinant sources. Traditionally, studies of the molecular recognition and electron transfer kinetics between wild-type TMADH and ETF have been performed using proteins derived exclusively from the native source, *Methylophilus methylotrophus*. However, due to the poor yields of ETF from this source, and due to the large quantities of W_3A_1 ETF required for subsequent analyses, it was decided that recombinant W_3A_1 ETF should be used. The genes for the two subunits of W_3A_1 ETF have been cloned, sequenced and expressed, and the recombinant protein has been purified (Chen & Swenson, 1994). This chapter describes the optimisation of the purification protocol for large-scale production of recombinant W_3A_1 ETF. To confirm that information derived from analysis of recombinant W_3A_1 ETF can be extrapolated to the properties of native W_3A_1 ETF, it is first necessary to ensure that the physical and chemical properties of both forms of the protein are identical. This chapter describes the characterisation of both native and recombinant W_3A_1 ETF using spectroscopic and kinetic techniques. Finally, this chapter also describes the stopped-flow kinetic techniques used to probe the effects of hydrodynamic friction on rates of electron transfer between TMADH and native or recombinant ETF.

3.2 Results

3.2.1 Preparation of Plasmid DNA

Large-scale preparation of plasmid DNA was performed using the Wizard™ *Plus* Maxiprep DNA Purification System, as described in Section 2.1.4. Plasmid DNA purified from TG1 cells incorporating the pKK-GEM ETF expression plasmid was

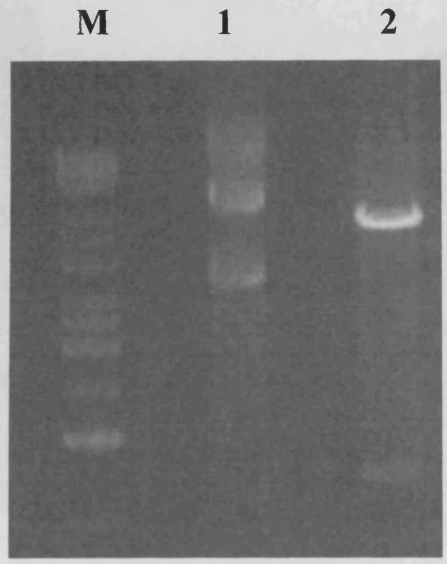

Figure 3.1
Agarose gel showing pure pKK-GEM expression plasmid, incorporating genes for the subunits of W_3A_1 ETF. Lane M is a 1kilobase DNA marker, Lane 1 is the purified pKK-GEM expression plasmid, and Lane 2 is the pKK-GEM expression plasmid digested with the *Eco* RI restriction enzyme.

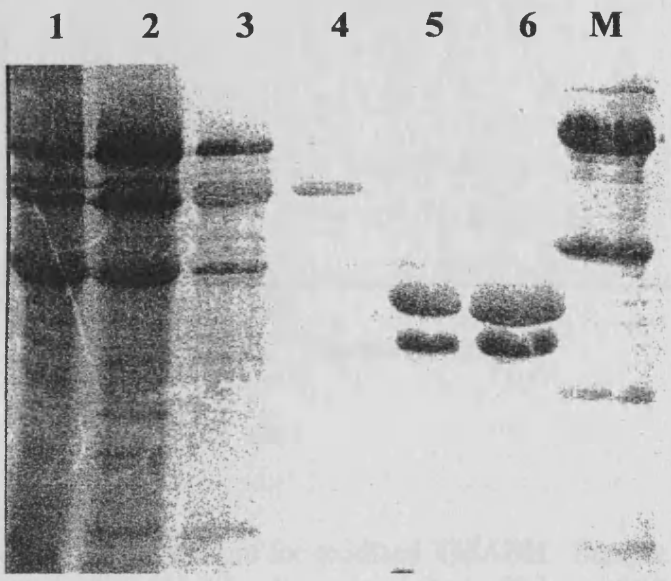

Figure 3.2
SDS PAGE gel showing purification of TMADH and ETF from *M. methylotrophus*. Lane M contains protein markers with molecular masses of 106 kDa, 43 kDa, 26 kDa and 15 kDa. Lane 1 contains the cell free extract; Lane 2 contains the 50%/80% ammonium sulphate fraction; Lane 3 contains TMADH eluted from the DE-52 chromatography step; Lane 4 contains TMADH eluted from the phenyl sepharose chromatography step; Lane 5 contains ETF eluted from the DE-52 chromatography step; Lane 6 contains ETF eluted from the hydroxyapatite chromatography step.

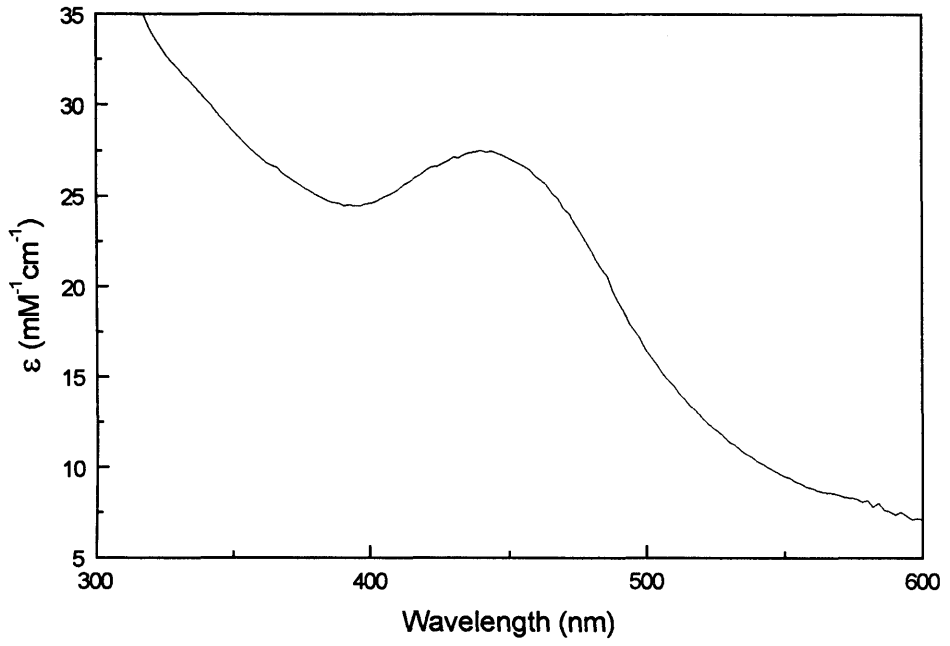

Figure 3.3
UV-visible absorption spectrum for oxidised TMADH. Sample was contained in 20 mM phosphate buffer, pH 7.5. An extinction coefficient of 27,300 M^{-1} cm^{-1} at 443 nm was used to calculate the concentration of oxidised TMADH.

obtained at a concentration of approximately 200 μg/ml. The purity of the plasmid DNA was determined by calculating the ratio of absorbance of the pure sample at 260 nm against its absorbance at 280 nm (A_{260}/A_{280}). The value of A_{260}/A_{280} for the purified plasmid was calculated as 1.84, which is sufficient for subsequent work (the minimum acceptable A_{260}/A_{280} for DNA work is 1.8), and an aliquot of the purified plasmid was run on an agarose gel (Figure 3.1).

3.2.2 Purification of TMADH from *Methylophilus methylotrophus*

Purification of native TMADH was performed as described in Section 2.3.1. A yield of approximately 2 mg of protein per litre of bacterial culture was obtained. Samples at each stage of the purification procedure were analysed by SDS PAGE to elucidate the purity of TMADH following each chromatographic step (Figure 3.2). A sample of pure TMADH was analysed by UV-visible absorbance spectroscopy (Figure 3.3). For oxidised, fully flavinylated TMADH, the ratio of the absorbance at 443 nm against the absorbance at 382 nm (A_{443}/A_{382}) has a value of 1.3. Hence, for the oxidised enzyme, this ratio can be used to calculate the flavin content of the enzyme.

3.2.3 Purification of ETF from *Methylophilus methylotrophus*

Purification of native ETF was performed as described in Section 2.3.1. A yield of approximately 0.15 mg of protein per litre of bacterial culture was obtained. Samples at each stage of the purification procedure were analysed by SDS PAGE to elucidate the purity of native ETF following each chromatographic step (Figure 3.2). Based on this SDS-PAGE analysis, the apparent molecular masses of the small and large subunits of native ETF are 38 kDa and 42 kDa, respectively. This observation confirms previous analyses of the electrophoretic behaviour of ETF (Davidson *et al.*, 1986). The abnormal migration of the small subunit (which has an apparent molecular mass of 42 kDa based on the migration in SDS-PAGE) is thought to be caused by unusually rigid secondary and/or tertiary structures, which lead to abnormal binding of SDS (Chen & Swenson, 1994). Pure native ETF was obtained primarily in the semiquinone form. Fully oxidised ETF was obtained by the addition of several crystals of potassium ferricyanide to a sample of purified ETF, which was subjected to gel filtration on a Bio-Rad 10 DG

disposable column to remove the oxidising agent. Semiquinone ETF was obtained by addition of 1 μg of TMADH to 1 mg of fully oxidised ETF in the presence of 10 mM TMA, and incubating at room temperature until reduction of ETF to the semiquinone form was complete. Samples of pure native ETF, in both oxidised and anionic semiquinone forms, were analysed by UV-visible absorbance spectroscopy (Figure 3.4).

3.2.4 Purification of Mutant TMADH

Purification of mutant TMADH was carried out as described in Section 2.3.3. Yields of approximately 10 mg of protein per litre of culture were obtained for Y442G TMADH, and similar yields were obtained for Y442L and Y442F mutants. Samples of pure Y442G, Y442L and Y442F TMADH were analysed by UV-visible spectroscopy (Figure 3.5). The flavin content of each enzyme was measured using the spectrophotometric method described in Scrutton *et al.*, (1994). The percentage of flavin present in the mutant protein sample can be determined using the following relationship;

$$\frac{A_{443}/A_{382} - 0.82}{0.48}.100 = \%flavinylatio$$

The flavinylation levels in the mutant TMADH enzymes are given in tabular form;

Sample	% flavinylation (determined spectrophotometrically)
Y442F TMADH	38
Y442L TMADH	38
Y442G TMADH	21

3.2.5 Expression and Purification of Recombinant ETF

Transformation competent *E.coli* (strain TG1) were produced as described in Section 2.2.5, and transformed with pKK-GEM ETF expression plasmid as described in Section 2.2.6. Purification of recombinant ETF was performed as described in Section 2.3.6. A yield of approximately 20 mg of protein per litre of culture was obtained.

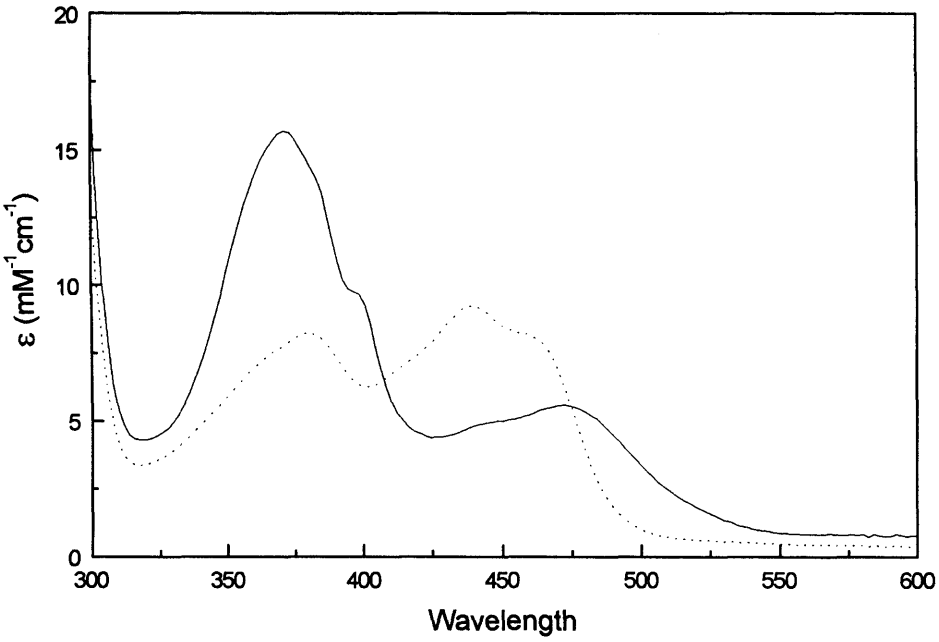

Figure 3.4
UV-visible absorption spectra for oxidised (dotted line) and semiquinone (solid line) W_3A_1 ETF. Samples were contained in 20 mM phosphate buffer, pH 7.5. An extinction coefficient of 11,300 M^{-1} cm^{-1} at 438 nm was used to calculate the concentration of oxidised ETF.

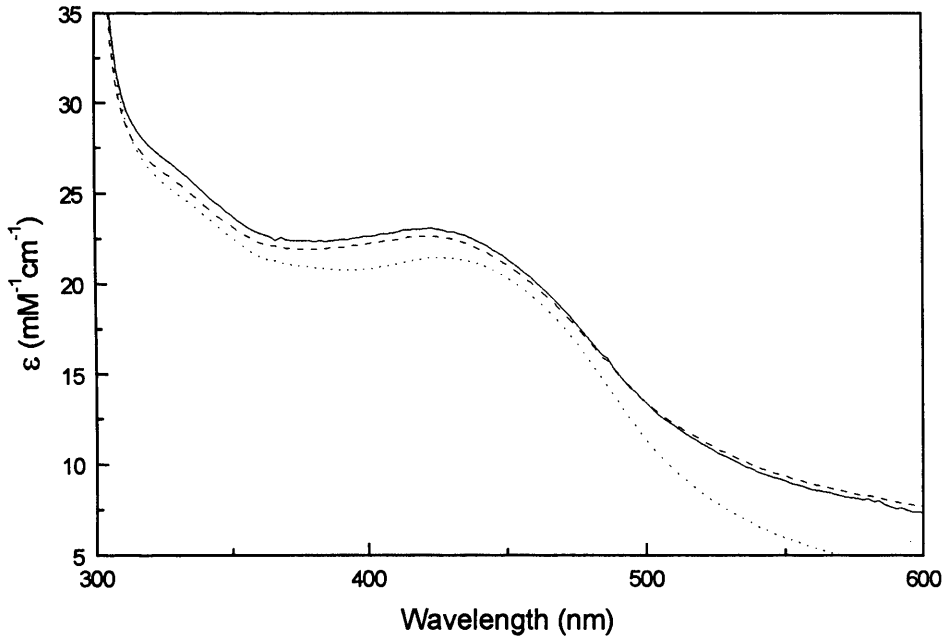

Figure 3.5
UV-visible absorption spectrum for Y442F (solid line), Y442L (dashed line) and Y442G (dotted line) TMADH. Samples were contained in 20 mM phosphate buffer, pH 7.5. An extinction coefficient of 20,000 M^{-1} cm^{-1} at 280 nm was used to calculate the concentration of mutant TMADH.

Samples of recombinant ETF at each stage of the purification procedure were analysed by SDS PAGE (Figure 3.6). The migration patterns of both subunits of recombinant ETF are identical to those of the native protein. Similarly to native ETF, recombinant ETF was obtained primarily in the semiquinone form. Fully oxidised recombinant ETF was obtained by the addition of several crystals of potassium ferricyanide to a sample of the pure protein, which was subjected to gel filtration on a Bio-Rad 10 DG disposable column to remove the oxidising agent. Semiquinone recombinant ETF was obtained by addition of 1 μg of TMADH to 1 mg of fully oxidised recombinant ETF in the presence of 10 mM TMA, and incubating at room temperature until reduction of ETF to the semiquinone form was complete. Samples of pure recombinant ETF, in both oxidised and anionic semiquinone forms, were analysed by UV-visible absorbance spectroscopy (Figure 3.7).

3.2.6 Comparison of Native and Recombinant ETF using UV-visible Spectroscopy

The absorbance spectra of native and recombinant ETF, in both their oxidised and semiquinone forms, were measured as described in Sections 3.2.3 and 3.2.5. Although there were very small differences in the absorbance spectra of native and recombinant ETF, the UV-visible spectral properties of native and recombinant ETF were essentially identical (Figure 3.8). For both forms of the protein, the A_{272}/A_{438} ratio for pure ETF in its fully oxidised form is 7.0. Also, the semiquinone form of both proteins is remarkably stable in air.

3.2.7 Fluorescence Spectroscopy Studies of Native and Recombinant ETF

Fluorescence spectroscopy was carried out as described in Section 2.3.7. The assumption behind these analyses was that if there were differences in the flavin environment between native and recombinant forms of the protein, this would be reflected in the fluorescence properties of the enzyme. Following excitation at 450 nm, the emission spectra for both forms of the enzyme were identical (Figure 3.9a). The same was true for the excitation spectra for both forms of the enzyme, which were taken measuring emission at 530 nm (Figure 3.9b). However, fluorimetric analysis of ETF revealed that, at ambient temperature (approx. 25 °C), the fluorescence of ETF (exciting

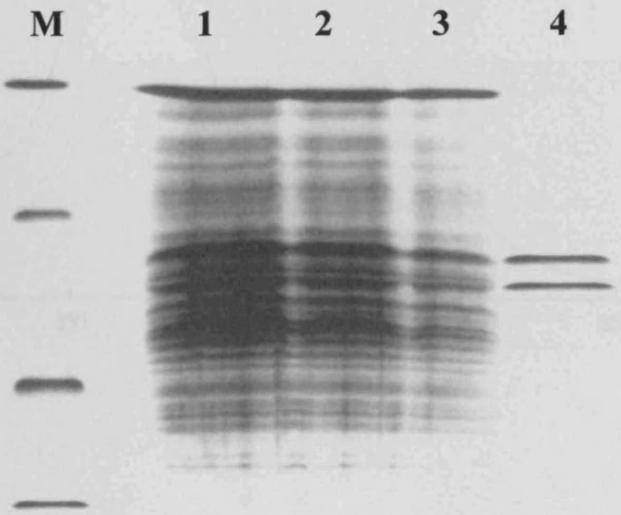

Figure 3.6
SDS PAGE gel showing purification of recombinant ETF from transformed TG1 cells. Lane M contains protein markers with molecular masses of 106 kDa, 43 kDa, 26 kDa and 15 kDa. Lane 1 contains the cell free extract; Lane 2 contains the 50%/80% ammonium sulphate fraction; Lane 3 contains ETF eluted from the DE-52 chromatography step; Lane 4 contains ETF eluted from the gel filtration step (to obtain ETF of sufficient purity for SAXS analysis).

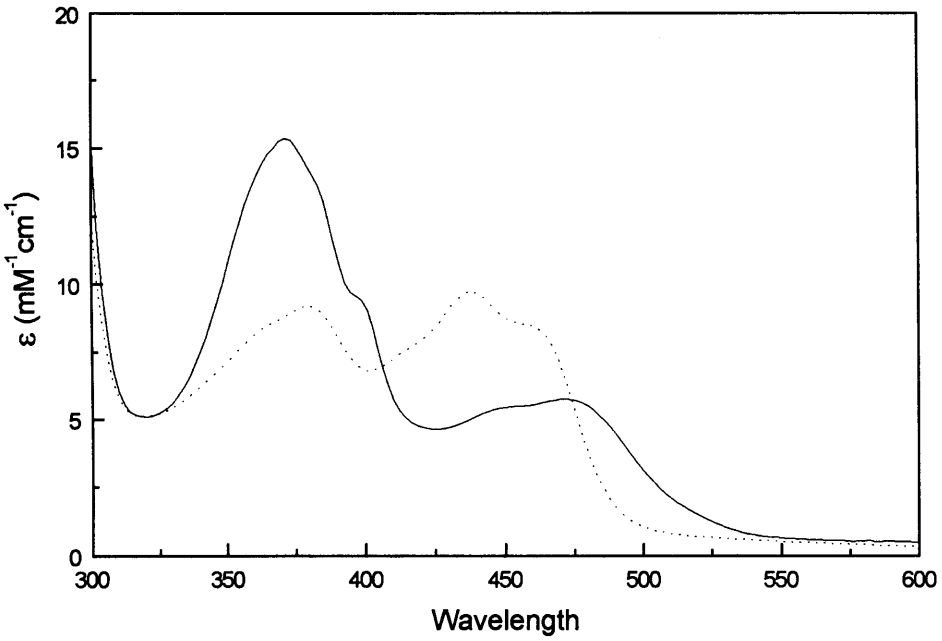

Figure 3.7
UV-visible absorption spectra for oxidised (dotted line) and semiquinone (solid line) recombinant ETF. Samples were contained in 20 mM phosphate buffer, pH 7.5. An extinction coefficient of 11,300 M^{-1} cm^{-1} at 438 nm was used to calculate the concentration of oxidised ETF.

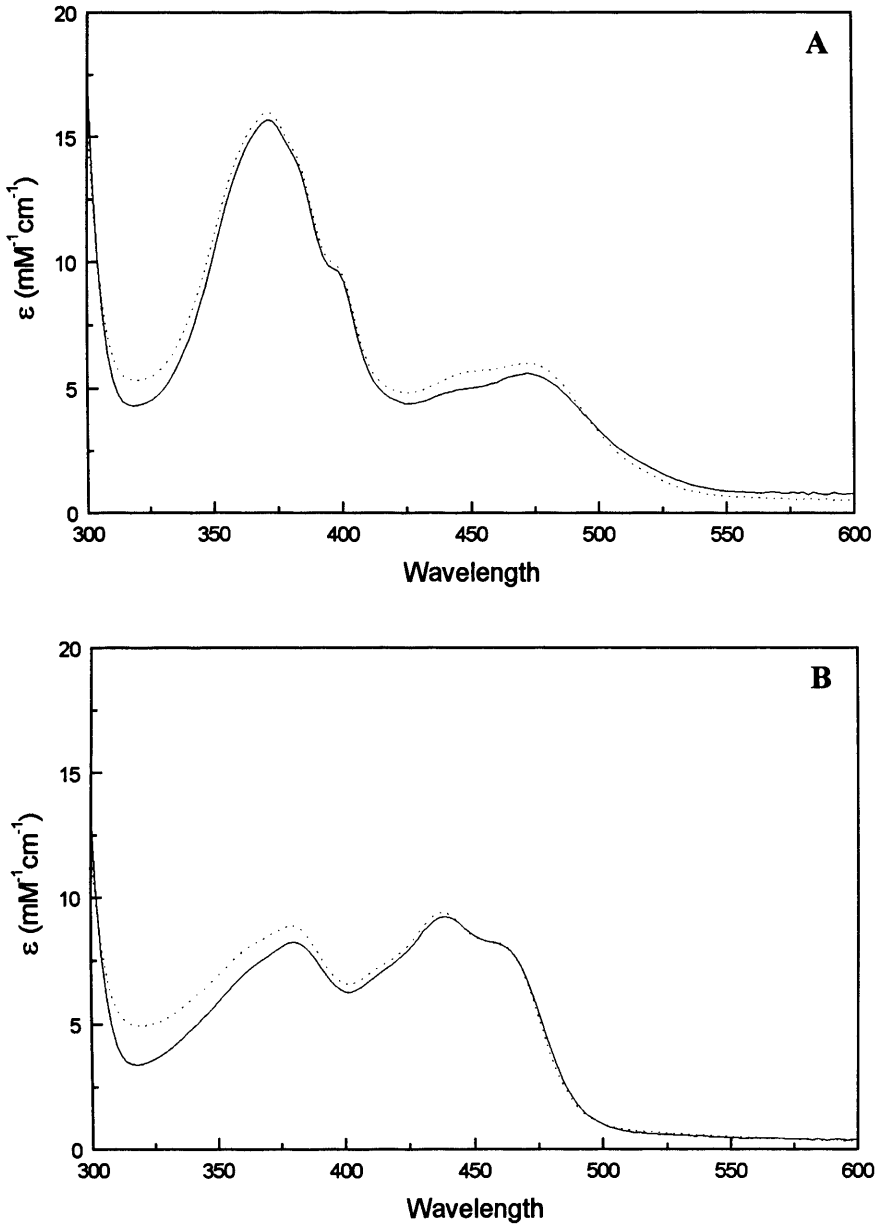

Figure 3.8

Panel A. UV-visible spectra of semiquinone native (solid line) and recombinant (dashed line) ETF. Samples were contained in 20 mM phosphate buffer, pH 7.2.

Panel B. UV-visible spectra of oxidised native (solid line) and recombinant (dashed line) ETF. Samples were contained in 20 mM phosphate buffer, pH 7.2. An extinction coefficient of 11,300 M^{-1} cm^{-1} at 438 nm was used to calculate the concentration of oxidised ETF.

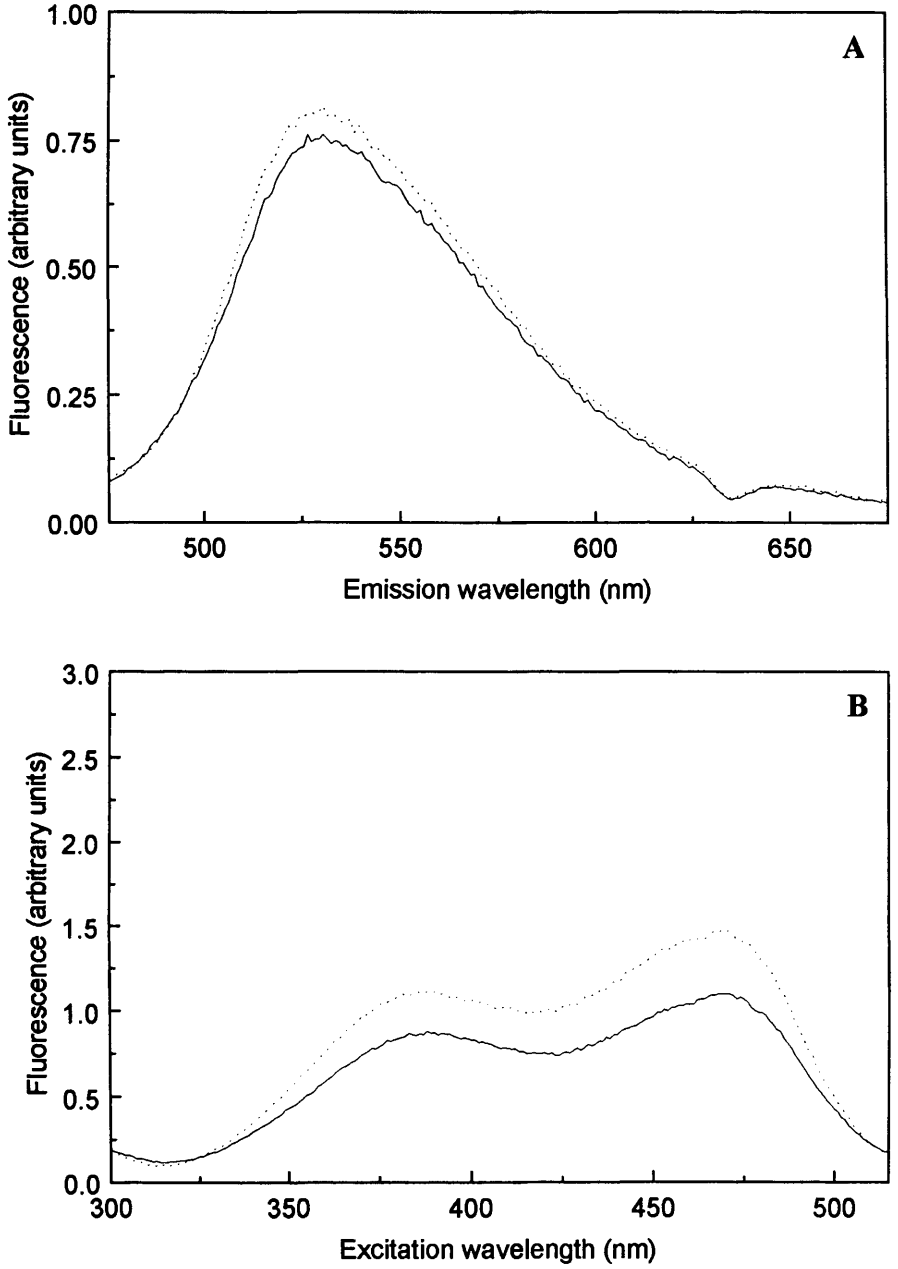

Figure 3.9

Panel A. Fluorescence emission spectra of oxidised native (dashed line) and recombinant (solid line) ETF. Samples were contained in 20 mM phosphate buffer, pH 7.2. Samples were subjected to excitation at 450 nm.

Panel B. Fluorescence excitation spectra of oxidised native (dashed line) and recombinant (solid line) ETF. Samples were contained in 20 mM phosphate buffer, pH 7.2. Emission was measured at 540 nm.

at 450 nm and measuring emission at 530 nm) increases as a function of time. The rate of increase in fluorescence was not dependent on the source of the enzyme (i.e. recombinant or native), but was dependent on the oxidation state of the enzyme. It was observed that the fluorescence of a 10 μM sample of semiquinone ETF increases at a rate of 2.28×10^{-4} per second, whereas the fluorescence of a 10 μM sample of oxidised ETF increases at a rate of 12.67×10^{-4} per second (Figure 3.10). This increase in fluorescence is thought to be due to dissociation of FAD from the ETF molecule. It was found that when a 10 μM sample of ETF (in either oxidation state) is subjected to denaturation by boiling for 5 min, its fluorescence at 540 nm increases by a value of 3.8. This value represents the total increase in flavin fluorescence that occurs when ETF is entirely dissociated from its FAD cofactor. Using this information, it was calculated that a 10 μM sample of semiquinone ETF loses its flavin at a rate of 0.45 % per minute when at room temperature, whereas oxidised ETF loses its flavin at a rate of 2 % per minute. These data suggest an altered conformation in oxidised ETF relative to the semiquinone form of the protein, the latter having a higher affinity for FAD. These data also explain previous observations that the oxidised form of ETF is highly unstable, and loses its ability to accept electrons over a number of days (Steenkamp & Gallup, 1978).

3.2.8 HPLC Studies of Native and Recombinant ETF

Native and recombinant ETF were analysed by HPLC as described in Section 2.3.8. These analyses were performed in order to confirm that both forms of the protein bind an equivalent amount of nucleotide cofactor. The concentrations of native and recombinant ETF were determined using the *DC* protein assay supplied by Bio-Rad, and 20 μM sample samples of each protein were boiled for 5 minutes prior to application to the column to denature protein and release any bound cofactors. The elution profiles for the cofactors of both forms of the protein were found to be identical (Figure 3.11). For both native and recombinant ETF, there are prominent absorption peaks at 436 nm after 6.4 minutes and 7.1 minutes. By comparison with nucleotide standards, these peaks were confirmed as representing FAD and FMN, respectively.

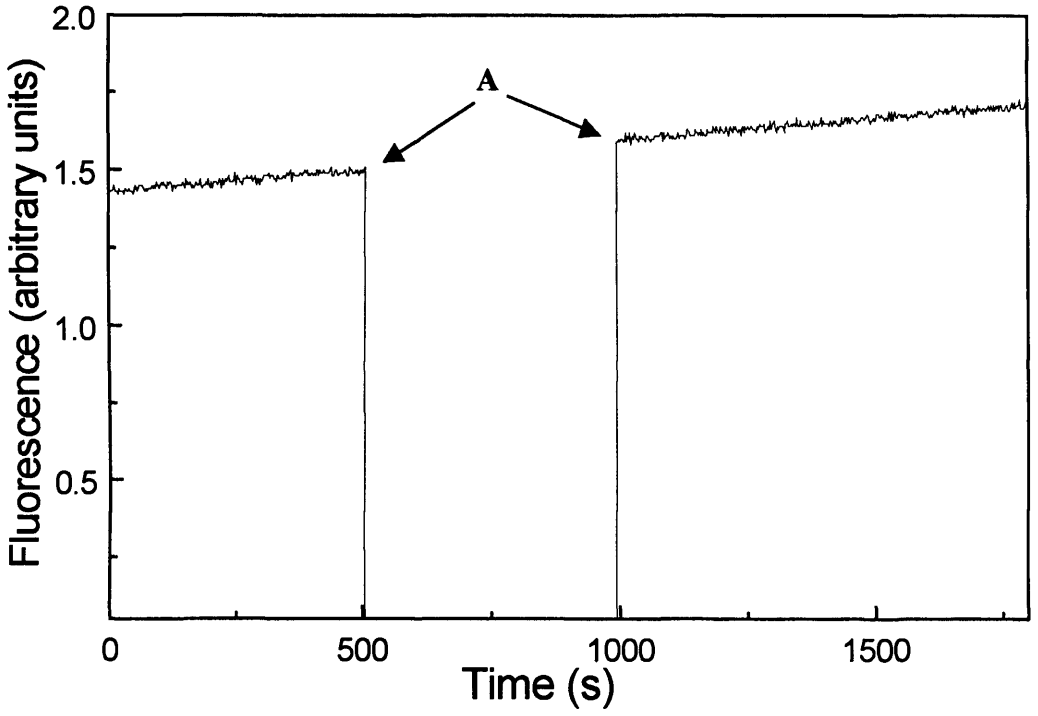

Figure 3.10
Fluorescence of oxidised recombinant ETF against time, exciting at 450 nm and measuring emission at 540 nm. Region A shows the period during which incident light was blocked from the sample to eliminate the effects of photo-bleaching (which causes a decrease in the fluorescence of the sample with respect to time). Region A was used to calculate the rate of increasing fluorescence (12.67 $x10^{-4}$ per second for oxidised recombinant ETF). This rate was identical for oxidised native ETF, but the rate of fluorescence increase with semiquinone ETF (both recombinant and native) was 2.28 $x10^{-4}$ per second (not shown).

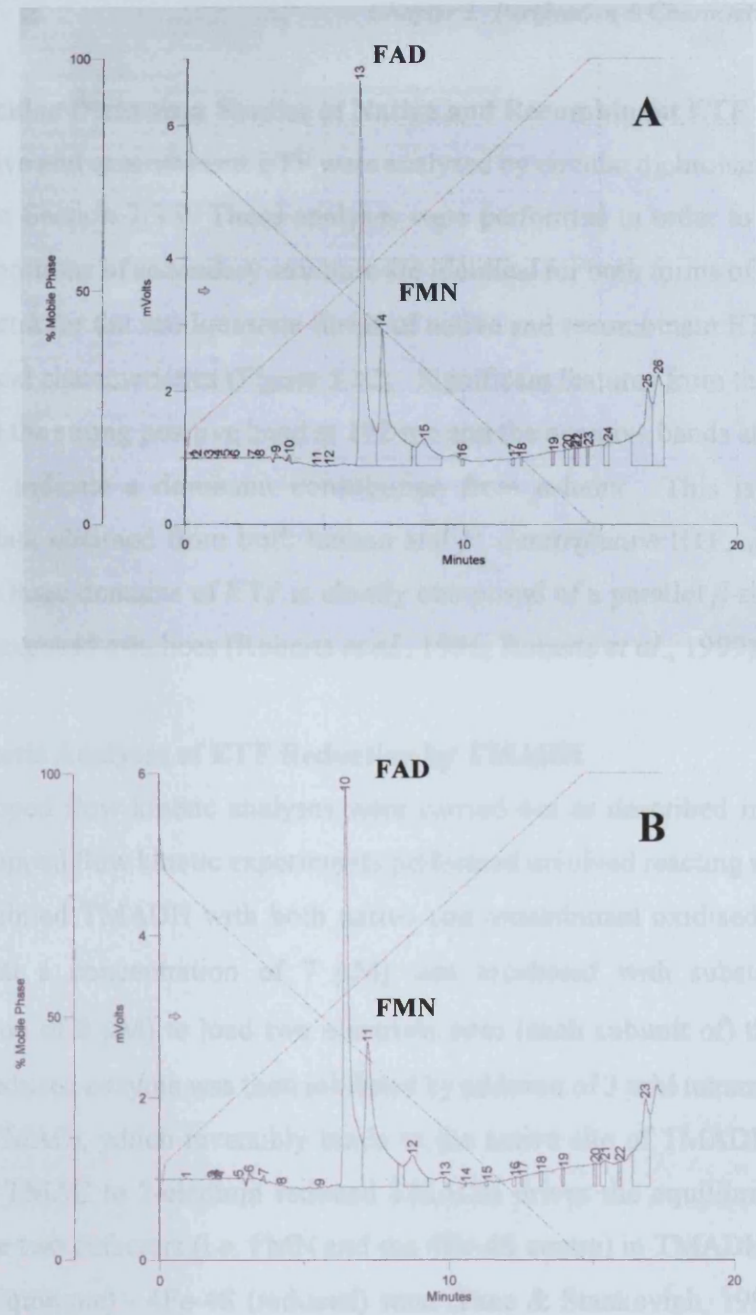

Figure 3.11
HPLC cofactor elution profiles for native (*Panel A*) and recombinant (*Panel B*) ETF. Cofactors were eluted with an increasing methanol gradient, and the eluate monitored at 436 nm. The identity of FAD and FMN in each elution profile was determined by comparison with the elution profile for a mixture of standard solutions of FAD and FMN (not shown). Peaks corresponding to FAD and FMN are marked (FMN is present due to degradation of the FAD cofactor).

3.2.9 Circular Dichroism Studies of Native and Recombinant ETF

Native and recombinant ETF were analysed by circular dichroism spectroscopy as described in Section 2.3.9. These analyses were performed in order to confirm that the overall proportions of secondary structure are identical for both forms of the protein. The far-UV spectra for the semiquinone forms of native and recombinant ETF were found to have identical characteristics (Figure 3.12). Significant features from the spectra of both proteins are the strong positive band at 192 nm and the negative bands at 208 nm and 220 nm, which indicate a dominant contribution from α-helix. This is consistent with structural data obtained from both human and *P. denitrificans* ETF, which shows that each of the three domains of ETF is chiefly composed of a parallel β-sheet core flanked by solvent exposed α-helices (Roberts *et al.*, 1996; Roberts *et al.*, 1999).

3.2.10 Kinetic Analyses of ETF Reduction by TMADH

Stopped flow kinetic analyses were carried out as described in Section 2.3.13. The first stopped flow kinetic experiments performed involved reacting substrate reduced TMAC-inhibited TMADH with both native and recombinant oxidised ETF. Oxidised TMADH (at a concentration of 7 μM) was incubated with substrate (TMA at a concentration of 8 μM) to load two electrons onto (each subunit of) the enzyme. The substrate-reduced enzyme was then inhibited by addition of 3 mM tetramethylammonium chloride (TMAC), which reversibly binds to the active site of TMADH. Significantly, binding of TMAC to 2-electron reduced TMADH drives the equilibrium of the redox states of the two cofactors (i.e. FMN and the 4Fe-4S centre) in TMADH in favour of the FMN (semiquinone) - 4Fe-4S (reduced) state (Pace & Stankovich, 1991). This means that substrate-reduced, TMAC-inhibited TMADH is reduced at its 4Fe-4S centre. TMADH treated in this way was reacted with oxidised recombinant ETF in a ratio of 3.5 μM : 45 μM (final concentration of reactants in the stopped flow reaction chamber) to ensure pseudo first-order kinetics. All reactions were carried out in 50 mM potassium phosphate buffer, pH 7.0, and the temperature in the reaction chamber was maintained at 25 °C. An average of twelve transients for the reaction with recombinant ETF is shown in Figure 3.13a. Results were identical for both native (not shown) and recombinant ETF. Transients were biphasic, the fast phase being representative of the rate of electron

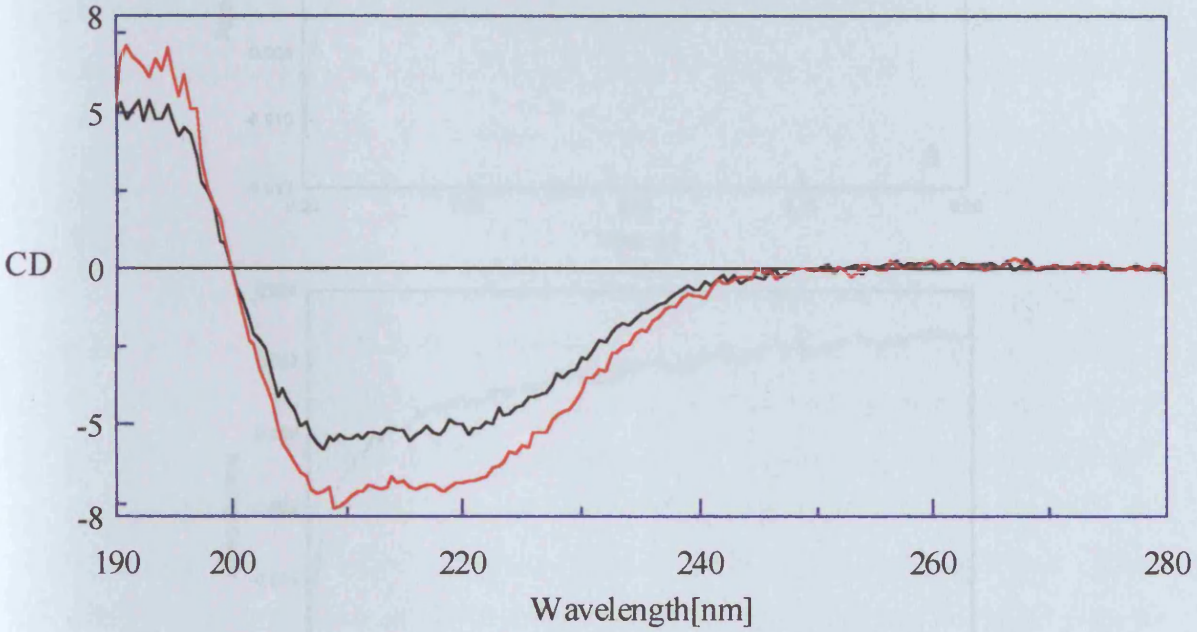

Figure 3.12
Far-UV CD spectra of native (*blue*) and recombinant (*red*) ETF (CD = Circular Dichroism, $[\theta]x10^{-3}$ degree cm^2). Spectra were recorded with a 10 mm path length at a protein concentration of 3 μM. Spectra were measured at 20 °C in 50 mM potassium phosphate buffer, pH 7.0. Ten scans were averaged for each protein sample

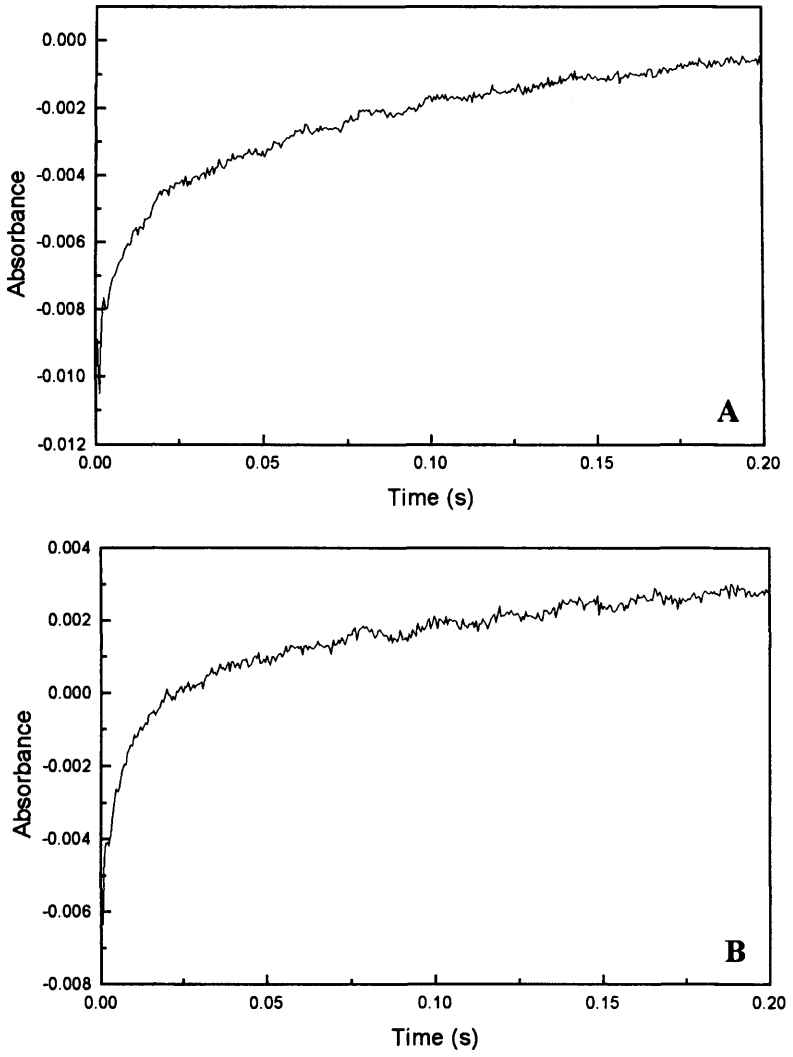

Figure 3.13

Panel A : Kinetic transient showing reduction of fully oxidised ETF by substrate reduced, TMAC-inhibited TMADH. The reaction was performed in 50 mM phosphate buffer, pH 7.0, at a temperature of 25 °C. Data were fitted to Equation 2.2 to obtain rates for the electron transfer reaction.

Panel B : Kinetic transient showing reduction of fully oxidised ETF by substrate reduced, TMAC-inhibited TMADH in the presence of 40 % (w/v) glycerol. The reaction was performed in 50 mM phosphate buffer, pH 7.0, at a temperature of 25 °C. Data were fitted to Equation 2.2 to obtain rates for the electron transfer reaction. Absorbance changes were measured at a wavelength of 438nm.

transfer from the 4Fe-4S centre of TMADH to the FAD of ETF, and the slow phase reporting on the rate of electron transfer from the FMN of TMADH to the flavin of ETF via the 4Fe-4S centre. Data were fitted to equation 2.2, and rate constants for the fast and slow rates of 168 s^{-1} and 12 s^{-1} respectively were obtained. The rate constant for electron transfer from the reduced 4Fe-4S centre of TMADH to the flavin of ETF (168 s^{-1}) is of the same order as previous analyses of the TMADH-ETF electron transfer reaction performed at similar protein concentrations and under identical buffer conditions (Huang *et al.*, 1995).

This experiment was repeated in the presence of glycerol. This was performed in order to increase the hydrodynamic friction in the reactant mixture, and hence to determine if this altered the rate of electron transfer by decreasing the rate of transition to the eT active conformation of ETF, according to the kinetic complexity model (Section 1.1.4.). Concentrations of glycerol from 5 % (w/v) to 40 % were used in this investigation, and all other reaction conditions were as previously described. It was found, however, that the observed rate constant for the reaction was not affected by the presence of glycerol. Results are shown below in tabular form. An average of nine transients for the reaction in the presence of 40 % glycerol is shown in Figure 3.13b.

Glycerol Concentration	Relative Viscosity	Observed Rate Constant for eT
0 %	1.0	168 s^{-1}
10 %	1.3	150 s^{-1}
20 %	1.7	171 s^{-1}
30 %	2.5	167 s^{-1}
40 %	3.8	179 s^{-1}

In the second set of stopped flow kinetic experiments, phenylhydrazine inactivated, dithionite-reduced TMADH was reacted with native and recombinant oxidised ETF. Treatment of TMADH with phenylhydrazine renders the FMN cofactor redox inactive by addition of a phenyl group to the C4a position of the isoalloxazine ring (Nagy *et al.*, 1979; Huang *et al.*,1995). Phenylhydrazine inactivation of TMADH was performed as described in Section 2.3.12. An aliquot of phenylhydrazine inactivated

TMADH was made anaerobic by bubbling with oxygen-free argon and reduced to the one electron level by titration with sodium dithionite, which transfers one electron directly onto the 4Fe-4S centre. TMADH treated in this way was reacted with oxidised ETF in a ratio of 3.5 μM : 45 μM (final concentration of reactants in the stopped flow reaction chamber) to ensure pseudo first-order kinetics. All operations were carried out under anaerobic conditions, and the temperature in the reaction chamber was maintained at 25 °C. An average of ten transients for this reaction is shown in Figure 3.14a. Results were identical for both native (not shown) and recombinant ETF. Transients were biphasic, the fast phase being representative of the rate of electron transfer from the reduced 4Fe-4S centre of TMADH to the FAD of ETF. Data were fitted to equation 2.2, and the rate constant for the fast rate of the reaction of 163 s^{-1} was obtained. The observed rate constant for the rate of electron transfer from the 4Fe-4S centre of TMADH to the flavin of ETF obtained in this study is of the same order as that suggested by previous analyses of the TMADH-ETF electron transfer reaction performed at similar protein concentrations and under identical buffer conditions (Huang *et al.*, 1995) and is almost identical to the value obtained using the TMAC/TMA system to investigate interprotein electron transfer rates (see above).

This experiment was repeated in the presence of glycerol. Concentrations of glycerol from 5 % (w/v) to 40 % were used in this investigation, and all other reaction conditions were as previously described. It was found that the observed rate constant for the reaction was not affected by the presence of glycerol, confirming the findings of the experiments using the TMAC/TMA system. Results are shown below in tabular form. An average of nine transients for the reaction in the presence of 40 % glycerol is shown in Figure 3.14b.

Glycerol Concentration	Relative Viscosity	Observed Rate Constant for eT
0 %	1.0	163 s^{-1}
10 %	1.3	178 s^{-1}
20 %	1.7	152 s^{-1}
30 %	2.5	159 s^{-1}
40 %	3.8	162 s^{-1}

Although these results appear to indicate that the rate of electron transfer from TMADH to ETF is independent of the viscosity of the medium, the concentrations of

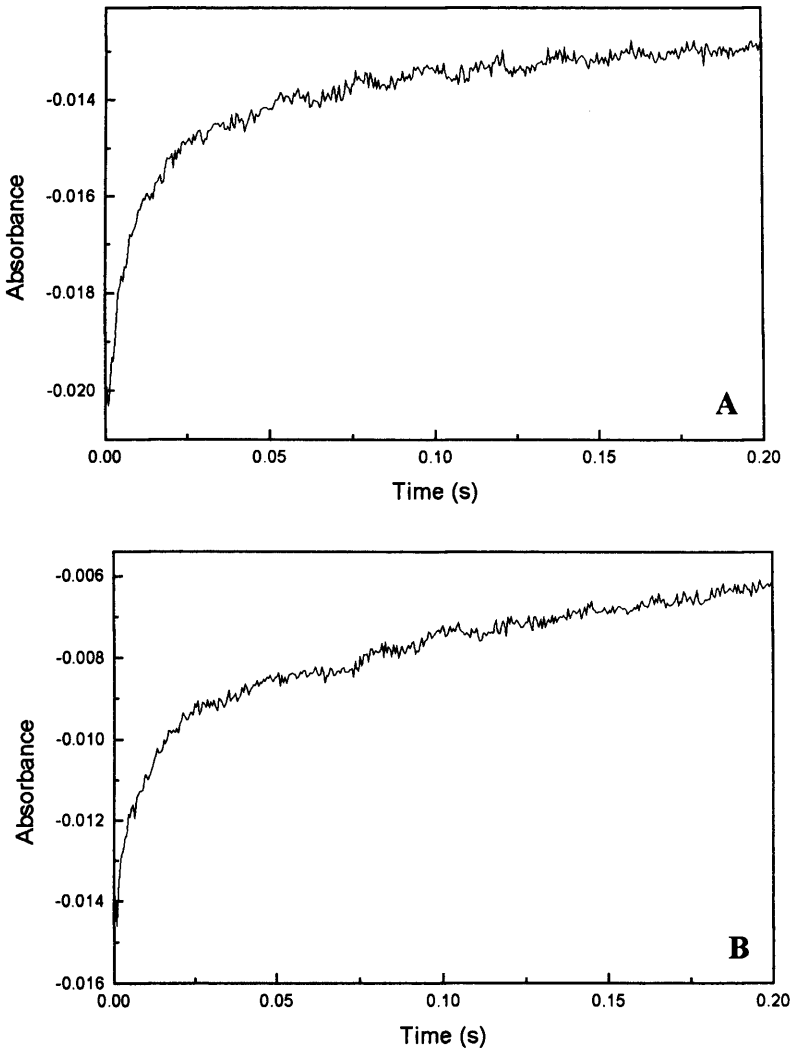

Figure 3.14

Panel A : Kinetic transient showing reduction of fully oxidised ETF by phenylhydrazine inactivated, dithionite reduced TMADH. The reaction was performed under anaerobic conditions in 50 mM phosphate buffer, pH 7.0, at a temperature of 25 °C. Data were fitted to Equation 2.2 to obtain rates for the electron transfer reaction.

Panel B : Kinetic transient showing reduction of fully oxidised ETF by phenylhydrazine inactivated, dithionite reduced TMADH in the presence of 40 % (w/v) glycerol. The reaction was performed under anaerobic conditions in 50 mM phosphate buffer, pH 7.0, at a temperature of 25 °C. Data were fitted to Equation 2.2 to obtain rates for the electron transfer reaction. Absorbance changes were measured at a wavelength of 438nm.

glycerol used in these studies may be insufficient to induce a noticeable decrease in the observed reaction rate. The degree of hydrodynamic friction in the medium may have to be increased further to cause a transition to a gated electron transfer scheme in this system. This is impractical using conventional stopped-flow technology, as mixing artifacts are associated with concentrations of glycerol in excess of 40 %.

3.3 Discussion

The protocol established for expression and purification of recombinant ETF yielded protein of sufficient purity for subsequent kinetic and spectroscopic analyses. However, the presence of small quantities of foreign protein means that the protocol is inadequate for production of protein for structural analyses, such as X-ray crystallography and small angle X-ray scattering (SAXS). Additional purification steps need to be included to obtain protein of sufficient purity for structural analyses, and these will be discussed in later chapters.

The primary goal of this exercise (*i.e.* to obtain high yields of pure ETF for subsequent kinetic and spectroscopic analyses) appears to have been achieved. Yields of pure ETF from the recombinant source are more than 100 fold greater than corresponding yields from *M. methylotrophus*. These high yields are vital for ensuring that sufficient quantities of pure protein are available for the experimental procedures to be employed, which often require concerted repetition and/or high concentrations of protein.

The results in the spectroscopic comparisons of native and recombinant ETF, together with the data obtained on the kinetic behavior of recombinant ETF in its reaction with TMADH, would strongly suggest that native and recombinant ETF are identical. This therefore validates the use of recombinant ETF in subsequent spectroscopic, kinetic and structural analyses, and extrapolation of the results to the properties of native ETF.

The fluorescence data, which indicate that samples of oxidised ETF increase in fluorescence at a greater rate than semiquinone ETF are interesting because they imply that the flavin in oxidised ETF dissociates from the enzyme at a greater rate than that of the semiquinone form of the enzyme. It has been noted previously that oxidised ETF loses its activity in a period of several hours when at room temperature (Steenkamp & Gallup, 1978), and these data could provide an explanation for this phenomenon and,

importantly, suggest that oxidised ETF has different physical, possibly conformational, properties to semiquinone ETF as regard the environment of its FAD cofactor.

The results of the initial kinetic analyses of oxidised ETF reacting with reduced TMADH are disappointing, as it was hoped that introduction of glycerol into the reaction mixture would limit the conformational flexibility of ETF and cause a transition from a true eT reaction to gated eT (according to kinetic complexity as described in Section 1.1.4.) causing a decrease in the observed rate constant for the reaction, and thus provide direct kinetic evidence for conformational gating in the TMADH/ETF interprotein electron transfer reaction. This did not seem to be the case. However, it has been determined in previous studies on a cytochrome electron transfer system (Qin & Kostic, 1994) that in order to cause significant changes in the observed rate constant of a gated interprotein electron transfer system it may be necessary to increase the concentration of glycerol in the medium to up to 80 %. At a glycerol concentration of 80 % (w/v), the relative viscosity of the medium is approximately 60, whereas at a glycerol concentration of 40 % the relative viscosity of the medium has a value of 3.8. Performing kinetic analyses of interprotein electron transfer at glycerol concentrations in excess of 40 % is impractical using conventional stopped flow methods, as there are mixing artifacts associated with such highly viscous solutions. However, kinetic analysis of reactions at high concentrations of glycerol may be possible using techniques such as laser flash photolysis. Laser flash photolysis studies of protein electron transfer complexes have previously been performed on cytochrome systems (Qin & Kostic, 1994; Orii, 1993) and flavoprotein systems (Hazzard *et al*, 1986; Hazzard *et al*, 1991; Hazzard *et al*, 1997)), and it is hoped that a suitable system for analysing the TMADH/ETF electron transfer reaction by laser flash photolysis may be devised in the future.

CHAPTER 4

ANALYSIS OF ELECTRON TRANSFERRING FLAVOPROTEIN USING SMALL ANGLE X-RAY SCATTERING

4.1 Introduction

In this chapter, the use of small angle X-ray scattering (SAXS) to investigate the solution structural characteristics of human, *P. denitrificans* and W_3A_1 ETF is described. SAXS has been used previously to determine the overall dimensions and volume of protein molecules, and also to provide information on the protein oligomerisation state, domain orientation and complex formation (Grossmann *et al.*,1993; Grossmann *et al.*, 1998; Chamberlain *et al.*, 1998; Gallagher *et al.*, 1999). SAXS has also been used to generate low resolution (~15 Å), model-independent molecular envelope structures for proteins in solution (Grossmann & Hasnain, 1997). As previous attempts at the crystallisation of W_3A_1 ETF have been unsuccessful (White *et al.*, 1994), it was thought that SAXS could be used to investigate the structural properties of this protein. This chapter describes the use of SAXS to determine the structural parameters of W_3A_1 ETF in solution, and to calculate a model-independent molecular envelope structure for the protein. This chapter also describes the use of SAXS to calculate structural parameters and molecular envelope structures for human and *P. denitrificans* ETF. Experimental scattering profiles from human, *P. denitrificans* and W_3A_1 ETF have been compared with simulated scattering profiles generated from molecular models.

4.1.1 The Utility of SAXS

X-ray solution scattering is a diffraction technique that can be used to gain information about the structural characteristics of a wide variety of biological molecules. The theoretical basis for this technique was developed in the 1950s (Guinier & Fournet, 1955). Since that time it has been used, for example, to study the crystallisation behaviour of cocoa butter in chocolate manufacture and the structural characteristics of detergent molecules (van Gelder *et al.*, 1995), as well as to study the structure of

biological macromolecules in solution (*e.g.* Glatter & Kratky, 1982; Perkins, 1988; Chamberlain *et al.*, 1997; Chamberlain *et al.*, 1998; Grossmann *et al.*, 1998; Gallagher *et al.*, 1999). SAXS has been used to investigate conformational changes induced in proteins in solution, for example those induced in transferrin when it binds ferric iron (Grossmann *et al.*, 1998) and those induced in the components of methane monooxygenase (MMO) on formation of the multicomponent enzyme complex (Gallagher *et al.*, 1999). SAXS has also been used to investigate the factors affecting the folding and unfolding of proteins in solution (Semisotnov *et al.*, 1996; Arai *et al.*, 1998; Kojima *et al.*, 2000). The chief advantage of using X-ray solution scattering is that it enables the characterisation of multiple parameters related to the gross structural features of biological macromolecules in an environment that approaches physiological conditions. Other advantages of the technique include its amenability to adjustments in sample conditions, such as temperature and pH (*e.g.* Kojima *et al.*, 2000), and its utility in the study of molecules with a wide range of molecular masses (*e.g.* Gallagher *et al.*, (1999), where the multicomponent MMO enzyme has a mass of over 300 kDa). Hydrodynamic techniques, by comparison, provide only one structural parameter derived from the sedimentation coefficient, which reports on the degree of structural elongation of the molecule. Electron microscopy requires that the sample is held in a vacuum and subjected to harsh preparatory techniques, both of which can give rise to artefacts. NMR spectroscopy requires complicated resonance assignment and is generally unsuitable for molecules larger than 30 kDa. Finally, X-ray crystallography provides no information on how biological macromolecules behave in solution, and the buffer conditions used in the crystallisation process are often very different from physiological conditions. The chief disadvantage of SAXS, in comparison to X-ray crystallography and NMR spectroscopy, is that the structural information yielded via this technique is of a very low resolution, typically around 15 Å. Other disadvantages of this technique are the high protein concentrations (typically 5 to 15 mg/ml) that are required for the sample scattering curve to be distinguishable from the background scattering of the solvent, and the fact that the data yielded from SAXS does not represent a static, unique structure.

4.1.2 The Theory of SAXS

In X-ray solution scattering, the incident X-ray beam is scattered by electrons from the solute molecules (and, to a lesser extent, by those from the solvent molecules), which are randomly oriented and dispersed in free solution. X-ray scattering profiles are expressed as a plot of intensity (I(s), measured in units relative to the mass and concentration of the measured particle) against the modulus of momentum transfer, s. The modulus of momentum transfer is a function of the scattering angle, and is defined as:

$$s = 2 \sin \Theta / \lambda ,$$

where 2Θ is the scattering angle and λ is the wavelength of the incident X-ray beam. It should be noted that s = 1/d, where d is the diffraction spacing specified by Bragg's Law of Diffraction, λ = 2 d sin Θ. At very small scattering angles, in the so-called Guinier region, the curvature of the scattering profile provides information on the overall dimensions of the molecule. The radius of gyration (R_g), which is defined as the root mean square of the distance of scattering centers (atoms) from the electronic centre of gravity, can be estimated using the Guinier approximation (Guinier, 1939). The Guinier approximation is accurate for sufficiently small scattering angles, and when ln $I(s)$ is plotted versus s^2, the radius of gyration (R_g) can be calculated from the slope m:

$$R_g^2 = -3m / 4\pi^2 ,$$

Another method to evaluate this structural parameter, and also to elucidate further structural information, involves determination of the distance distribution function, $p(r)$. This function represents the distribution of all intramolecular distances between scattering centres (atoms) in the solute molecule. Determination of the $p(r)$ function involves an indirect Fourier transform procedure (Svergun *et al.*, 1988):

$$R_g^2 = \frac{\int_0^D r^2 p(r)dr}{2\int_0^D p(r)dr},$$

which utilises the entire experimental scattering profile and hence provides a more accurate approximation of R_g than is possible via the Guinier method. The $p(r)$ function has a value of 0 for $r > D$, where D is the maximum dimension (D_{max}) of the molecule. Determination of values for R_g and D_{max} via this approach assumes that the solute molecules are dilute, monodisperse and non-interacting. The features of the $p(r)$ function can also provide information on the gross structural characteristics of the molecule.

Recently, the program GNOM has been developed to implement the indirect Fourier transform method and thus to calculate the $p(r)$ function from experimental scattering data (Semenyuk & Svergun, 1991). This program enables the determination of values for R_g and D_{max}. Also, the program also enables determination of the forward scattering intensity (I_o) by reverse transformation of the $p(r)$ function. The relative molecular mass of the molecule can be calculated from I_o/c (where c is the sample concentration) when referenced against the scattering profile of a sample of known molecular mass. The volume (V) of the solute molecule can be deduced form the scattering profile using the following relationship (Feigin & Svergun, 1987):

$$V = 2\pi^2 / Q_0,$$

where Q_o is the Porod invariant (Porod, 1951):

$$Q_0 = \int_0^\infty s^2 (I(s)/I_0)ds,$$

calculated from the normalized scattering intensity ($I(s)/I_o$). All volume calculations incorporated a correction factor to account for the limited experimental scattering range.

Determination of the molecular envelope structure utilises the multipole expansion method proposed by Stuhrmann (1970) and developed by Svergun *et al.* (1997). Assuming that the X-ray scattering is caused by a globular molecule of uniform density, its molecular envelope can be defined by a two-dimensional angular function $F(\theta, \varphi)$, which describes the envelope such that the particle density $\rho(r)$ is unity inside the molecular boundary and vanishes elsewhere. The function $F(\theta, \varphi)$ can be expanded into a series of spherical harmonics $Y_{lm}(\theta, \varphi)$ (Stuhrmann, 1970):

$$F(\theta,\varphi) = R_0 \sum_{l=0}^{L} \sum_{m=-l}^{l} f_{lm} Y_{lm}(\theta,\varphi),$$

where f_{lm} are the complex multipole coefficients and L represents the multipole order. R_0 is a scale factor [$\approx (3V / 4\pi)^{1/3}$], where V is the volume of the particle. The function $Y_{lm}(\theta, \varphi)$ is defined as follows:

$$Y_{lm}(\theta,\varphi) = \left[\frac{(2l+1)(l-m)!}{4\pi(l+m)!}\right]^{1/2} P_l^m(\cos\theta)\exp(im\varphi),$$

where $P_l^m(\cos\theta)$ are the associated Legendre functions (with argument $\cos\theta$) and l and m are integers with $-l \leq m \leq l$. A computational procedure to evaluate the multipole coefficients from the experimental scattering profile was developed by Svergun and Stuhrmann (1991).

The range of the experimental scattering data typically allows the determination of 15-20 variables in the shape description (Svergun *et al.*, 1996). This imposes an upper limit on the multipole order (L) of the expansion and hence on the resolution of the calculated molecular envelope, because the number of independent parameters derived from the spherical harmonics series is $(L + 1)^2 - 6$ (arbitrary rotations and translations of the molecule do not alter the scattering curve and hence lead to a reduction of six variables). Therefore, shape calculations for asymmetric molecules can be performed up to a multipole order of $L = 4$, which characterises the molecular envelope in terms of 19 free parameters. However, the presence of molecular symmetry allows certain multipole

coefficients to be omitted, which allows multipole expansions with $L = 6$ or $L = 7$ to be achieved. The higher the degree of symmetry, the more multipole coefficients may be omitted and hence the greater the resolution of the calculated molecular envelope.

The multipole expansion method has been used to generate model-independent molecular envelope structures for both symmetric (Grossman & Hasnain, 1997) and asymmetric (Grossmann *et al.*, 1998) proteins in solution, which have provided excellent agreement with the corresponding crystal structures.

4.2 Results

4.2.1 Scattering Data for W_3A_1 ETF

SAXS analysis was performed on both oxidised and semiquinone forms of W_3A_1 ETF. The protein was purified as described in Section 2.3.4, and oxidised ETF was obtained using the method described in Section 2.3.6. SAXS analyses were carried out at a range of protein concentrations between 0.3 and 15 mg/ml to investigate any concentration dependent changes in the scattering profile. The solution scattering curves and intra-particle distance distributions for the oxidized and semiquinone forms of W_3A_1 ETF are shown in Figure 4.1. The figure clearly demonstrates the very close similarity between the scattering profiles for oxidized and semiquinone forms of the protein. The concentration dependent low-angle scattering region ($s \leq 0.01$ Å^{-1}) and the calculated radii of gyration at different protein concentrations are emphasized in Figure 4.2. The intensity of the scattering profiles at low scattering angles was found to increase as a function of ETF concentration for both the oxidized and semiquinone forms of the protein, indicating that inter-particle interactions occur. Hence, low concentration (≤ 2 mg/ml) measurements were crucial. By analysis of scattering data collected in different time frames during the experiment it was found that the intensity scattering profile in the low-angle region increases as a function of time for both forms of ETF. Calculation of I_o from the initial frames of the scattering profile (*i.e.* those taken during the first five minutes of X-ray exposure) was used to determine initial values of I_o for both forms of ETF over a range of protein concentrations. Hence, careful I_o analysis established that both forms of W_3A_1 ETF behaves as a free heterodimeric protein (~60 kDa) in solution. The interactions between ETF molecules in the X-ray beam may have been caused by

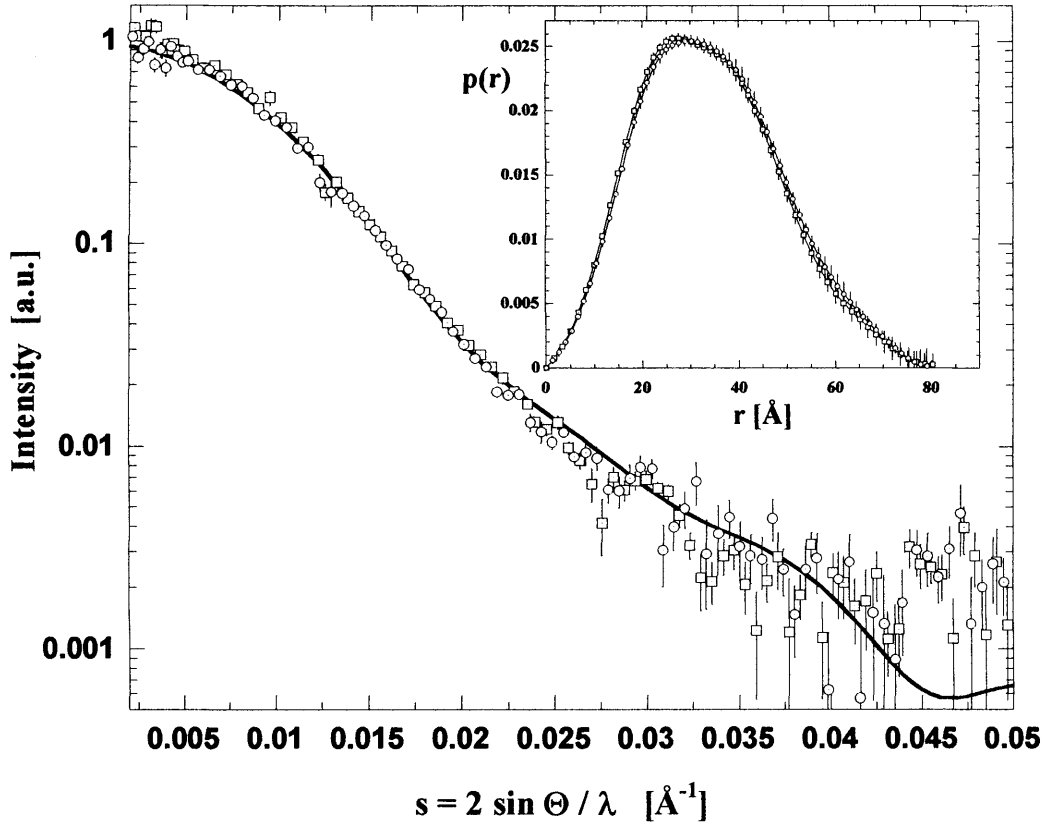

Figure 4.1
Experimental SAXS results for solutions of oxidized and semiquinone (reduced) *M. methylotrophus* ETF. This graph shows a representation of the scattering curves for oxidized (squares) and reduced (circles) ETF using the combined low and high concentration data for the low angle and outermost scattering region, respectively. Error bars are based on counting statistics (only every third experimental data point is shown for each scattering profile). Calculated distance distribution functions are shown for both ETF forms (see inset). I(s) and p(r) functions for both protein states have been normalized so that I(0) and the area under p(r) are scaled to unity. The fit (solid line) to the experimental SAXS curves represents the scattering from the restored molecular envelope.

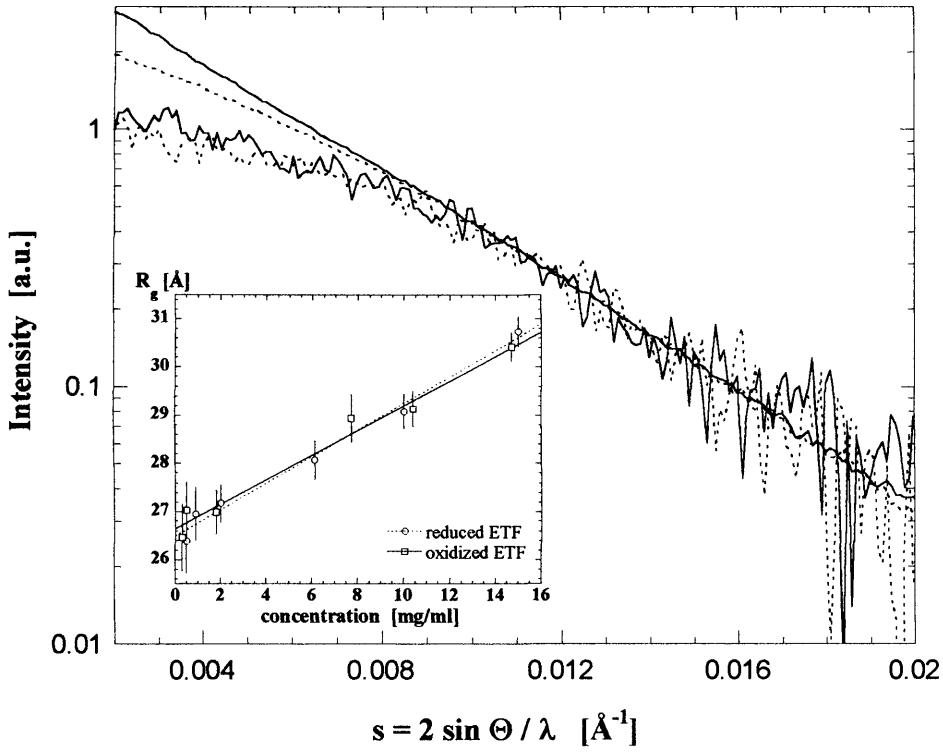

Figure 4.2
The effect of protein concentration on small angle scattering. The concentration effect at low angle is highlighted for scattering profiles shown for oxidized ETF at 14.7 mg/ml and 0.5 mg/ml (solid lines) and for reduced ETF at 10 mg/ml and 0.3 mg/ml (dotted lines). The concentration dependence of the radii of gyration and linear regression curves are shown as inset graph.

aggregation effects and/or radiation damage induced during X-ray exposure (after examination of data collected in different time frames). The R_g (radius of gyration) values were obtained by extrapolation to zero concentration for oxidized and semiquinone ETF, and were found to be virtually identical (26.6 ± 0.4 Å and 26.5 ± 0.4 Å, respectively). Furthermore, maximum dimension and volume of both forms of ETF revealed equivalent values within error limits (D_{max} = 80 Å ± 4%, V = 110 000 Å^3 ± 5%). This illustrated that no large conformational transformation had occurred as a result of changing the redox state of W_3A_1 ETF. Moreover, the features of the $p(r)$ function (with a characteristic shoulder at ~ 40 Å) indicate that W_3A_1 ETF in solution has a spread-out Y-shaped conformation with distinct domain features, as opposed to a compact, globular structure. The distance distribution function for globular structures typically resemble a skewed normal distribution, and do not posses distinctive features similar to those observed in the present study (Grossmann *et al.*, 1998).

4.2.2 Simulated Scattering Profiles from Molecular Models of W_3A_1 ETF

ETF has previously been modeled in two conformations (Chohan *et al*, 1998). The first (the so-called eT-inactive conformation, analogous to that of the crystal structure for human ETF) was obtained from modeling studies in which the structure of *M. methylotrophus* ETF was built by homology using the crystal coordinates of human ETF (Figure 4.3a). The second conformation (the eT-active conformation) is that obtained by rotating domain II by 50° with respect to domains I and III, such that it produces a complementary fit with the ETF-binding site seen in the crystal structure of TMADH (Figure 4.3b). Using the molecular coordinates for these models, simulated x-ray scattering profiles were generated for each solvated ETF conformer and fitted against the experimental scattering data for W_3A_1 ETF (Figure 4.4). It can be seen that the experimental scattering profile for W_3A_1 ETF does not match agreeably with the simulated profile generated from the structural model for the eT-inactive conformation. The experimental SAXS profiles for both forms of ETF lack the pronounced shoulder in the intermediate-wide angle range (0.02 Å^{-1}≤ s ≤ 0.04 Å^{-1}) that is associated with the static lobed structure of the eT-inactive model. Significant differences in the low angle (s ≤ 0.01 Å^{-1}) and intermediate angle (0.017 Å^{-1}≤ s ≤ 0.025 Å^{-1}) range result only in a fit

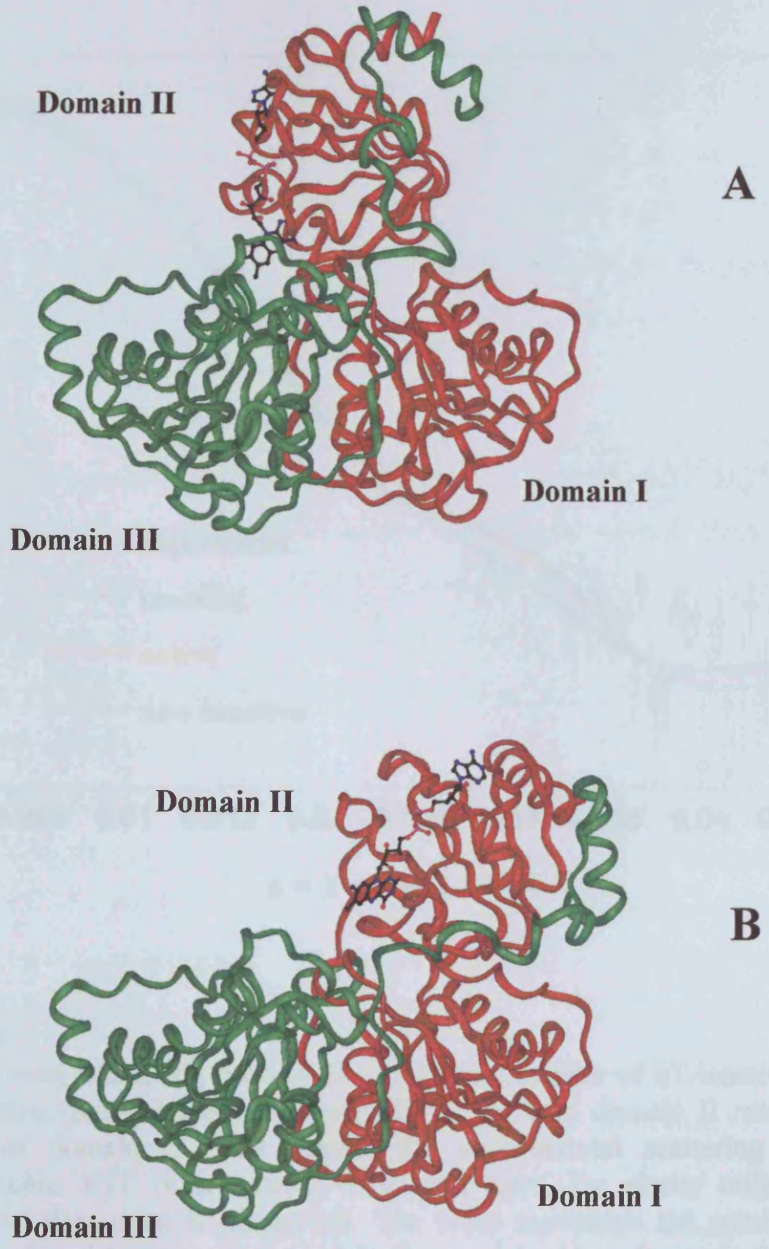

Figure 4.3
(a) Molecular model of "eT-inactive" *M. methylotrophus* ETF, showing the polypeptide backbone of the α (red) and β (green) subunits comprising domains I, II and III. Also shown is the FAD, which forms the redox center of *M. methylotrophus* ETF. (b) Molecular model of "eT-active" *M. methylotrophus* ETF, which corresponds to eT-inactive *M. methylotrophus* ETF with domain II rotated 50° relative to domains I and III.

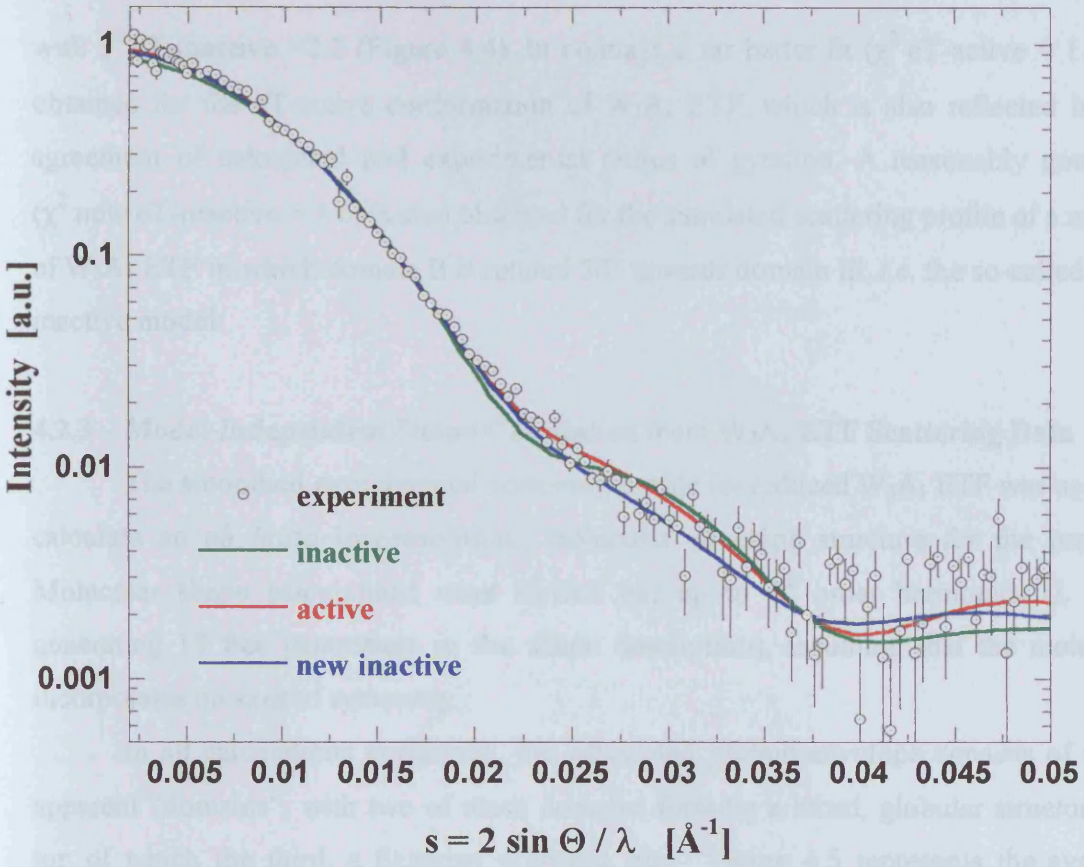

Figure 4.4
Simulated x-ray scattering profiles for molecular models of eT-inactive ETF (green) and eT-active (red) *M. methylotrophus* ETF, i.e. with domain II rotated 50° in the direction of domain I, fitted against the experimental scattering curve for *M. methylotrophus* ETF (black circle with error bars, for clarity only every second experimental data point is displayed). The latter represents the combined scattering curve of reduced ETF as illustrated in Figure 4.1. Also shown is the fit using the further molecular model of eT-inactive *M. methylotrophus* ETF where domain II is rotated 50° in the direction of domain III and thus burying the cofactor in the domain interface (blue). The radii of gyration for the active, inactive and new inactive model are 26.1 Å, 24.9 Å and 26.0 Å, respectively.

with χ^2 eT-inactive =2.2 (Figure 4.4). In contrast, a far better fit (χ^2 eT-active = 1.5) is obtained for the eT-active conformation of W_3A_1 ETF, which is also reflected in the agreement of calculated and experimental radius of gyration. A reasonably good fit (χ^2 new eT-inactive = 1.6) is also obtained for the simulated scattering profile of a model of W_3A_1 ETF in which domain II is rotated 50° towards domain III, *i.e.* the so-called new inactive model.

4.2.3 Model-Independent Shape Calculation from W_3A_1 ETF Scattering Data

The smoothed experimental scattering profile for reduced W_3A_1 ETF was used to calculate an *ab initio* low-resolution, molecular envelope structure for the protein. Molecular shape calculations were carried out up to 4th order harmonics (L = 4, generating 19 free parameters in the shape description), assuming that the molecule incorporates no axes of symmetry.

In all calculations performed, the calculated protein envelope consists of three apparent "domains", with two of these domains forming a lobed, globular structure on top of which the third, a flattened ellipsoid, sits. Figure 4.5 represents the average molecular envelope taking into account several calculations starting from different initial shapes. Manual fitting of the molecular models of W_3A_1 ETF into this molecular envelope structure resulted in an excellent fit between domains I and III of the model with the two globular "domains" forming the base of the molecular envelope. With domains I and III of the model fitted to the envelope structure in this orientation, domain II of the model sits at the centre of the third "domain" of the envelope structure, with the latter forming a flattened "halo" around domain II.

4.2.4 Scattering Data for Human and *P. denitrificans* ETF

The solution scattering curves and intra-particle distance distributions for the oxidized forms of human, *P. denitrificans* and W_3A_1 ETF are shown in Figure 4.6. Human and *P. denitrificans* ETF were the kind gift of Prof. Frank E Frerman from the Department of Pediatrics at the University of Colorado School of Medicine, Denver, Colorado, and W_3A_1 ETF was purified as described in Section 2.3.4. The scattering profiles illustrate the very close similarity between the scattering profiles of the three

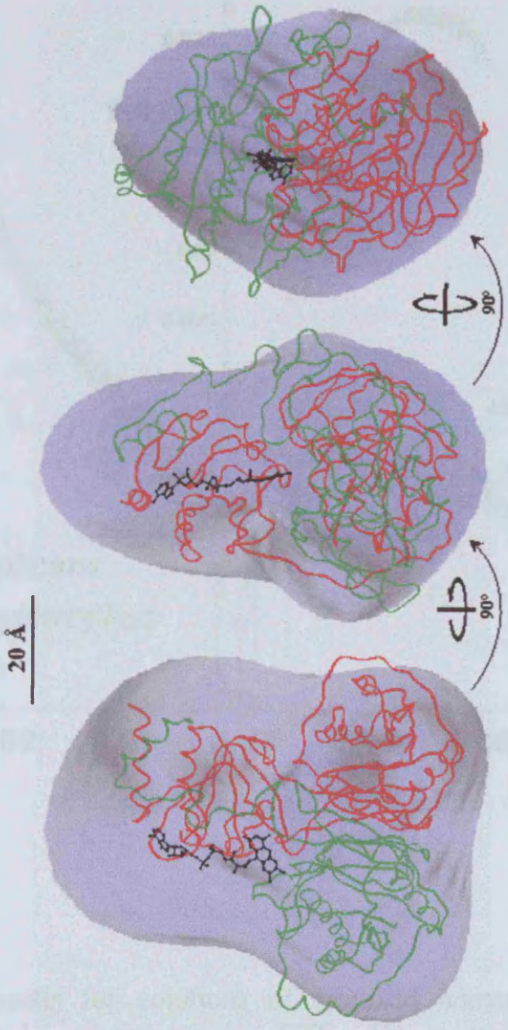

Figure 4.5

Three orientations of the calculated molecular envelope structure for *M. methylotrophus* ETF, superimposed over the molecular model of *M. methylotrophus* ETF (based on homology with the crystal structure of human ETF; the α and β subunits are red and green, respectively). This shows the excellent fit between the globular base of the envelope structure and domains I and III of the model, as well as the "halo" formed around domain II by the molecular envelope.

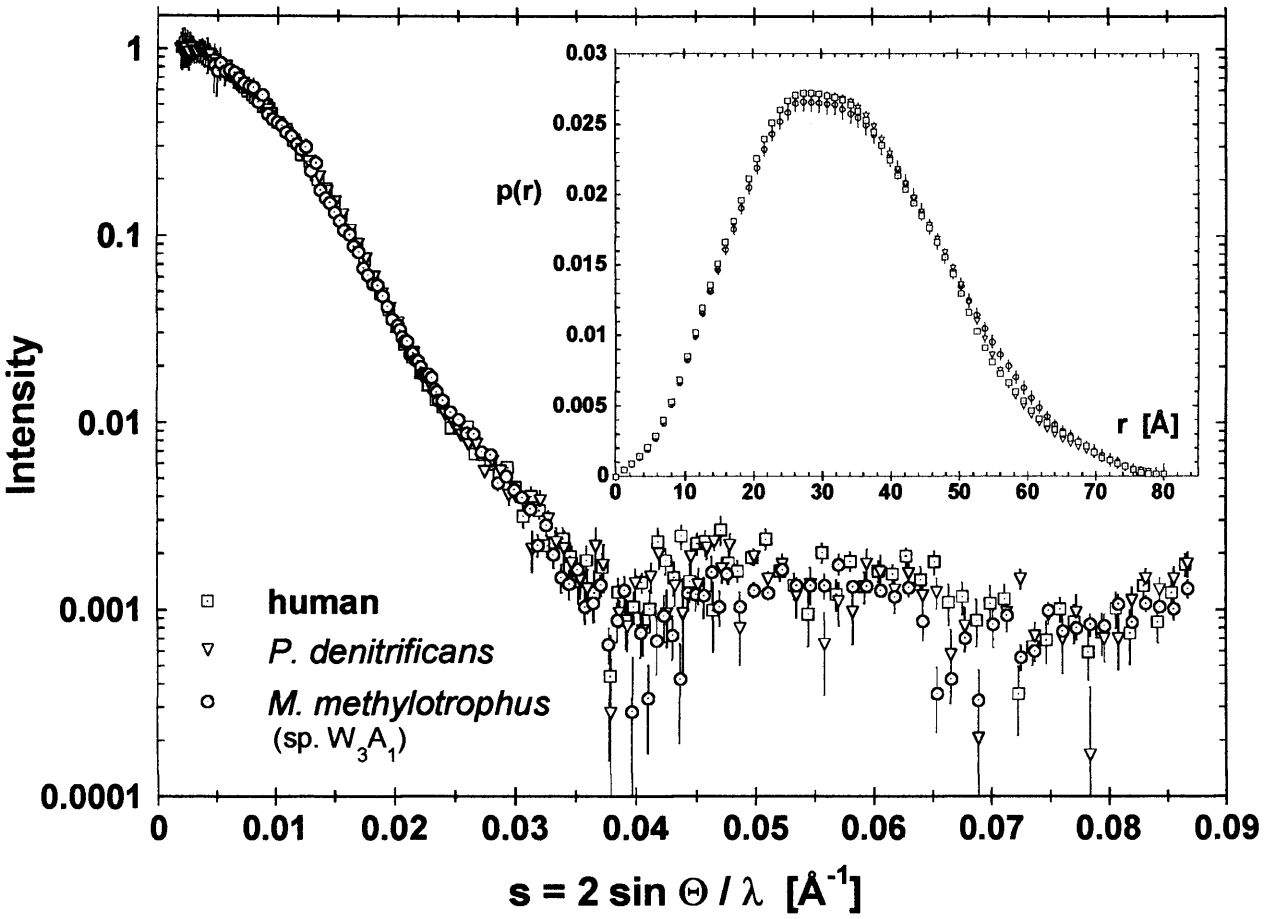

Figure 4.6
Experimental SAXS results for solutions of oxidized human and *P. denitrificans* ETFs, and semiquinone *M. methylotrophus* ETF. The scattering curves of all three ETFs are represented by a combination of low and high concentration data for the low angle and outermost scattering region, respectively. Error bars are based on counting statistics (for clarity only a third of the experimental data points are displayed). Calculated distance distribution functions are shown for all three ETFs (see inset). I(s) and p(r) functions for the three proteins have been normalized so that I(0) and the area under p(r) are scaled to unity. The fit (solid line) to the experimental SAXS curves represents the scattering from the restored shape of human ETF (Figure 4.8). Deviations between the fit representing the uniform molecular envelope and experiment for high scattering angles ($s > 0.045$ Å^{-1}) are attributable to internal structural inhomogeneities, the effects of which become more pronounced at higher scattering angles.

forms of ETF in the low ($s \leq 0.01$ Å^{-1}) and intermediate (0.017 Å$^{-1} \leq s \leq 0.025$ Å^{-1}) scattering angle ranges. The experimental SAXS profiles for all three forms of ETF lack the pronounced shoulder in the intermediate-wide angle range (0.02 Å$^{-1} \leq s \leq 0.04$ Å^{-1}) that is associated with the static lobed structure of the crystalline state (Figure 4.4). Unlike W_3A_1 ETF, the intensity of the scattering profiles at low scattering angles was not dependent on the concentration of human/*P. denitrificans* ETF used in each experiment, indicating that human and *P. denitrificans* ETF are not affected by the inter-particle interactions that occur in W_3A_1 ETF. I_o analysis established that both forms of ETF behaved as a heterodimeric protein (~60 kDa) in solution. The R_g (radius of gyration) values obtained for human and *P. denitrificans* ETF are 25.2 ± 0.4 Å and 24.8 ± 0.4 Å, respectively, slightly smaller than that obtained for W_3A_1 ETF (26.4 ± 0.4 Å from data collected in this study). Furthermore, the maximum dimension and volume of all three forms of ETF are identical within experimental error limits (D_{max} = 80 Å ± 4%, V = 110 000 Å^3 ± 5% for W_3A_1 ETF, 108 000 Å^3 ± 5% for human ETF and 110 000 Å^3 ± 5% for *P. denitrificans* ETF). As with W_3A_1 ETF, the $p(r)$ function for each protein possesses a characteristic shoulder at 36 - 40 Å, indicating rather a spread out, Y-shaped conformation (with distinct domain features) as opposed to a compact, globular structure. However, there are small differences between the $p(r)$ function of W_3A_1 ETF and those of human and *P. denitrificans* ETF, particularly in the distribution of higher intraparticle distances (between 50 and 70 Å).

4.2.5 Simulated Scattering Profiles from Molecular Models of Human and *P. denitrificans* ETF

The crystal structures for both human and *P. denitrificans* ETF have been determined previously (Roberts *et al.*, 1996; Roberts *et al.*, 1999). Simulated X-ray scattering profiles were generated for each solvated ETF conformer and fitted against the experimental scattering data for the corresponding form of ETF (Figure 4.7). It was hypothesized that human and *P. denitrificans* ETF may, in solution, posses a static conformation that differs substantially from that suggested by their respective crystal structures. Both human and *P. denitrificans* ETF posses two polypeptide loop regions (between domains I and II and domains II and III), analogous to those present in W_3A_1

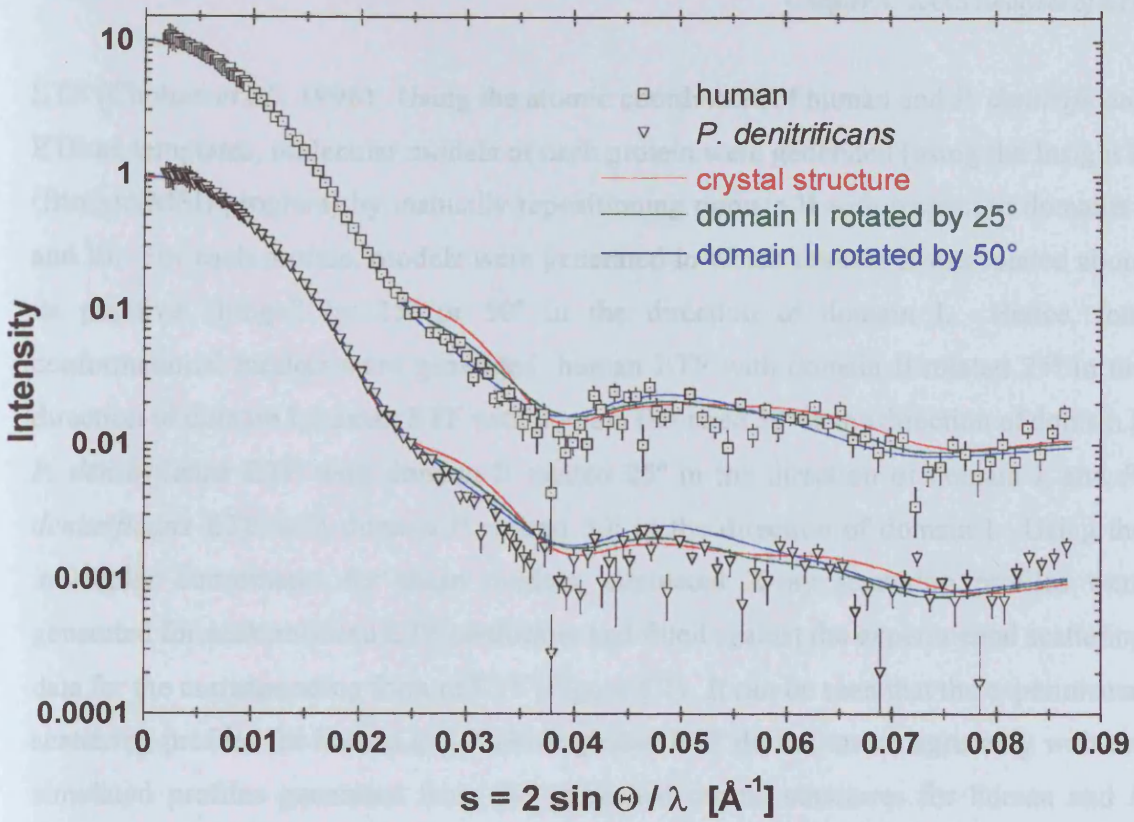

Figure 4.7
Simulated X-ray scattering profiles for molecular models of human and *P. denitrificans* ETFs with domain II rotated 0° (red), 25° (green) and 50° (blue) towards domain I relative to the respective crystal structure. These have been fitted against the experimental scattering curve for the corresponding ETF (the two experimental curves are those from Figure 1, for the sake of clarity the curves for human ETF have been shifted by one order of magnitude). The simulations for human (*P. denitrificans*) ETF resulted in R_g values of 25.1 Å (24.6 Å), 25.2 Å (24.8 Å) and 25.5 Å (25.1 Å) using the crystal structure, 25° and 50° domain rotation models, respectively.

ETF (Chohan *et al.*, 1998). Using the atomic coordinates of human and *P. denitrificans* ETF as templates, molecular models of each protein were generated (using the Insight II (Biosym/MSI) program) by manually repositioning domain II with respect to domains I and III. For each protein, models were generated in which domain II was rotated about its putative "hinge" by 25° or 50° in the direction of domain I. Hence, four conformational models were generated: human ETF with domain II rotated 25° in the direction of domain I, human ETF with domain II rotated 50° in the direction of domain I, *P. denitrificans* ETF with domain II rotated 25° in the direction of domain I, and *P. denitrificans* ETF with domain II rotated 50° in the direction of domain I. Using the molecular coordinates for these models, simulated X-ray scattering profiles were generated for each solvated ETF conformer and fitted against the experimental scattering data for the corresponding form of ETF (Figure 4.7). It can be seen that the experimental scattering profiles for human and *P denitrificans* ETF do not match agreeably with the simulated profiles generated from the published crystal structures for human and *P denitrificans* ETF. Significant differences between the experimental scattering profile and the simulation in the low angle ($s \leq 0.01$ Å^{-1}) and intermediate angle (0.017 Å$^{-1} \leq s \leq 0.025$ Å^{-1}) ranges result in fits with only χ^2 human =2.37 and χ^2 *P. denitrificans* =2.17. Furthermore, experimental scattering profiles for human and *P denitrificans* ETF do not match agreeably with the simulated profiles generated from the molecular models of the respective proteins. Although the fits to the experimental data are improved when compared to simulations from the crystallographic structure (χ^2 human_25° =2.16, χ^2 human_50° =2.19, χ^2 *P. denitrificans*_25° =1.92 and χ^2 *P. denitrificans*_50° =1.98) they nonetheless do not adequately describe the scattering of either protein in solution.

4.2.6 Model-Independent Shape Calculation from Human ETF Scattering Data

The smoothed experimental scattering profile for human ETF was used to calculate an *ab initio* low-resolution, molecular envelope structure for the protein. Molecular shape calculations were carried out up to 4th order harmonics (L = 4, generating 19 free parameters in the shape description), assuming that the molecule incorporates no axes of symmetry.

The calculated protein envelope consists of three apparent "domains", with two of these domains forming a lobed, globular structure on top of which the third, a flattened, lobed ellipsoid, sits. Figure 4.8 represents the average molecular envelope taking into account several calculations starting from different initial shapes. Manual fitting of the crystal structure of human ETF into this molecular envelope structure resulted in an excellent fit between domains I and III of the structure and the two globular "domains" forming the base of the molecular envelope. With domains I and III of the model fitted to the envelope structure in this orientation, domain II of the model lies within of the third "domain" of the envelope structure. This region, in contrast to the envelope structure of W_3A_1 ETF, does not form a symmetrical "halo" around domain II of the protein but instead is biased towards one side of the molecule.

4.2.7 Molecular Modeling of the Human ETF-MCAD Complex

This work was carried out by Dr Michael Sutcliffe and Kamaldeep Chohan at the Department of Chemistry, Leicester University. It has been suggested previously that rotation in W_3A_1 ETF of domain II by ~ 50° (with respect to its position relative to domains I and III in the crystal structure of human ETF) was required for electron transfer from its redox partner TMADH (Chohan *et al.*, 1998). The SAXS data presented above suggest that such large conformational changes could also occur in human ETF upon complex formation with MCAD. To test this hypothesis, it was assumed that the conformation of MCAD remains essentially unchanged during complex formation. This enabled the modeling of the MCAD-human ETF complex (Figure 4.9) and calculation of the intrinsic electron transfer rates (Table 4.1). The method used for calculating electron transfer rates (Page *et al.*, 1999) considers the density of the protein packing between redox centers without regard to specific "pathways".

These calculations suggest that domain II has to be rotated by ~ 50° towards domain I to maximize electronic coupling between the two redox centers. For a robust electron transfer system, the distance between the redox centers should be less than ~ 14 Å (Page *et al.*, 1999). Therefore, a robust and productive electron transfer complex will likely be formed when domain II of human ETF is rotated by between ~ 30° and ~ 60° (Table 4.1) towards domain I. However, a rotation of ~ 60 ° can be ruled out because this

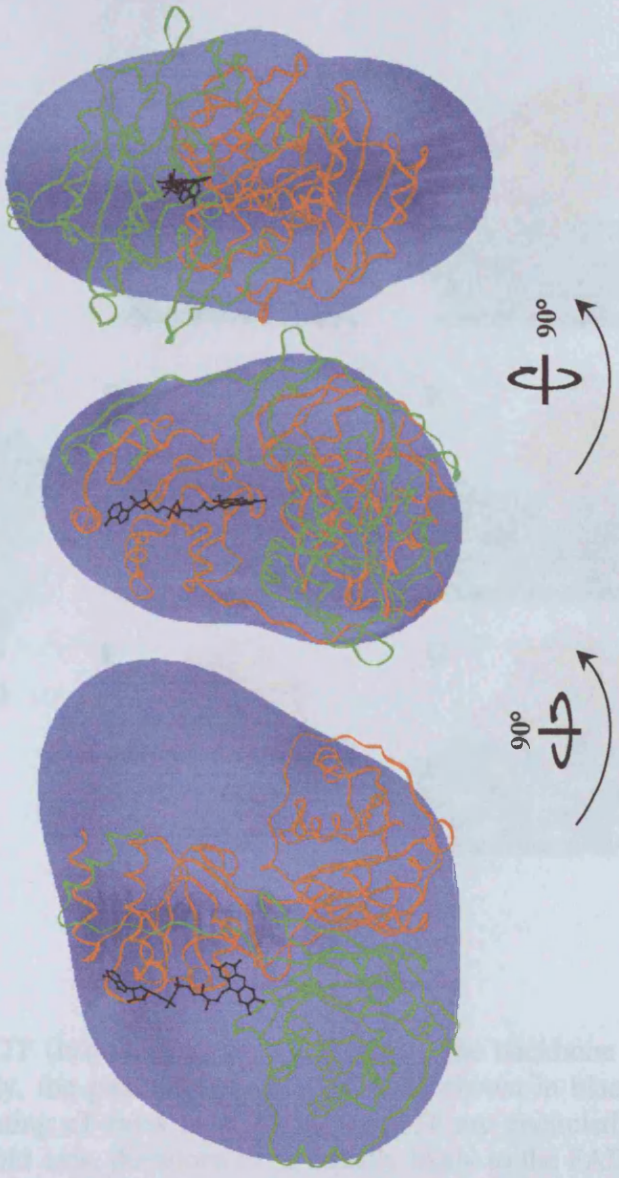

Figure 4.8
Three orientations of the calculated molecular envelope structure for human ETF, superimposed over its crystal structure. Since the scattering results for human and *P. denitrificans* ETF are virtually identical, the restored shape of human ETF also represents a good approximation to the molecular envelope of *P. denitrificans* ETF. The shape displays the excellent fit between the globular base of the envelope structure and domains I and III, and highlights the conformational flexibility of domain II. Since this envelope represents an average conformation, it appears that domain II occupies the space towards one side of the molecule (shown here towards domain I) more frequently than the other, which agrees with the results of the scattering pattern simulations (Figure 4.7).

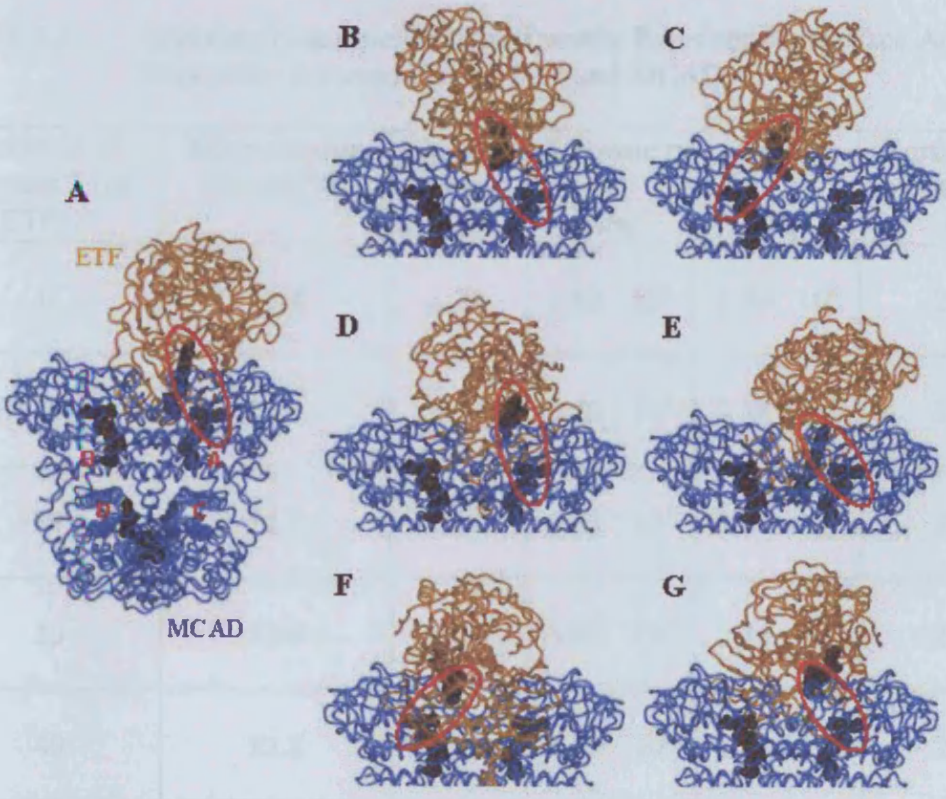

Figure 4.9
Dockings of human ETF (brown) onto MCAD (blue). The backbone of each protein is shown schematically, the positions of the FADs are shown in black CPK and the flavins used in calculating eT rates from MCAD to ETF are encircled in red (MCAD contains a pseudo 2-fold axis, therefore eT is equally likely to the FAD in either chain A or chain B; in all cases, the second flavin in MCAD, related by the pseudo 2-fold axis, is much further away than the flavin to which eT is indicated). Each panel illustrates the docking onto MCAD (the orientation of MCAD is identical in all panels) of: (A) ETF with domain II rotated 0° towards domain I with respect to the crystal structure of human ETF, with the flavins in the four subunits of the MCAD tetramer labelled, (B) ETF with domain II rotated 10° towards domain I, (C) ETF with domain II rotated 20° towards domain I, (D) ETF with domain II rotated 30° towards domain I, (E) ETF with domain II rotated 40° towards domain I, (F) ETF with domain II rotated 50° towards domain I, and (G) ETF with domain II rotated 60° towards domain I. In each model, ETF has been positioned such that the surface area of interaction between the two proteins is maximised and the distance between their redox centres is minimised.

Table 4.1 Calculated Intrinsic Electron Transfer Rates and the Surface Area of Interaction Between Human ETF and MCAD

Rotation of domain 2 (of ETF) /°	Edge-to-edge distance[a] /Å	Packing density[b], ρ	Intrinsic rate constant, k_{eT} /s^{-1} ox/sq	sq/hq	Surface area of interaction /Å^2
0	18.4	0.72	2.83×10^2	1.79×10^2	2653
10	19.8	0.71	3.62×10^1	2.28×10^1	2534
20	18.7	0.66	3.93×10^1	2.48×10^1	2466
30	13.4	0.72	3.46×10^5	2.18×10^5	2830
40	12.2	0.71	1.75×10^6	1.11×10^6	2690
50	11.6	0.74	7.13×10^6	4.50×10^6	2653
60	12.4	0.81	7.66×10^6	4.83×10^6	2306

[a] The edge-to-edge distance is the "shortest" distance between the FAD in MCAD and the FAD in human ETF (Calculated by ET_RATES; Page *et al.*, 1999).

[b] The packing density, ρ, is the fraction of the volume between redox centers that is within the united atom van der Waals radius of intervening atoms. When the protein medium is fully packed, ρ = 1. In principle, the packing density can vary from 0 to 1 (Calculated by ET_RATES; Page *et al.*, 1999).

results in severe steric overlap between domains I and II, suggesting that rotations of between ~ 30° and ~ 50° are required for a productive eT complex. Implicit in the above discussion is the concept of a two step "collision plus electron transfer" process. However, it is likely that electron transfer occurs not from a single bound conformation of ETF, but from an "ensemble" of thermodynamically metastable complexes (*i.e.* this comprises both a range of conformations of ETF *and* a range of orientations of each conformation in the eT complex). Within the ensemble of MCAD-ETF structures, a range of intrinsic electron transfer rates (*e.g.* Table 4.1) will be present, most of which will likely be much faster than the observed rates of electron transfer in stopped-flow experiments. By utilizing an ensemble of structures where the intrinsic electron transfer rate far exceeds the observed rate, the system is not reliant on adopting a unique geometry for the productive electron transfer complex, and all the conformational sampling and thermodynamic restrictions that this imposes. Most experimentally observed and physiological interprotein electron transfer rates are in the range 10^2 to 10^3 s^{-1}, *i.e.* much slower than the values calculated when domain II is rotated by between ~ 30° and 50° with respect to domains I and III (Table 4.1). In this regime where the intrinsic rate of electron transfer is much greater than the observed rate, given the efficient coupling between redox centers, the observed electron transfer rate can be maintained from a number of different electron transfer complex geometries. This is yet another example of a 'robust engineering principle', and builds on the idea that naturally occurring mutations can be accommodated in a redox protein without affecting significantly the electron transfer rate (Page *et al.*, 1999).

4.3 Discussion

It was initially considered, on the basis of the fluorescence spectroscopy data described in Section 3.2.7, that the oxidation state of W_3A_1 ETF may play a role in the predisposition of the protein to favour either the eT-active or the eT-inactive conformation. As oxidised ETF appears to dissociate from its flavin cofactor more rapidly than semiquinone ETF it was argued that the oxidation state of the protein could act as a "switch" between different conformational states. However, the scattering data indicate that this is not the case, as the SAXS profiles for both oxidised and semiquinone

ETF are practically indistinguishable, indicating that both forms have an essentially identical molecular conformation in solution.

The experimental SAXS profiles for W_3A_1 ETF closely resembled the simulated profile for the eT-active conformation, as opposed to the eT-inactive conformation. This initially led to the belief that the conformation of W_3A_1 ETF in solution resembles that of the postulated eT-active form. With regard to protein function, however, it would be surprising if the protein existed predominantly in its active conformation in free solution, as this would render the isoalloxazine ring susceptible to oxidative attack by molecular oxygen. Significantly, because of the pseudo-symmetry of the W_3A_1 ETF molecule about the interface between domains I and III, the simulated scattering profile for the "new inactive" model (where domain II is rotated 50° in the direction of domain III) is very similar to that for the eT-active model. Consequently, in terms of the low resolution molecular shape it is difficult to distinguish between a conformation of W_3A_1 ETF which resembles the model for eT-active ETF and one which resembles the "new inactive" model. Indeed, the simulated scattering profile for the "new inactive" model of ETF is as good a fit to the experimental data (χ^2 new-inactive = 1.6) as the simulated profile for the eT-active model (χ^2 eT-active = 1.5). However, it is difficult to imagine that the oxidation state of the protein acts as a conformational "switch" between the eT-active conformation and the "new inactive" conformation, even though the scattering profiles alone cannot exclude this possibility. It is more likely that the W_3A_1 ETF molecule is continuously sampling both conformations in solution, and in so doing also populates a range of other conformations between these two extremes. Such flexibility could account for the difficulties faced when attempting to crystallize W_3A_1 ETF. Hence, the fact that oxidised and semiquinone ETF share an identical scattering profile would suggest that this conformational flexibility is independent of the oxidation state of the protein.

The continuous sampling of a range of conformations between the extremes discussed above is consistent with the structure of the W_3A_1 ETF envelope, as calculated from the experimental scattering data. If there was a significant energy barrier between the two extreme conformations (leading to a "flipping" between the eT-active conformation and the "new inactive" conformation, and vice versa) one would expect to observe a more lobed, triangular envelope structure. However, the calculated molecular

envelope forms a flattened "halo" around the locus of domain II. Examining the dimensions of domain II of the W_3A_1 ETF model it is apparent that domain II cannot occupy all areas of its corresponding "halo" simultaneously. As is the case with all scattering measurements, the deduced molecular envelope structure represents an average over time. Combining these factors, it seems reasonable to deduce that W_3A_1 ETF is sampling a range of conformations in solution, corresponding to a rotation of domain II about the axis formed by the two polypeptide hinge regions connecting it with domains I and III. Also, because the "halo" surrounding domain II is flattened in the direction of the rotation, one can conclude that rotation of domain II with respect to domains I and III occurs mainly in one dimension, with very little "side to side" movement.

The experimental SAXS data can hence be used to refine the original model for domain motion in W_3A_1 ETF (Chohan *et al.*, 1998). Rather than activation of the ETF-TMADH electron transfer complex being associated with a simple 50° rotation of domain II of ETF (*i.e.* a discrete transition from an eT-inactive to an eT-active conformation) as originally proposed, complex formation stabilises the eT-active conformation of ETF. During complex formation, the highly dynamic nature of W_3A_1 ETF is transiently "frozen" when forming the eT-active conformation. This suppression of ETF dynamics is achieved via an induced fit mechanism for the interaction of ETF with TMADH.

The fact that the experimental scattering profiles for human and *P. denitrificans* ETF are almost identical to the experimental scattering profile for W_3A_1 ETF in the intermediate angle range suggests that all three forms of ETF possess very similar molecular dimensions, and that all three proteins possess a similar domain arrangement in solution. A corollary of this is that human and *P. denitrificans* ETF are likely to sample a range of conformations in solution corresponding to a rotation of domain II relative to domains I and III, as discussed above in the case of W_3A_1 ETF. The slightly larger apparent size of W_3A_1 ETF (V = 110 000 Å^3 ± 5% for W_3A_1 ETF, 108 000 Å^3 ± 5% for human ETF and 110 000 Å^3 ± 5% for *P. denitrificans* ETF) may be due to the intrinsic structural characteristics of the protein, or alternatively it arise from a greater degree of flexibility in W_3A_1 ETF. As discussed in Chohan *et al.* (1998) and in Section 1.4.4, increased flexibility in W_3A_1 ETF may be contributed to by the two putative "hinge" regions within the W_3A_1 ETF molecule: i) the intrinsically flexible domain I-domain II

linker (amino acid sequence $^{\alpha 193}$GGG$^{\alpha 195}$, *c.f.* $^{\alpha 205}$TKS$^{\alpha 207}$ and $^{\alpha 183}$AES$^{\alpha 185}$ in human and *P. denitrificans* ETFs, respectively), and ii) the much longer loop section in the C-terminal part of the β-subunit (residues β228-β245, *c.f.* β229-β236 and β226-β233 in human and *P. denitrificans* ETFs, respectively). Additionally, differences in domain-domain interactions between the three forms of ETF may be present due to the 31 % and 33 % sequence identities between W_3A_1 and human and *P. denitrificans* ETFs, respectively. The small differences between the $p(r)$ function of W_3A_1 ETF and those of human and *P. denitrificans* ETF at higher intraparticle distances (between 50 and 70 Å) reflect the increased flexibility of W_3A_1 ETF relative to human and *P. denitrificans* ETF.

The observation that the experimental scattering profiles for human and *P denitrificans* ETF do not correspond well to the simulated profiles generated from the published crystal structures for human and *P denitrificans* ETF demonstrates that in both cases the crystallographic structures do not adequately describe the molecular structures of these proteins in solution. A close inspection of the molecular arrangements in the crystalline lattice of both ETF structures reveals that, in both cases, there are several close contacts of domain II with domains from neighboring molecules. Low-energy, non-covalent interactions can effectively influence protein conformation, particularly in the case of multidomain proteins. Consequently, the crystal packing forces arising from non-covalent interactions are likely to alter or stabilise specific domain orientations. Furthermore, the fact that none of the simulated scattering profiles for the static molecular models of human and *P. denitrificans* ETF can be unambiguously fitted to the experimental scattering data for these proteins suggests that neither the structure for human ETF nor the structure for *P. denitrificans* ETF can be represented by a static conformational model. Structural flexibility would certainly be advantageous in terms of the physiological function of human ETF, as the protein has to recognise a wide range of different redox partners.

The calculated molecular envelope structure for human ETF confirms that the protein samples a range of different conformations in solution. The calculated envelope structure exhibits an excellent fit with domains I and III of the corresponding crystal structure, and modeled in this orientation domain II of the molecule lies in a large "domain" of the envelope structure. As was the case for W_3A_1 ETF, domain II of human

ETF cannot occupy all areas of its corresponding molecular envelope "domain" simultaneously. However, the fact that the region of the human ETF molecular envelope that corresponds to domain II of ETF is predominantly located toward one side of the structure indicates that domain II of human ETF occupies one side of the molecule more frequently than the other. Because human ETF possesses a pseudo two-fold axis of symmetry about the interface of domains I and III, a conformation of ETF in which domain II is rotated in the direction of domain I would possess an essentially identical scattering profile to a conformation of ETF in which domain II is rotated to an equivalent degree in the direction of domain III. Consequently, one cannot determine from the calculated envelope structure whether, in free solution, domain II of human ETF predominantly occupies the region adjacent to domain I or that adjacent to domain III.

However, the data obtained by molecular modeling of the structure of human ETF in complex with one of its physiological redox partners, MCAD, strongly suggest that rotation of domain II in the direction of domain I would enhance the degree of electronic coupling between the two proteins. The modeling studies suggest that rotation of domain II of human ETF by 30° - 50° in the direction of domain I would increase intrinsic electron transfer rates between the two proteins by more than three orders of magnitude. Hence it seems more probable that domain II of human ETF is biased toward occupation of the region adjacent to domain I in free solution. The molecular modeling studies suggest that a significant change in the conformation of ETF creates a regime in which the intrinsic electron transfer rate is elevated well above typical values observed in physiological electron transfer complexes (10^2 to 10^3 s^{-1}). This regime introduces a 'robust engineering principle', relaxing the specificity required between MCAD and ETF without compromising the observed electron transfer rates.

The present study is an excellent illustration of how static molecular models and crystal structures may be compared with structures investigated under close physiological conditions (*i.e.* in solution) using the small-angle x-ray scattering technique. Furthermore, this study demonstrates how SAXS analyses may be used to elucidate the dynamic properties of proteins in solution.

CHAPTER 5

SPECTROSCOPIC ANALYSIS OF THE DYNAMIC INTERACTION BETWEEN ETF AND TMADH

5.1 Introduction

This chapter describes the use of fluorescence and absorption spectroscopies to study the assembly of the TMADH-ETF complex. Previous studies using difference spectroscopy have established that small spectral changes in the flavin absorption region (~ 350 – 550 nm) are associated with the interaction of oxidised wild-type ETF with wild-type TMADH (Jang *et al.*, 2000). This chapter describes the extension of those studies to investigate the interactions of ETF in both redox states (oxidised and anionic semiquinone) with wild-type and mutant TMADH. This chapter also describes the use of steady-state and lifetime fluorescence spectroscopy to investigate changes in the fluorescence properties of ETF associated with its interaction with TMADH. Fluorescence spectroscopy is commonly used to provide information on the size, shape, flexibility and molecular environment of fluorescent moieties within proteins (Dewey, 1991; Lakowicz, 1998). Furthermore, this chapter describes the use of stopped-flow spectroscopy to characterise the reaction of semiquinone ETF with inorganic electron acceptors. These experiments were performed using semiquinone ETF both prior to and after incubation with TMADH. The results of the fluorescence and stopped-flow spectroscopic analyses indicate that ETF undergoes a stable conformational change as a result of its transient interaction with TMADH. This conformational change is termed molecular imprinting, or structural imprinting.

5.1.1 The Definition of Molecular Imprinting

5.1.1.1 Molecularly Imprinted Polymers (MIPs)

The terms "molecular memory" and "molecular imprinting" are used to describe several phenomena in biochemistry. One of the most topical applications of molecular imprinting is in the development of synthetic compounds with specific molecular recognition properties. One such technique is the synthesis of molecularly imprinted

polymers, or MIPs (Ansell *et al.*, 1996). The concept of MIPs has been in existence since the 1940s (Pauling, 1942). In practical terms, there are two approaches to the synthesis of MIPs: the self-assembly approach (Lindsey, 1991) and the pre-organised approach (Mosbach & Ramström, 1996), which differ in terms of the pre-polymerisation interaction of the monomer precursors with the template molecule. The self-assembly molecular imprinting approach involves the formation of precursor-target complexes stabilised by weak intermolecular interactions, such as hydrogen bonding, hydrophobic interactions and ionic interactions. These complexes are established spontaneously in the liquid phase and then sterically fixed by polymerisation with a high degree of cross-linking. Elimination of the target molecules results in a macroporous matrix containing multiple recognition sites for the molecule of interest. The pre-organised molecular imprinting approach involves formation of reversible covalent compounds (*e.g.* imines, ketals and boronate esters) of the monomer precursors with the target molecules. The target molecules must be derivatized with the monomer precursors prior to the polymerisation reaction. After polymerisation of the monomer precursors, cleavage of the covalent bonds that attach the target molecules to the polymer once again results in a macroporous matrix containing multiple recognition sites for the molecule of interest.

Thus far, MIPs have been prepared using a wide variety of molecular templates, such as proteins, nucleotides, amino acids, vitamins and pharmaceuticals (Mosbach, 1994; Mosbach & Ramström, 1996). For example, polymeric hydrogels have been prepared from enzymically-generated sugar acrylates for the chiral separation of Z-Asp (Liu and Dordick, 1999). These MIPs were able to achieve a separation factor of almost 2.5. Also, MIPs prepared against morphine using methacrylic acid-ethylene glycol copolymers have been used to mimic the binding sites of opioid receptors (Anderson *et al.*, 1995). These MIPs expressed a high binding affinity for morphine ($K_d = 10^{-7}$ M), and their specificity was similar to that of monoclonal antibodies. The chief advantage of using MIPs is that they can be developed for species against which it is difficult to raise monoclonal antibodies. Other advantages include their long-term chemical stability and their resistance to harsh chemical environments (Kriz & Mosbach, 1995).

5.1.1.2 Imprinting Enzymes for Use in Organic Media

Another topical use of the term "molecular imprinting" derives from the preparation of enzymes for use in organic media. The availability of enzyme catalysis in organic solvents can be invaluable to synthetic organic chemists (Khmelnitsky & Rich, 1999). However, most enzymes have a very low activity in organic solvents compared to their activity in aqueous media (Dordick, 1992). This may be due in part to the fact that enzymes suspended in organic media are more rigid than when they are suspended in aqueous media (Affleck *et al.*, 1992; Klibanov, 1995). This phenomenon is probably due to increases in electrostatic interactions and hydrogen bonding between surface residues (Hartsough & Merz, 1992). Fortunately, because of this increased rigidity it is possible to modify the activity of enzymes in organic media in a stable manner by pre-incubation with substrate or substrate analogues (Russell & Klibanov, 1988; Stahl *et al.*, 1990; Stahl *et al.*, 1991; Rich & Dordick, 1997). Addition of an appropriate ligand to the enzyme prior to lyophilisation is thought to stabilise a conformation of the enzyme that is favourable for catalysis. This process has been termed molecular imprinting.

It was found that the activity of subtilisin for the transesterification of *N*-acetyl-L-amino acid with n-propanol in octane could be enhanced up to 100 fold by lyophilising the enzyme in the presence of a competitive inhibitor, *N*-Ac-L-Tyr-NH_2 (Russell & Klibanov, 1988). The activity of the enzyme in the organic solvent increased in proportion to the concentration of inhibitor present in the pre-lyophilisation aqueous solution. The stereo-specificity of enzymes can be enhanced or reversed via the process of molecular imprinting. For example, α-chymotrypsin incubated with *N*-Ac-D-Trp and precipitated from aqueous buffer by cooling in 1-propanol has been used to catalyse the synthesis of D-amino acid esters (Stahl *et al.*, 1990). Furthermore, molecular imprinting can alter the substrate specificity of enzymes in organic media. For example, the specificity of α-chymotrypsin was altered in favour of Phe or Tyr by incubation with the appropriate *N*-acetylated substrates in the aqueous buffer (Stahl *et al.*, 1991). More recently, it has been shown that the activity and substrate specificity of subtilisin in catalysing the acylation of nucleosides in organic media can be controlled by lyophilizing the enzyme from an aqueous solution containing the appropriate substrate (Rich & Dordick, 1997). Kinetic data revealed that the increased activity of the imprinted enzyme

in organic media is largely the result of changes in the catalytic components of enzyme activity as opposed to binding components; large increases in k_{cat} were accompanied by only modest changes in K_m. Molecular modeling studies and molecular dynamics simulations revealed that the residues which form the catalytic "triad" of subtilisin undergo a structural change during imprinting (Rich & Dordick, 1997). However, the precise mechanism of this form of molecular imprinting is still not fully understood. Studies using FTIR spectroscopy have revealed that changes in the secondary structure of enzymes can occur during imprinting (Griebenow & Klibanov, 1995). Other studies have revealed that non-specific lyoprotectants can also enhance enzyme activity in organic solvents (Dabulis & Klibanov, 1993). The increases in enzyme activity caused by non-specific lyoprotectants and those caused by substrate analogues are not additive, indicating that both processes may operate via the same mechanism. It has been postulated that this form of molecular imprinting may operate by limiting reversible denaturation during lyophilisation.

5.1.1.3 Imprinting of Enzymes in Multi-Enzyme Complexes

Finally, one of the more recent applications of the term "imprinting" in biochemistry concerns the observation that certain enzymes can retain transient catalytic properties on dissociation from their corresponding multi-enzyme complexes. These transient kinetic properties can differ from the properties of the stable enzyme in solution and from the properties of the enzyme in the multi-enzyme complex. The most extensive studies of this phenomenon have been carried out on the glyceraldehyde-3-phosphate dehydrogenase – phosphoribulokinase (GAPDH-PRK) complex from *Chlamydomonas reinhardtii* (Lebreton *et al.*, 1997a; Lebreton *et al.*, 1997b; Avilan *et al.*, 1997; Lebreton & Gontero, 1999). Kinetic studies of the GAPDH-PRK complex have revealed that the complex dissociates to give a metastable reduced form of PRK, the catalytic activity of which is increased approximately 10-fold relative to free, stable PRK and to the enzyme in complex with GAPDH (Lebreton & Gontero, 1999). Analysis of the thermodynamic parameters of ligand binding for stable and metastable PRK indicated that the energy barrier for catalysis might be decreased by stabilisation energy (-6 kJ/mol) derived from a conformational change in PRK within the complex. This stabilisation energy, stored

during complex association, corresponds to a transfer of energy from GAPDH to PRK. Site-directed mutagenesis has suggested that Arg-64 of PRK may be significant in stabilisation of the GAPDH-PRK complex and in the transfer of energy to PRK (Avilan *et al.*, 1997).

There is much evidence to suggest that macromolecules are very closely packed within living cells (Srere, 1982; Goodsell, 1991). Therefore, the effects of protein-protein interactions on the catalytic activity of metabolic enzymes are of great significance to the role of those enzymes *in vivo*. In this context, elucidation of the mechanisms and effects of phenomena such as molecular imprinting may result in a more complete understanding of the biochemistry of metabolism.

5.2 Results

5.2.1 Difference Spectroscopy and Kinetic Studies of Complex Assembly

Difference spectroscopy was carried out as described in Section 2.3.10. The primary goal of these experiments was to examine changes in the spectral properties of ETF when it forms a complex with TMADH. Previous studies using difference spectroscopy have established that there are small spectral changes associated with the mixing of oxidised ETF with TMADH (Jang *et al.*, 2000). These spectral changes, coupled with the ability to reduce ETF to the 2-electron (dihydroquinone) level when in complex with TMADH have been interpreted as evidence of a structural reorganisation of ETF during complex assembly.

In the present study, initial experiments involved mixing oxidised TMADH with wild-type recombinant ETF in both the oxidised and semiquinone states. ETF was reacted with TMADH at ambient temperature (~25 °C) in a ratio of 15μM : 10μM (final concentration of reactants after mixing in the split-cell cuvette). The pre-mixing and post-mixing absorbance spectra for each experiment, together with the corresponding difference spectra (post mixing - pre mixing) for these experiments, are shown in Figure 5.1. There were small spectral changes associated with the mixing of oxidised TMADH and oxidised ETF, which confirm the findings of Jang *et al* (2000). Furthermore, mixing of semiquinone ETF with oxidised TMADH gives rise to a large spectral change in the

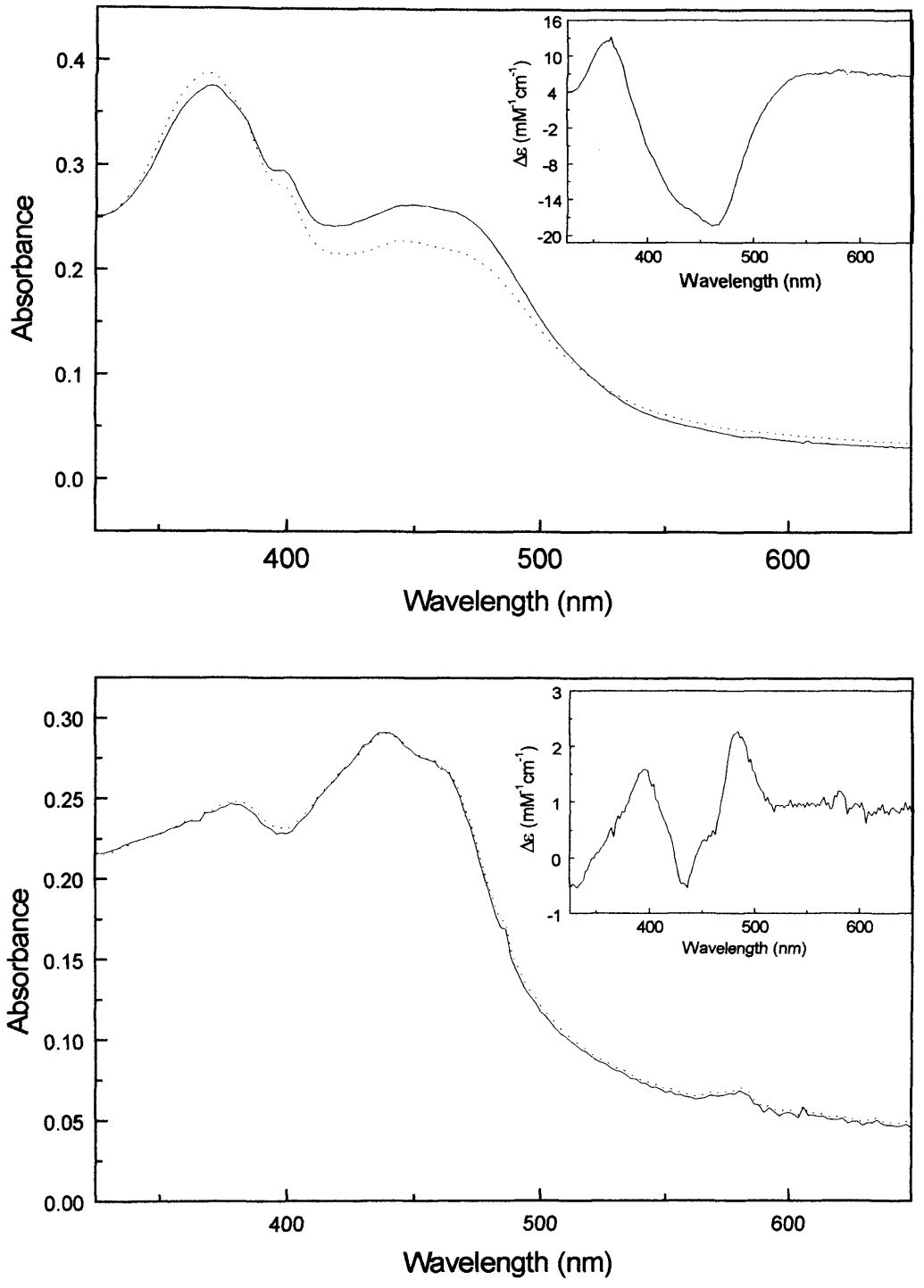

Figure 5.1
Spectral changes associated with the formation of the TMADH-ETF electron transfer complex. *Panel A*: Absorption spectrum of TMADH and semiquinone ETF before (solid line) and after (dashed line) mixing. *Inset*: Difference absorption spectrum (after mixing minus before mixing). *Panel B*: Absorption spectrum of TMADH and oxidised ETF before (solid line) and after (dashed line) mixing. *Inset*: Difference absorption spectrum (after mixing minus before mixing). Conditions: 15 μM ETF, 10 μM TMADH, 50 mM potassium phosphate buffer, pH 7.0, 25 °C.

region of 400 - 500 nm. These spectral changes are thought to be indicative of a change in the environment of the flavin in ETF when it forms a complex with TMADH.

As a continuation of these investigations, experiments were carried out to investigate the interaction of wild-type ETF with mutant forms of the TMADH enzyme. Three mutant species of the TMADH enzyme were used in these investigations; Y442F TAMDH, Y442L TMADH and Y442G TMADH. Significantly, these are the same species that were used to investigate the kinetics of electron transfer between wild-type ETF and mutant TMADH (Wilson *et al.*, 1997; Basran *et al.*, 2000). Purification of mutant forms of TMADH was performed as described in Section 2.3.4. It was found that the difference spectra for the mixing of oxidised ETF with mutant TMADH have almost identical features to the difference spectrum for the mixing of oxidised ETF with wild-type TMADH, regardless of which mutant of TMADH was used in the experiment. The difference spectrum for the mixing of oxidised ETF with Y442G TMADH is shown in Figure 5.2A. Similarly, the difference spectra for the mixing of semiquinone ETF with mutant TMADH are identical to the difference spectra for the mixing of semiquinone ETF with wild type TMADH. The difference spectrum for the mixing of semiquinone ETF with Y442G TMADH is shown in Figure 5.3A. However, dependent on the mutant form of TMADH used in each experiment there was a great variation in the time taken for each reaction to proceed to completion. For example, whereas the spectral changes observed on the mixing of oxidised or semiquinone ETF with wild type TMADH occur apparently instantaneously upon manual mixing, the spectral change observed on the mixing of semiquinone ETF with Y442F TMADH takes approximately 10 minutes to fully evolve, and the spectral change observed on the mixing of oxidised ETF with Y442G TMADH takes more than one hour to reach the point where no further change in the difference spectrum can be observed. Therefore, it was deemed necessary to subject the binding reaction of ETF and TMADH to quantitative kinetic analysis using absorbance and stopped-flow spectroscopy. In all experiments, ETF was reacted with TMADH in a ratio of 15μM : 10μM (final concentration of reactants in the stopped flow chamber), i.e. the same ratio that was used in the difference spectroscopy experiments. All reactions were carried out in 50 mM phosphate buffer, pH 7.0, and the temperature in the reaction chamber was maintained at 25 °C. For reactions of oxidised ETF with

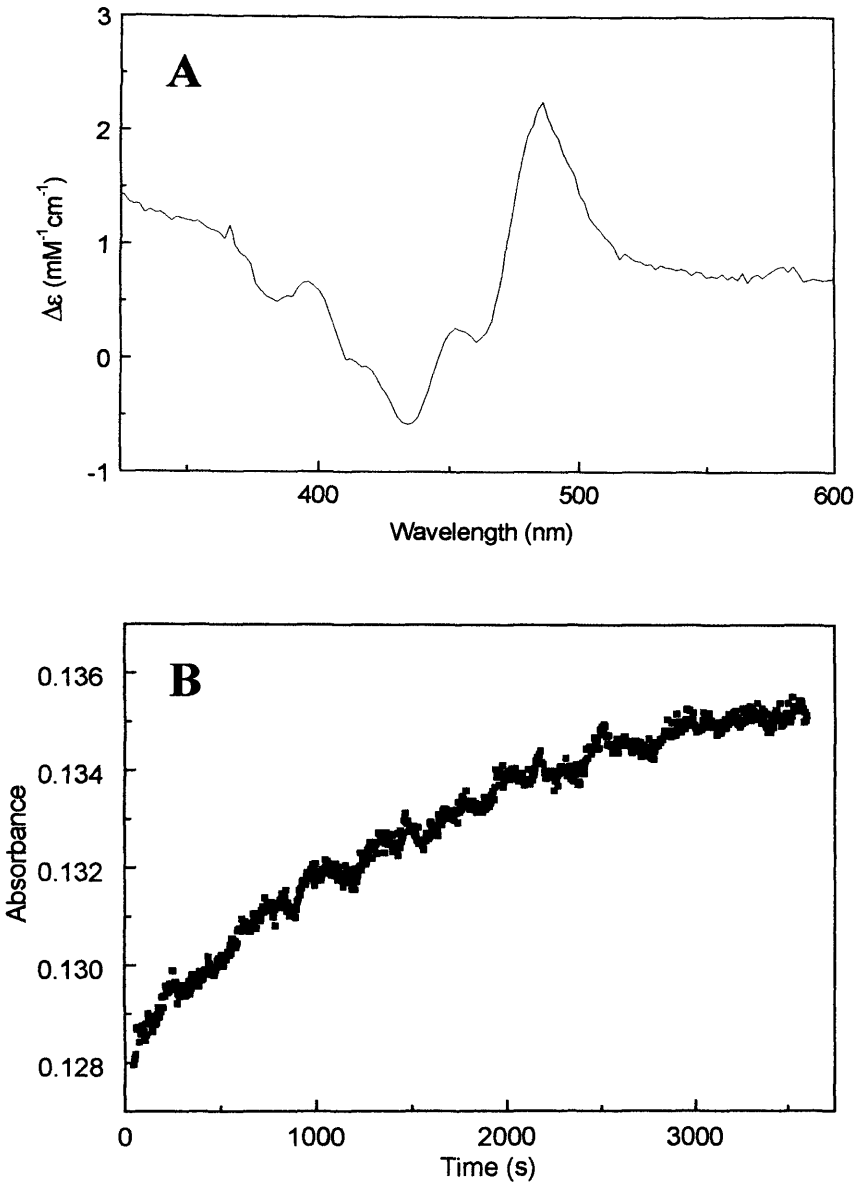

Figure 5.2
Static difference spectrum and kinetics of assembly for the Y442G TMADH-ETF_{ox} and Y442G TMADH-ETF_{sq} complex. *Panel A*: Difference spectrum (spectrum after mixing minus spectrum before mixing) for Y442G TMADH (10 μM) and ETF_{ox} (15 μM). *Panel B*: kinetic transient at 482 nm showing the absorbance change on mixing of ETF_{ox} with Y442G TMADH. The rates of absorption change were obtained by approximating first-order fitting (using Equation 2.1) to the early parts of the reaction transient. Conditions: 50 mM potassium phosphate buffer, pH 7.0, 25 °C.

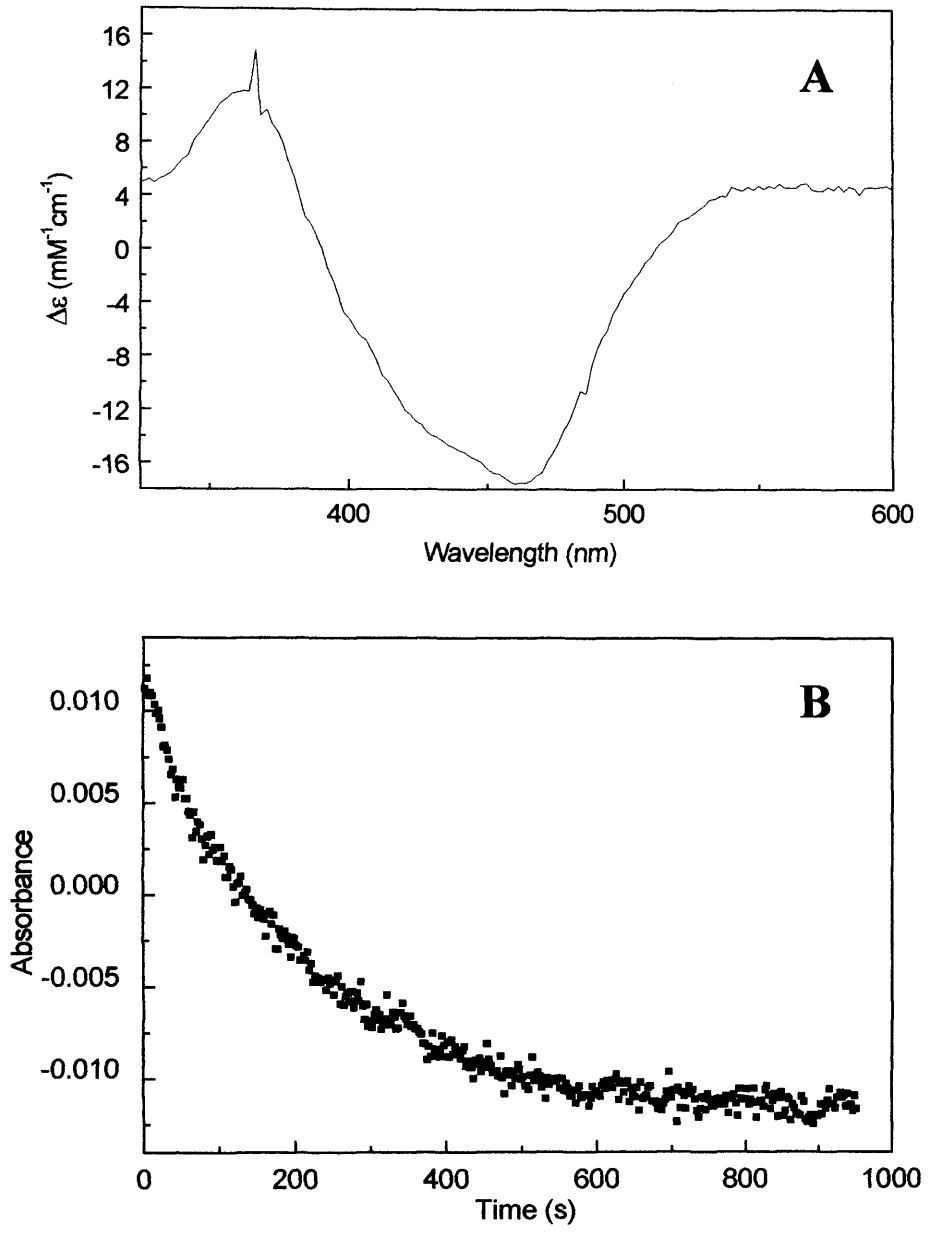

Figure 5.3
Static difference spectrum and kinetics of assembly for the Y442G TMADH-ETF_{ox} and Y442G TMADH-ETF_{sq} complex. *Panel A*: Difference spectrum (spectrum after mixing minus spectrum before mixing) for Y442G TMADH (10 μM) and ETF_{sq} (15 μM). *Panel B*: kinetic transient at 460 nm showing the absorbance change on mixing of ETF_{sq} with Y442G TMADH. The rates of absorption change were obtained by approximating first-order fitting (using Equation 2.1) to the early parts of the reaction transient. Conditions: 50 mM potassium phosphate buffer, pH 7.0, 25 °C.

TMADH, the reaction was monitored by measuring the absorbance change at 482 nm, and for reactions of semiquinone ETF with TMADH, the reaction was monitored by measuring the absorbance change at 460 nm. Results for all of these experiments are shown below in tabular form;

Table 5.1; Observed Rate Constants for ETF/TMADH Binding

TMADH;	ETF_{ox}	ETF_{sq}
Wild Type	ND (fast)	$9.27x10^{-1}$ s^{-1}
Y442F	ND (fast)	$8.43x10^{-3}$ s^{-1}
Y442L	ND (fast)	$3.06x10^{-3}$ s^{-1}
Y442G	$3.63x10^{-4}$ s^{-1}	$2.75x10^{-3}$ s^{-1}

The rates of absorbance change were analysed by approximating first order fitting to the early parts of the reaction profiles, as all of the reactions are second order with respect to TMADH and ETF. Where no value is presented for an experiment, this indicates that the expected change in absorbance on reaction of ETF/TMADH was observed, but reaction rates could not be measured as the absorbance change occurred in the "dead time" (mixing phase) of the reaction, and was thus too rapid to be measurable by stopped flow spectroscopy. Formation of the Y442G-oxidised ETF complex occurs on a much longer time scale than the corresponding rate of electron transfer when normalized to the equivalent concentrations of the component proteins (Basran *et al.*, 2000), which suggests that electron transfer occurs in a thermodynamically metastable complex.

5.2.2 Fluorescence studies of ETF-TMADH Complex and its Components

Fluorimetric analyses were performed as described in Section 2.3.7, and fluorescence quantum yields were determined by A. Bobrov and N. Vekshin at the Institute of Cell Biophysics, Pushchino, Russia. Preliminary studies were carried out to investigate the fluorescence properties of ETF and TMADH. The excitation spectrum of FAD in oxidised ETF coincides with that of free FAD (Figure 3.9). Little, if any, Trp or

Tyr contribution was observed at 280-nm in the excitation spectrum for ETF-bound FAD, revealing the absence of resonant energy transfer from Trp and Tyr to FAD. The quantum yield of FAD emission for semiquinone ETF is about of 5-10 % of that for free FAD. The slow increase in the intensity of the flavin emission over time, commensurate with the slow release of FAD from the protein (Figure 3.10), indicates that a quenching group reduces the FAD emission in ETF. The fluorescence lifetime of FAD in semiquinone ETF is relatively long (4.5 ± 0.2 ns), and is about twice that for free FAD in water (2.5 ± 0.3 ns). Dynamic deactivation of excited FAD by the adenosine moiety is well known for FAD in aqueous solution (Chen *et al.*, 1994). The fluorescence data for ETF-bound FAD suggests the adenosine moiety does not contact the isoalloxazine ring, which is consistent with the X-ray data for human ETF (Roberts *et al.*, 1996) and the model of *M. methylophilus* ETF (Chohan *et al.*, 1998). The fluorescence quantum yield of oxidised ETF is about 50% that of semiquinone ETF, and the lifetime of the fluorescence emission for ETF_{ox} is 2.9 ± 0.2 ns.

The quantum yield of fluorescence emission for the 6-*S*-cysteinyl FMN in TMADH is very small (~ 0.04 % of that for free FAD), and fluorescence from the 6-*S*-cysteinyl FMN is probably quenched as a result of the proximity of the flavin to the 4Fe-4S centre. The lifetime of fluorescence is ~ 6 ns, compared with 5 ns for free FMN in water. The very low quantum yield, and the long fluorescence lifetime, suggest that the emission at 540 nm may not be attributable to the 6-*S*-cysteinyl FMN in native TMADH. The origin of the fluorescence emission is uncertain, but possibilities include minor contaminating flavoproteins or a small population of non-native TMADH. The very low quantum yield of fluorescence emission for preparations of TMADH has allowed us to investigate flavin fluorescence changes associated solely with ETF on interaction with TMADH.

Incubation of ETF (in either redox state) with an equivalent concentration of TMADH at ambient temperature (~25 °C) leads to a gradual ~4-fold increase in ETF flavin fluorescence, which reaches a plateau after about 2 hours (Figure 5.4A). No similar change in the flavin fluorescence was observed for single preparations of either TMADH or ETF, other than those attributable to leaching of the FAD cofactor from free ETF (as described in Section 3.2.7). The rate at which fluorescence increases in a

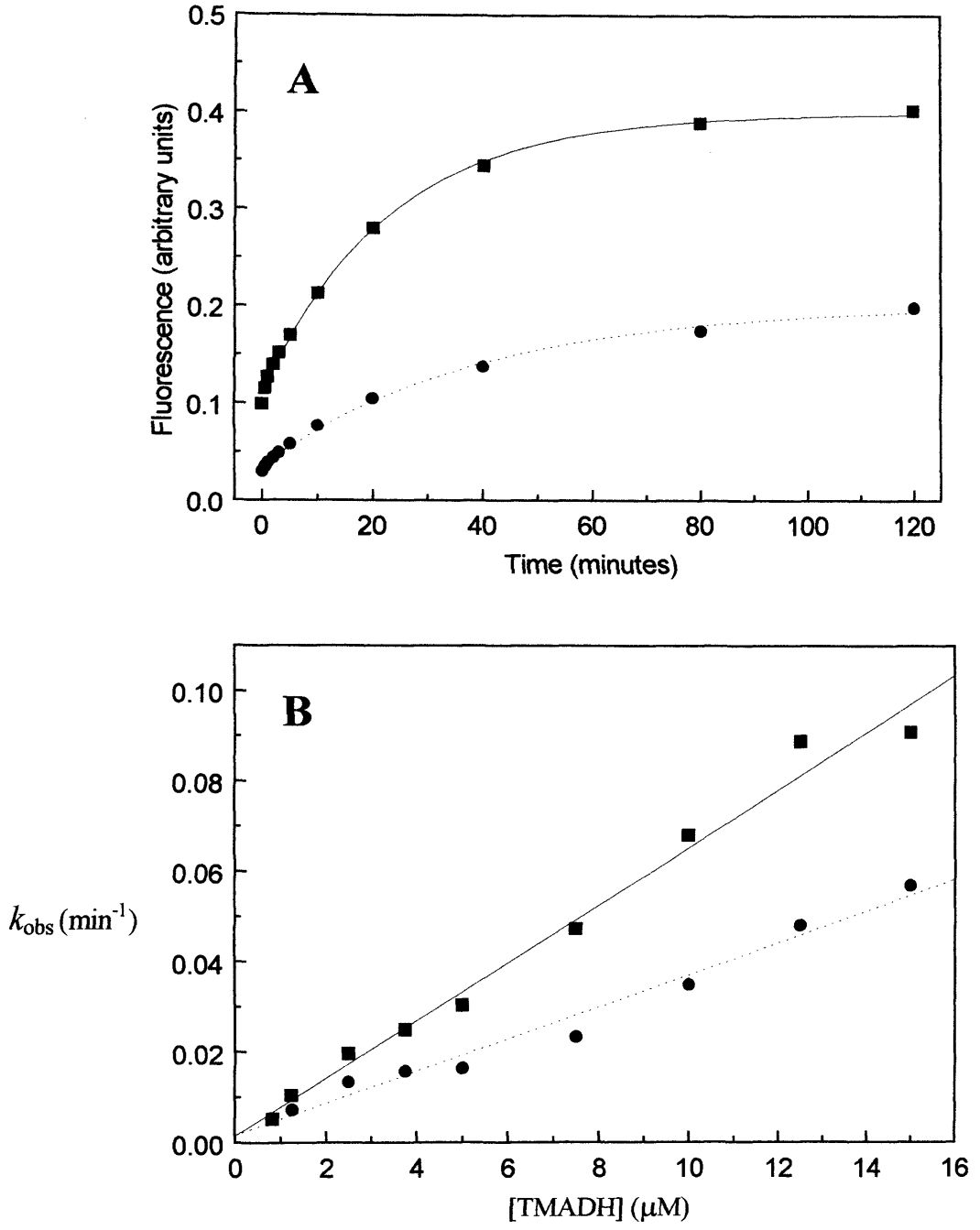

Figure 5.4
TMADH-induced flavin fluorescence emission in ETF_{ox} and ETF_{sq}. *Panel A*: Time dependence of induced emission (540 nm) following excitation (450 nm) of the FAD in ETF. *Circles*, ETF_{ox}; *squares*, ETF_{sq}. Conditions: TMADH (5 μM), ETF (5 μM), 50 mM potassium phosphate buffer, pH 7.0, 25 °C. *Panel B*: Plot of the rate of development of induced flavin fluorescence as a function of TMADH concentration. ETF was held at a concentration of 5 μM throughout. Symbols are the same as in panel A. Similar enhancements in flavin fluorescence were also observed in imprinting reactions with ETF_{ox} and ETF_{sq} purified from *M. methylotrophus* (not shown).

mixture of ETF and TMADH is directly proportional to the concentration of TMADH present in the reaction mixture. The relationship between the rate of fluorescence increase and TMADH concentration is illustrated in Figure 5.4B. Rates of increase in fluorescence were analysed by approximating first order fitting to the early parts of the reaction curves (strictly speaking, the reaction is second order with respect to TMADH and ETF).

It was originally considered that this increase in fluorescence may be due to a slow release of FAD from ETF. To test this possibility, absorption spectra for semiquinone ETF were measured before and after incubation with sub-stoichiometric amounts (*i.e.* less than 5 %) of TMADH. It was found that the absorption spectrum of the reaction mixture following prolonged incubation (>48 h) with TMADH is characteristic of the anionic semiquinone form of FAD (Figure 5.5). If FAD were released from semiquinone ETF during incubation with TMADH it would rapidly oxidise ($t_{1/2}$ of reduced FAD when free in solution is < 1s). However, there is a small increase in the absorption at 450 nm and a small decrease at 360 nm, which could suggest partial oxidation of the FAD bound to ETF. The structurally altered ETF spectrum was, however, resistant to further reduction on addition of trimethylamine to the incubation mixture, suggesting that partial oxidation of the ETF-bound FAD had not occurred. The fact that the flavin moiety remains bound to ETF during incubation with TMADH led to the suggestion that ETF may undergo a stable structural change in the presence of TMADH, and that this structural change may give rise to the slow increase in fluorescence. This structural change was termed "imprinting", and ETF that has been exposed to prolonged incubation with TMADH (*i.e.* such that its fluorescence emission reaches a plateau) will henceforth be termed "imprinted ETF".

Following imprinting of oxidised ETF by incubation with TMADH, the ETF-bound FAD is readily reduced by addition of the TMADH substrate trimethylamine, thus indicating that imprinted oxidised ETF is catalytically active. The importance of complex formation with TMADH in facilitating the imprinting reaction is apparent in studies of ETF imprinting catalysed by mutant TMADH enzymes. Mutation of Tyr-442 in TMADH leads to ~10-20-fold reduction in the rate of structural imprinting for semiquinone ETF (Figure 5.6), presumably as a result of the impaired interaction

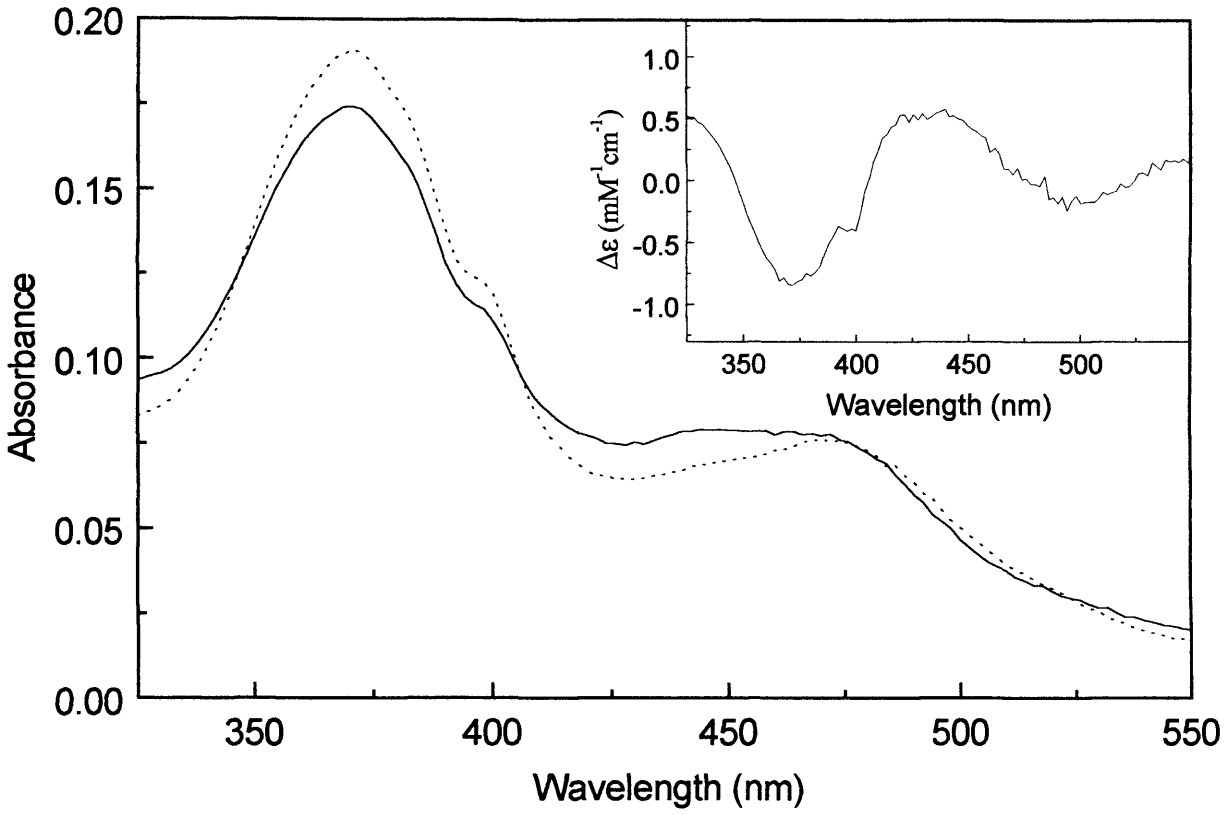

Figure 5.5
Absorbance spectrum of ETF_{sq} prior to and after incubation with TMADH. Method: ETF_{sq} (20 μM) incubated with TMADH (1 μM) and flavin fluorescence (540 nm) monitored over a 48 h period to ensure the reaction was completed. The spectrum of TMADH was subtracted from the acquired spectrum to yield the spectrum of imprinted ETF_{sq}. *Dashed line*, ETF_{sq} prior to incubation with TMADH; *solid line*, ETF_{sq} after incubation and removal of the TMADH spectrum. *Inset*: difference spectrum (spectrum after incubation minus spectrum before incubation with TMADH). Conditions: 50 mM potassium phosphate buffer, pH 7.0; 25 °C.

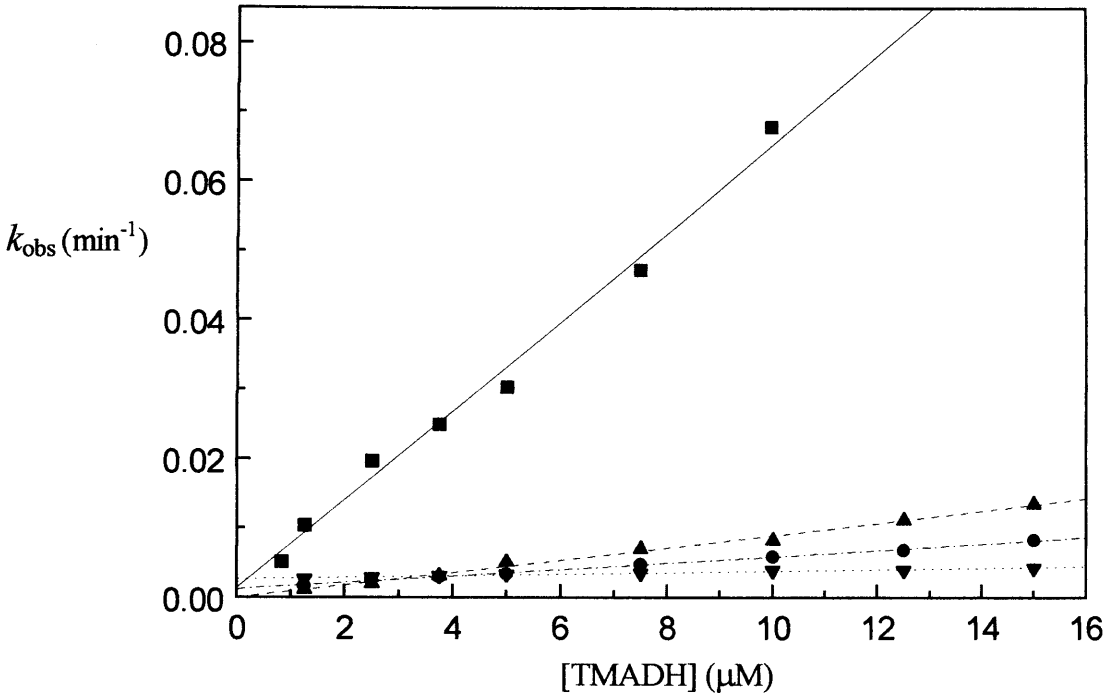

Figure 5.6
Kinetics of imprinting of ETF_{sq} with mutant TMADH enzymes altered at residue position 442. Rates for reactions performed with wild-type, Y442F, Y442G and Y442L TMADH enzymes are represented by *squares*, *triangles*, *circles* and *inverted triangles*, respectively. Imprinting reactions performed with wild-type TMADH and αR237A were substantially compromised (not shown) as a result of the known very slow rate of complex assembly determined by difference spectroscopy ETF (Talfournier *et al.*, 2001). Conditions: 5μM ETF, 50 mM potassium phosphate buffer, pH 7.0; 25 °C.

between ETF and the binding surface on TMADH. Similar results were obtained for imprinting reactions performed with oxidised ETF and the mutant TMADH enzymes (not shown). Previous studies have indicated that an interaction between Tyr-442 of TMADH and Arg-237 of ETF is implicated in the assembly of the wild-type complex (Chohan *et al.*, 1998; Talfournier *et al.*, 2001).

5.2.3 Solution Structural and Dynamic Properties of Imprinted ETF

In order to examine the effects of imprinting on the gross molecular structure of ETF, both imprinted and non-imprinted (*i.e.* as purified) ETF were subjected to analysis by small angle X-ray scattering (SAXS). Non-imprinted ETF was purified as described in Section 2.3.3, and imprinted by incubation with a sub-stoichiometric (*i.e.* less than 5 %) amount of TMADH. Scattering profiles for imprinted and non-imprinted ETF are shown in Figure 5.7. The two scattering curves are virtually identical (as indicated by their superimposition), which indicates that there are no significant changes in the global domain structure as a result of the imprinting reaction. Therefore, the calculated envelope model generated from SAXS data for non-imprinted semiquinone ETF (Section 4.2.3) can adequately describe the gross structural features of both imprinted and non-imprinted ETF.

Fluorescence anisotropy and lifetime measurements for the FAD cofactor in both imprinted and non-imprinted ETF were performed in order to gain information on the mobility and environment of the fluorophore. Results of these analyses are presented in Table 5.2. Calculated values for the rotational correlation time (θ) of the fluorophore were obtained from the Perrin equation,

$$r = \frac{r_0}{1+(\tau/\theta)} \quad ,$$

where r is the measured anisotropy, r_0 is the fundamental anisotropy and τ is the fluorescence lifetime of the fluorophore. The data indicate that the anisotropy values for imprinted ETF (in both oxidised and semiquinone forms) are less than the corresponding values for non-imprinted ETF. The major effect in accounting for this reduction in

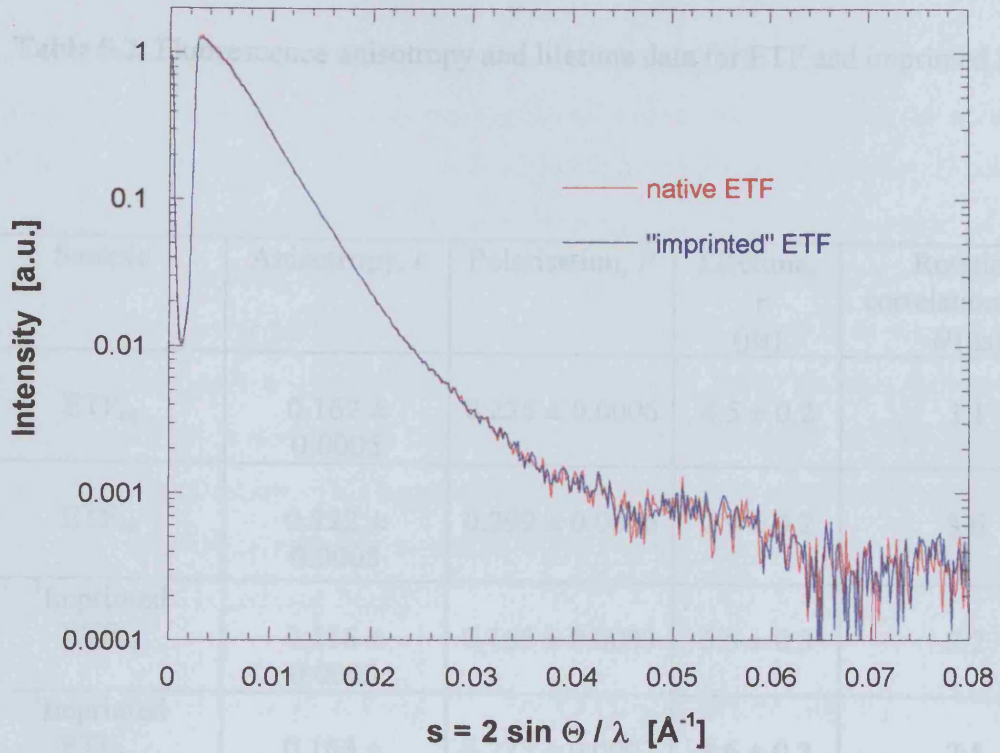

Figure 5.7
X-ray solution scattering profiles of native (red) and imprinted (blue) *M. methylotrophus* ETF_{sq}. Both curves were measured at 4° C and a protein concentration of approx. 15 mg/ml.

Table 5.2. Fluorescence anisotropy and lifetime data for ETF and imprinted ETF

Sample	Anisotropy, r	Polarisation, P	Lifetime, τ (ns)	Rotation correlation time, θ (ns)
ETF_{sq}	0.162 ± 0.0005	0.225 ± 0.0006	4.5 ± 0.2	3.1
ETF_{ox}	0.222 ± 0.0005	0.299 ± 0.0006	2.9 ± 0.2	3.6
[1]Imprinted ETF_{sq}	0.116 ± 0.0003	0.165 ± 0.0003	5.5 ± 0.3	2.2
[1]Imprinted ETF_{ox}	0.163 ± 0.0005	0.227 ± 0.0007	3.6 ± 0.2	2.5
[2]Imprinted ETF_{sq}	0.113 ± 0.0005	0.161 ± 0.0006	ND	ND

[1]ETF imprinted with TMADH in the following reaction: ETF (5 μM) + TMADH (5 μM), 50 mM potassium phosphate buffer, pH 7.0; incubated at 20 ° C for 2 hours.

[2]ETF imprinted with TMADH in the following reaction: ETF (5 μM) + TMADH (0.25 μM), 50 mM potassium phosphate buffer, pH 7.0, incubated at 20 ° C for 48 hours.

anisotropy is a decrease in the rotational correlation time. Small increases in the lifetime of the fluorophore are also apparent, but the effect of these changes on the anisotropy of the fluorophore is small. Therefore, the FAD fluorophore in structurally imprinted ETF undergoes a larger angular displacement between absorption and emission of a photon than in non-imprinted ETF. This suggests that the FAD fluorophore is bound more loosely in imprinted ETF, and hence that the imprinting reaction involves a structural change in the local environment of the FAD moiety. Also, the data indicate that the anisotropy of imprinted ETF is not affected by the concentration of TMADH present in the imprinting reaction. This suggests that the nature of the structural change associated with the imprinting reaction is not affected by the concentration of ETF-TMADH complex in the imprinting mixture.

5.2.4 Purification of Imprinted ETF by Analytical Gel Filtration

Analytical gel filtration was carried out as described in Section 2.3.5. Imprinted ETF was obtained by incubation of non-imprinted semiquinone ETF with a sub-stoichiometric (*i.e.* less than 5 %) amount of TMADH. Analytical gel filtration was used in an attempt to purify imprinted ETF from a mixture of ETF and TMADH. Although this goal was achieved and samples of pure imprinted ETF were obtained by gel filtration, on examination of the eluate fractions by both spectrophotometric and spectrofluorimetric techniques it was found that imprinted ETF purified in this manner is almost exclusively in the *apo* form, and that the FAD cofactor of ETF is eluted in a separate fraction. As a control, a sample of pure (*i.e.* of a purity sufficient for SAXS analysis) non-imprinted ETF was subjected to gel filtration under the same conditions as those used in the purification of imprinted ETF, and the eluate fractions analysed by spectrofluorimetry. Figure 5.8 shows the fluorescence intensity (exciting at 450 nm and measuring emission at 530 nm) for fractions eluted during gel filtration of both imprinted and non-imprinted ETF. Although SDS-PAGE analysis of the eluate fractions revealed that both forms of the protein are eluted at identical volumes (results not shown), the results of the fluorescence analyses clearly show that, for non-imprinted ETF, the majority (~80%) of the flavin present in the initial sample remains bound to ETF in the *holo*-enzyme. These results indicate that non-imprinted ETF has a far greater affinity for

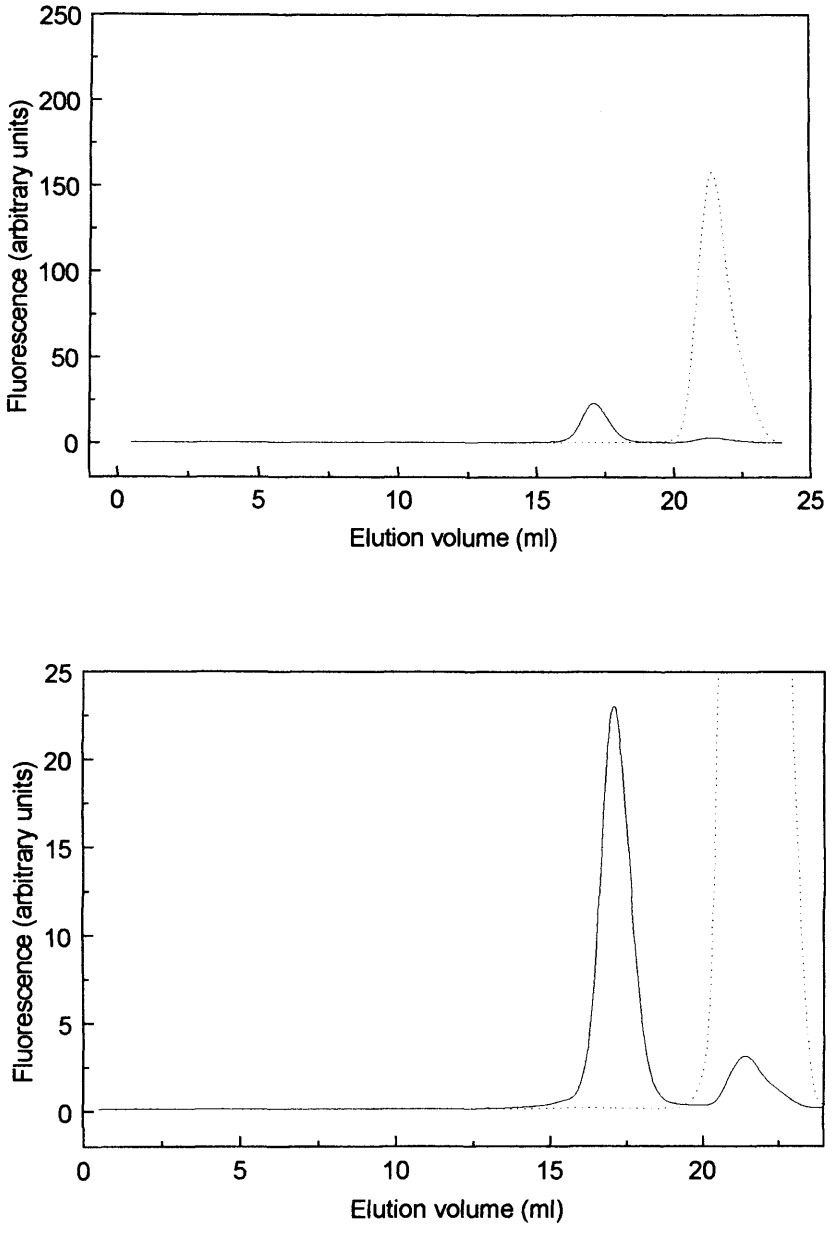

Figure 5.8
Fluorescence elution profiles of imprinted (*dotted line*) and non-imprinted (*solid line*) ETF_{sq}. Both panels show the same experiment, but in *Panel B* the Y-axis is magnified 10-fold relative to *Panel A*. Conditions: the analytical gel filtration column was equilibrated with 50 mM potassium phosphate buffer, pH 7.0, at 4 °C, and a flow rate of 0.3 ml per minute was used. 200 µl of a 2 mg/ml protein solution was loaded onto the column, and eluate fractions of 0.5 ml were collected. Eluate fractions were analysed using fluorescence spectroscopy (exciting at 450 nm and measuring emission at 530 nm). Fluorescence peaks at 17.5 ml and 21.5 ml represent protein-bound flavin and free flavin, respectively.

its FAD cofactor than imprinted ETF under the conditions used in the gel filtration experiment, and are further evidence that there is a structural change associated with the ETF imprinting reaction.

5.2.5 The Electron Transfer Reactions of ETF with Inorganic Redox Partners

A great deal of work has been carried out to investigate the reactions of biological molecules with non-physiological, inorganic redox partners (for examples, see Dennison *et al*, 1994, Kyritsis *et al*, 1991, Kyritsis *et al*, 1994 and Zhang *et al*, 1992). It was thought that investigation of the interaction of imprinted and non-imprinted ETF with inorganic redox partners may provide useful information concerning the redox behavior of the ETF, and provide a valuable means for making kinetic comparison between the two forms of the protein.

The first inorganic redox partner used in these investigations was ferricenium hexafluorophosphate. The ferricenium ion is a potent oxidising agent (E_m = +380 mV) which carries a positive charge (Figure 5.9);

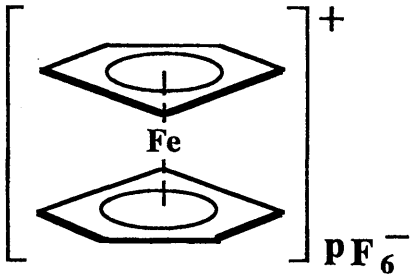

Figure 5.9 The Chemical Structure of Ferricenium

In stopped flow experiments, 15 μM semiquinone ETF was reacted with ferricenium hexafluorophosphate in 50 mM potassium phosphate buffer, pH 7.0. Concentrations of ferricenium from 0.2 mM to 1mM were used, and the experiments performed over a temperature range from 5 °C to 35 °C. Results for these experiments are shown in figure 5.10. For imprinted ETF, all transients obtained were monophasic (an average of four transients for the reaction of imprinted semiquinone ETF with 0.25

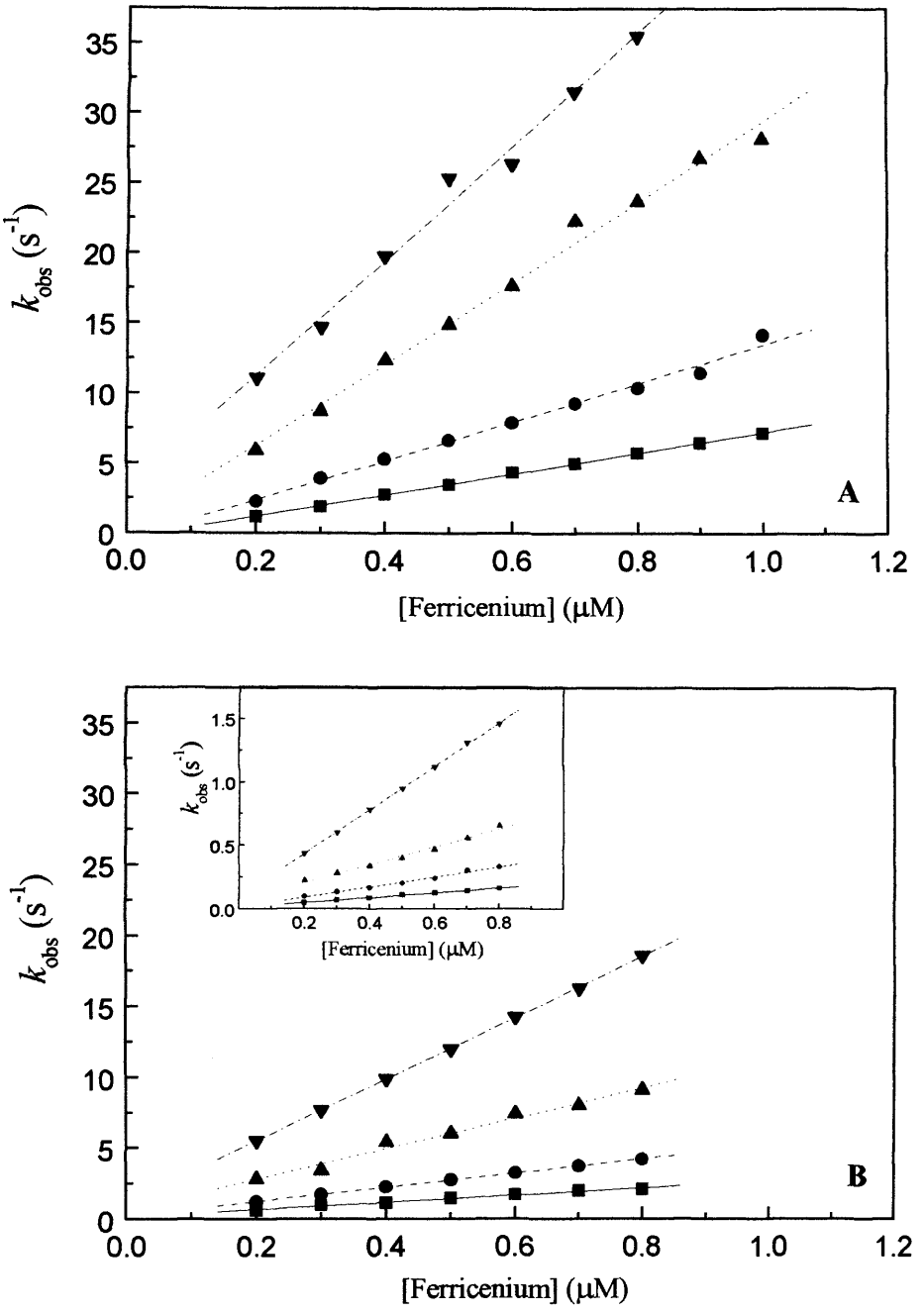

Figure 5.10
Electron transfer kinetics for reactions of imprinted and non-imprinted ETF with ferricenium. *Panel A*: plot of observed rate constant, k_{obs} against ferricenium concentration for the oxidation of imprinted ETF_{sq}. Reactions were performed at temperatures of 278 K (*squares*), 288 K (*circles*), 298 K (*triangles*) and 308 K (*inverted triangles*). For the imprinting reaction, ETF_{sq} (40 μM) and TMADH (2 μM) were mixed; the progress of the imprinting reaction was monitored by fluorescence emission (540 nm) following excitation (450 nm). Conditions: ETF concentration 15 μM; 50 mM phosphate buffer, pH 7.0. *Panel B*: plot of observed rate constant (fast phase), k_{obs} against ferricenium concentration for the oxidation of 'as-purified' ETF_{sq}. Reactions were performed at temperatures of 278 K (*squares*), 288 K (*circles*), 298 K (*triangles*) and 308 K (*inverted triangles*). Conditions as for panel A. *Inset*: plot of observed rate constant (slow phase), k_{obs} against ferricenium concentration for the oxidation of 'as-purified' ETF_{sq}. In all cases, absorbance change was monitored at 438 nm.

mM ferricenium at 25 °C is shown in figure 5.11B), and fitting to equation 1 provided rate constants for the reaction. However, for non-imprinted ETF, all transients obtained were biphasic (an average of four transients for the reaction of non-imprinted ETF_{sq} with 0.25 mM ferricenium at 25 °C is shown in figure 5.11A), and fitting to equation 2 provided rate constants for each phase of the reaction. The observed rate constants for the slow phase of the non-imprinted semiquinone ETF/ferricenium electron transfer reaction were approximately 10-fold lower than the rate constants for the fast phase of the reaction. All of the observed rate constants obtained in these experiments were considerably lower than expected for intrinsic rates of electron transfer, which indicates that rates are limited by a non-eT reaction step. Saturation kinetics were not observed; and reaction rates expressed a linear dependence on the concentration of ferricenium. The slope of this linear dependence is equivalent to the second order rate constant of the reaction. Fitting these data to the unimolecular rate equation to obtain a linear plot (as described in Craig *et al*, 1998) enabled the determination of the apparent enthalpy ($\Delta H^{\ddagger}$) and entropy ($\Delta S^{\ddagger}$) terms for the reactions of imprinted and non-imprinted ETF with ferricenium hexafluorophosphate (Figure 5.12). The altered kinetic and thermodynamic parameters for electron transfer between ETF and ferricenium provide additional evidence that a conformational change occurs in the environment of the redox cofactor during the imprinting reaction.

It was considered that, as ferricenium is a positively charged molecule, unfavourable electrostatic forces might be responsible for limiting the reaction rates between ferricenium and ETF. Therefore, the analysis of imprinted semiquinone ETF was repeated at a single temperature (25 °C) using ferricyanide, a negatively charged inorganic oxidising agent, as an electron acceptor. All other reaction conditions were identical to those described previously. All transients obtained were monophasic, and fitting to Equation 2.1 provided rate constants for the reaction. The reaction rates for this experiment were found to be comparable to those for the reaction of imprinted semiquinone ETF with ferricenium, as shown in Figure 5.13. This suggests that electrostatic interactions are not responsible for the low observed rates of electron transfer between semiquinone ETF and inorganic redox partners.

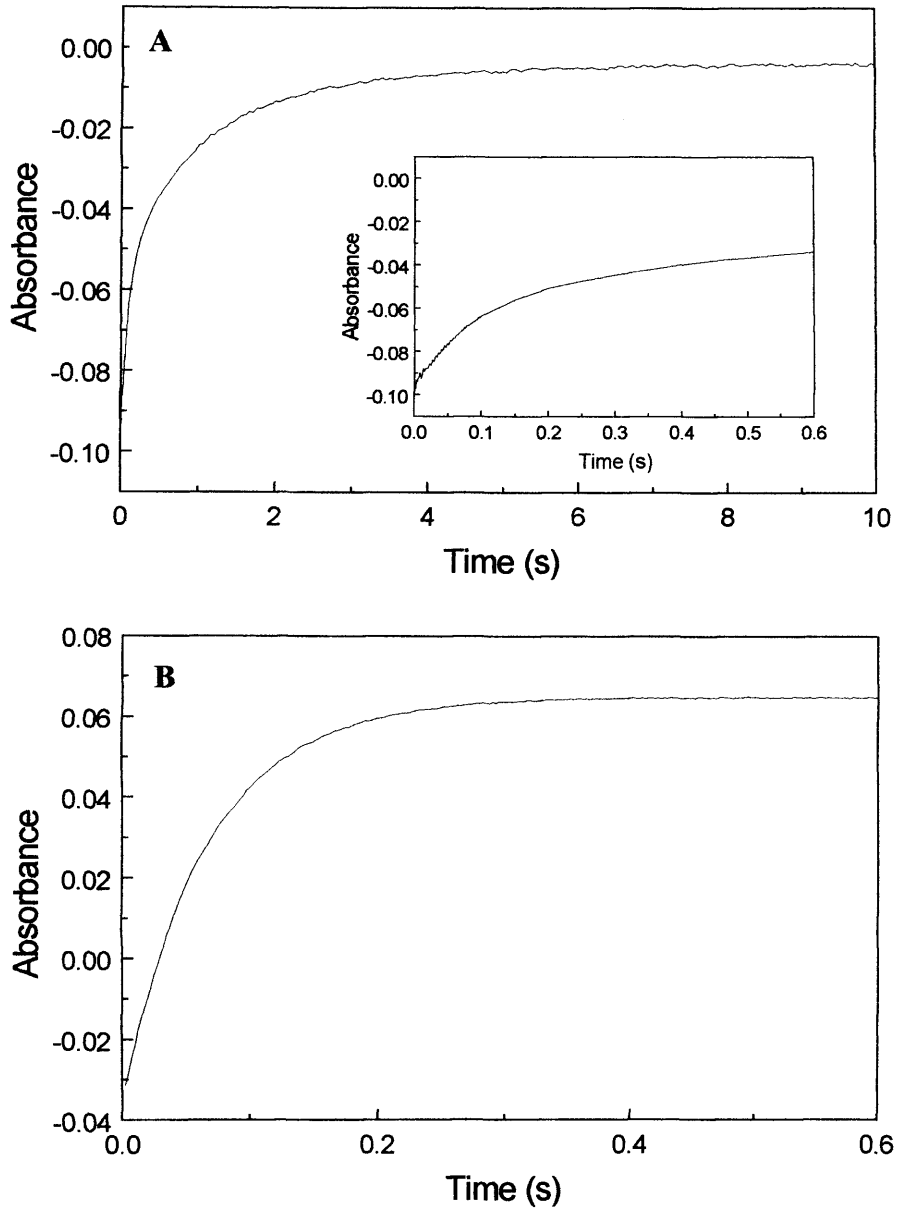

Figure 5.11
Absorption transients for the reaction of imprinted and as-purified ETF_{sq} with ferricenium ion. *Panel A*: reaction of 15 μM ETF_{sq} (as-purified) with 500 μM ferricenium hexafluorophosphate, in 50 mM phosphate buffer, pH 7.0, 298 K. Transient measured over 10 s. Fitting to Equation 2.2 gave values for k_{fast} and k_{slow} of 6.0 s^{-1} and 0.4 s^{-1}, respectively. *Inset*: the same transient shown in the main panel, but over a shorter time scale. Each phase contributes equally to the total absorption change. *Panel B*: reaction of 15μM ETF_{sq} (imprinted) with 500 μM ferricenium hexafluorophosphate, in 50 mM phosphate buffer, pH 7.0, 298 K. Fitting to Equation 2.1 gave value for the rate of the absorption change, k_{obs}, of 14.9 s^{-1}.

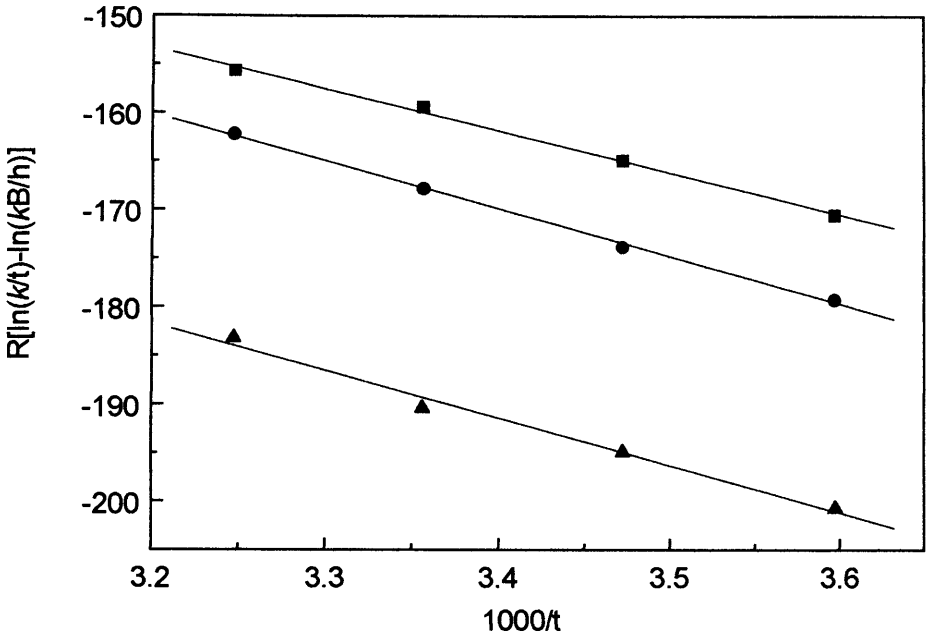

Figure 5.12
Temperature dependence plot of second-order rate constants for the reaction of imprinted and non-imprinted ETF_{sq} with ferricenium (obtained from Figure 5.10) at temperatures from 278 to 308 K. Thermodynamic parameters obtained by fitting to the unimolecular rate equation are as follows: for imprinted ETF (*squares*), $\Delta H^{\ddagger} = 43 \pm 2.2$ kJ mol^{-1}, $\Delta S^{\ddagger} = -17 \pm 7.5$ J mol^{-1} K^{-1}; : for non-imprinted ETF (fast reaction - *circles*), $\Delta H^{\ddagger} = 49 \pm 1.8$ kJ mol^{-1}, $\Delta S^{\ddagger} = -4 \pm 4.1$ J mol^{-1} K^{-1}; for non-imprinted ETF (slow reaction - *triangles*), $\Delta H^{\ddagger} = 49 \pm 2.3$ kJ mol^{-1}, $\Delta S^{\ddagger} = -26 \pm 8.6$ J mol^{-1} K^{-1}.

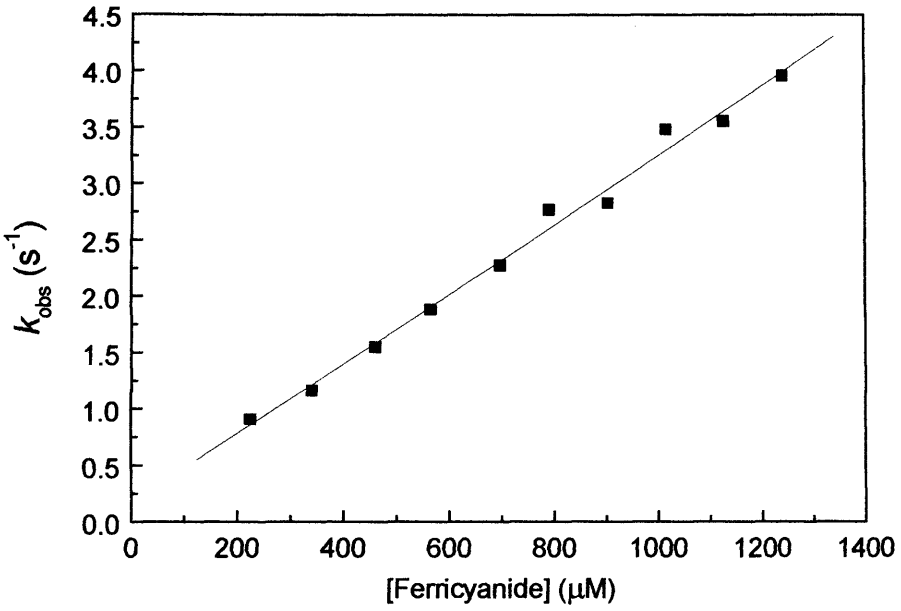

Figure 5.13
Electron transfer kinetics for reactions of imprinted ETF_{sq} with ferricyanide. The concentration of ETF_{sq} used was 15 μM and concentrations of ferricyanide used were from 0.2 mM to 1.2 mM. This experiment was performed at 298 K, in 50 mM phosphate buffer, pH 7.0.

5.3 Discussion

5.3.1 Difference Spectroscopy Data

The spectral changes observed during ETF-TMADH complex formation are indicative of a change in the environment of the flavin in ETF. It was shown in the previous chapter that the SAXS profiles of oxidised and semiquinone ETF indicate that both redox forms of ETF have equivalent structural characteristics in solution. In combination, the difference spectroscopy data and the SAXS data strongly suggest that both redox forms of ETF undergo a localised conformational change during complex assembly.

Mutation of tyrosine 442 of TMADH does not alter the character of the spectral change observed on the interaction of TMADH with ETF, indicating that the physical nature of the conformational change that occurs in ETF on binding TMADH is unaffected. However, the fact that mutation of Tyr-442 causes a decrease in the rate of the spectral change observed on the binding of TMADH to ETF strongly supports the hypothesis put forward by Basran *et al.* (2000) that Tyr-442 is responsible for coupling to ETF (specifically, to residue Arg-237) and formation of the active electron transfer complex. It has been postulated that the decrease in electron transfer rate that is observed when Tyr-442 is mutated is the product of an impaired rate of conformational change and/or structural realignment necessary for subsequent electron transfer (Basran *et al.*, 2000). According to this model, electron transfer between TMADH and ETF can be described using the following kinetic scheme;

$$A + B \underset{k_{-a}}{\overset{k_a}{\rightleftharpoons}} (AB)_1 \underset{k_{-r}}{\overset{k_r}{\rightleftharpoons}} (AB)_2 \xrightarrow{k_{eT}} (A^{+}B^{-}) \longrightarrow A^{+} + B^{-}$$

SCHEME 1

where A is oxidised ETF, B is semiquinone TMADH, $(AB)_1$ is a non-productive electron transfer complex, $(AB)_2$ is the productive electron transfer complex that forms following

structural realignment of complex $(AB)_1$, and (A^+B^-) is the product complex following electron transfer. An analytical rate equation for the observed electron transfer rate constant (k_{obs}) measured in stopped-flow studies can be derived for such a scheme (Eq. 5.1; Basran *et al.*, 2000);

$$k_{obs} = \frac{k_a k_r k_{eT}[A]}{k_{-a}(k_{eT} + k_{-r}) + k_r k_{eT} + k_a(k_{eT} + k_r + k_{-r})[A]} \qquad \text{(Eq. 5.1)}$$

In the regime where the *intrinsic* electron transfer rate (k_{eT}) is fast, and also where $k_r >> k_{-a} + k_a[A]$, Eq. 5.1 is approximated by a linear relationship between k_{obs} and [A], and this situation pertains for the wild-type complex (Basran *et al.*, 2000). Saturation behaviour is observed for mutant complexes altered at residue 442, and this was previously inferred to represent a rate-limiting conformational change [conversion of $(AB)_1$ to $(AB)_2$], rather than a rate-limiting intrinsic electron transfer rate [k_{eT}; (Basran *et al.*, 2000)]. In the present study, the difference spectroscopy data concerning complexes formed between ETF and mutant TMADH enzymes provide substantial evidence for impaired structural realignment during mutant complex formation. Evolution of the spectral changes accompanying the assembly of complexes between semiquinone ETF and Y442F, Y442L and Y442G mutant TMADH enzymes occurs with rate constants ~ 2 orders of magnitude lower than that for formation of the wild-type complex. The rate of spectral change observed on the interaction of oxidised ETF with Y442G TMADH is also substantially slower than that for the corresponding wild-type complex. The spectral changes accompanying the assembly of Y442F, Y442L mutant TMADH enzymes with oxidised ETF are too rapid to follow using stopped-flow methods. It is clearly not possible to perform interaction studies with 1 electron reduced TMADH and oxidised ETF in the absence of electron transfer. However, the difference spectroscopy studies with mutant oxidised TMADH- oxidised ETF and oxidised TMADH- semiquinone ETF combinations indicate that mutation of Tyr-442 in TMADH impairs complex assembly, and this is likely to translate to the assembly of the electron transfer competent complex involving 1-electron reduced TMADH and oxidised ETF. The molecular model of the electron transfer complex (Chohan *et al.*, 1998) suggests a close interaction between Tyr-

442 of TMADH and Arg-237 of ETF, and this interaction may be important in facilitating the structural reorganisation which forms the productive electron transfer complex. Difference spectroscopy studies with ETF mutated at Arg-237 (R237A), which also indicate impaired complex assembly, are consistent with this model (Talfournier *et al.*, 2001). Significantly, the experiments with mutant TMADH enzymes show slow rates of complex assembly (especially with the Y442G-ETF complex) in comparison to the rates of electron transfer within the corresponding electron transfer complex (Basran *et al.*, 2000). This suggests that electron transfer in these mutant complexes does not occur in the most thermodynamically stable state, but that a metastable form of the complex is competent in transferring electrons from TMADH to ETF.

5.3.2 Fluorescence Analysis of the ETF Imprinting Reaction

The large, long time-scale changes in the fluorescence emission of the FAD cofactor of ETF indicate that interaction of with TMADH induces a conformational change in ETF, probably localised around the environment of the FAD moiety. It has been determined that the observed increase in fluorescence signal cannot be due to a release of flavin from ETF. The fact that the rate of the ETF imprinting reaction increases as a linear function of TMADH concentration indicates that TMADH is acting as a true catalyst for ETF imprinting. Mutation of Tyr-442 of TMADH causes significant reduction in rates of imprinting for both oxidised and semiquinone ETF which, in the light of previous conclusions about the importance of Tyr-442 in the formation of the active electron transfer complex, suggests that formation of the active complex is a vital precursor to the ETF imprinting reaction. The finding that rates for the imprinting reaction were faster when catalysed by Y442G TMADH than when catalysed by Y442L TMADH was unexpected, as rates for both interprotein electron transfer (Wilson *et al*, 1997; Basran *et al*, 2000) and active-complex formation are more severely compromised in Y442G TMADH than in Y442L TMADH. As the imprinting reaction is likely to be a complex molecular dynamic interaction within the active complex, it is difficult to interpret this result. However, it may be related to the observation noted during kinetic analysis of the ETF/TMADH electron transfer reaction that the dissociation constant for the complex is significantly elevated for Y442G TMADH (Wilson *et al*, 1997).

5.3.3 Solution Structural Properties of Imprinted ETF

The results of the SAXS analyses of ETF (Chapter 4) reveal that domain II of ETF is conformationally mobile with respect to domains I and III. It was clear from the scattering profile simulations that restricted motion of domain II would have a pronounced effect on the scattering profile of ETF, most notably at the low scattering angles ($s \leq 0.02$ Å^{-1}). The experimental scattering data presented in this chapter hence confirm that no gross change in the domain structure or dynamics of ETF occurs during the imprinting reaction. However, because the resolution of the structural information obtainable by SAXS is very low (~ 15 Å), local changes in conformation such as those resulting from side-chain reorientations cannot be excluded. This suggests that the structural change that occurs during imprinting of ETF consists of small side-chain reorientations localised around the FAD moiety. One possible candidate for the conformational change that occurs during imprinting can be deduced by examination of the time scale of the imprinting reaction. The half-life for imprinting of ETF, at approximately 30 minutes, is comparable to the time scale expected for a proline *cis-trans* isomerism. The suggestion that proline isomerism may be responsible for the imprinting reaction is further substantiated by analysis of the structure of ETF. There is a proline residue (Pro-238) immediately adjacent to Arg-237, the residue which has been implicated in stabilisation of the semiquinone form of ETF and in complex formation (Chohan *et al.*, 1998; Talfournier *et al.*, 2001).

5.3.4 Dynamic Properties of the FAD Cofactor of ETF

Measurement of fluorescence anisotropy and lifetime of fluorescent moieties within protein molecules can provide valuable information on the structural and dynamic characteristics of the protein, or on the structure and flexibility of the fluorophore. The anisotropy/lifetime data reveal that the decreased values for anisotropy observed for imprinted ETF relative to those observed for non-imprinted ETF are largely the product of reduced rotational correlation times for the fluorescent moiety. This suggests that imprinted ETF binds its FAD cofactor more loosely than non-imprinted ETF. Loose binding of the FAD may facilitate electronic coupling between ETF and TMADH, as the

molecular model of the ETF-TMADH complex predicts that the isoalloxazine ring of FAD might enter a small groove on the surface of TMADH adjacent to Tyr-442 (Chohan *et al.*, 1998).

5.3.5 The Electron Transfer Reactions of ETF with Inorganic Redox Partners

The analyses of the reactions of imprinted and non-imprinted ETF with ferricenium confirm that the changes observed in the fluorescence properties of ETF when it interacts with TMADH are reflected in a change in the kinetic and thermodynamic properties of ETF. The stopped flow data thus provide further evidence that a conformational change occurs in the environment of the redox cofactor during the imprinting reaction. The observation that the rate constants for electron transfer from imprinted ETF to ferricenium are faster than the corresponding rate constants for electron transfer from non-imprinted ETF to ferricenium supports the hypothesis that the FAD cofactor is more loosely bound in imprinted ETF. The fact that kinetic transients for electron transfer from ETF to ferricenium are biphasic for non-imprinted ETF and monophasic for imprinted ETF suggests a more conjugated mechanism for electron transfer from non-imprinted ETF. Although this result is difficult to interpret, the more complex kinetic scheme for electron transfer from non-imprinted ETF does suggest a change in the environment and/or orientation of the FAD cofactor in ETF. Analysis of the reaction between ETF and ferricyanide confirmed that electrostatic forces do not limit the observed electron transfer rates between ETF and inorganic molecules.

5.3.6 Implications for Study of Interprotein Electron Transfer Reactions *in vivo*

There are very few structures solved of soluble, physiological and transiently formed electron transfer complexes. Examples include the methylamine dehydrogenase-amicyanin-cytochrome *c* (Chen *et al.*, 1994) and cytochrome *c* peroxidase:cytochrome *c* (Pelletier & Kraut, 1992) complexes. In these cases, the structures of the protein components in the complex resemble those of the uncomplexed molecules, giving rise to a colliding "billiard ball" representation of complex assembly. These structural studies thus provide little insight into the extent and role of dynamics in electron transfer. However, kinetic studies have revealed that small-scale conformational changes occur in

electron transfer from cytochrome *c* to ferricytochrome *b*5 (Qin & Kostic), from cytochrome *c* to plasticyanin (Zhou & Kostic, 1992; Zhou & Kostic, 1993) and from methanol dehydrogenase to cytochrome *c*551i (Harris *et al.*, 1994). Also, X-ray studies have suggested that large-scale conformational change may be a prerequisite for efficient electron transfer; for example in the cytochrome *bc*1 complex (Zhang *et al.*, 1998), sulfite reductase (Gruez *et al.*, 2000) and, to a lesser extent, the components of the bovine adrenodoxin reductase-adrenodoxin electron transfer complex (Ziegler *et al.*, 1999). The results presented in this chapter, together with the results of the SAXS analyses, have indicated that ETF also undergoes a large-scale conformational change on formation of the active electron transfer complex. Furthermore, comparison of kinetic data for the ETF-TMADH electron transfer reaction (Basran *et al.*, 2000) with the kinetic data for the ETF-TMADH binding reaction have indicated that, for interactions of ETF with mutant TMADH, this rearrangement does not lead to the thermodynamically most stable state (which is formed too slowly), but to one or more rapidly-formed metastable states that are themselves productive electron transfer complexes.

Previous research conducted on the enzyme phosphoribulokinase has demonstrated that imprinting transiently alters the kinetic parameters of enzyme catalysis and the thermodynamic parameters of ligand binding on dissociation from the multienzyme complex (Lebreton *et al.*, 1997a; Lebreton *et al.*, 1997b; Avilan *et al.*, 1997; Lebreton & Gontero, 1999). In this study it has been deduced that imprinting of an electron transfer protein by interaction with its physiological redox partner can give rise to alterations in the protein's spectral, kinetic and thermodynamic characteristics. Taking into account previous conclusions about the importance of Tyr-442 in the formation of the active electron transfer complex, the slow rate of the imprinting reaction observed during complex formation with mutant TMADH indicates that formation of the active complex is an essential component of the ETF imprinting reaction. These results are consistent with previous analyses of the phosphoribulokinase system, which indicate that mutation of residues responsible for complex stabilization can affect information transfer between proteins in the complex (Avilan *et al.*, 1997). The long-term effects on the properties of ETF via transient interaction with TMADH have important implications for our understanding of biological electron transfer reactions *in vivo*, since ETF encounters

TMADH constantly in the cell. This suggests that the kinetic scheme proposed previously (Basran *et al.*, 2000) for the oxidative half-reaction (Scheme 1) is applicable to the *in vivo* situation with the modification that the ETF is in the structurally imprinted, rather than non-imprinted, form. Thus, Scheme 1 becomes (Scheme 2):

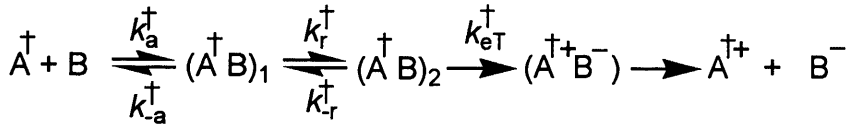

SCHEME 2

Here, $A^{\dagger}$ is (imprinted) ETF_{ox}, B is $TMADH_{sq}$, $(A^{\dagger}B)_1$ is a non-productive (imprinted) electron transfer complex, $(A^{\dagger}B)_2$ is the (imprinted) productive electron transfer complex that forms following structural realignment of complex $(A^{\dagger}B)_1$, and $(A^{\dagger+}B^{-})$ is the (imprinted) product complex following electron transfer. The situation *in vitro* is somewhat more complex, as the ETF is initially in the non-imprinted form. However, as the reaction proceeds (some of) the ETF will become imprinted, leading to a more complex kinetic scheme (Scheme 3):

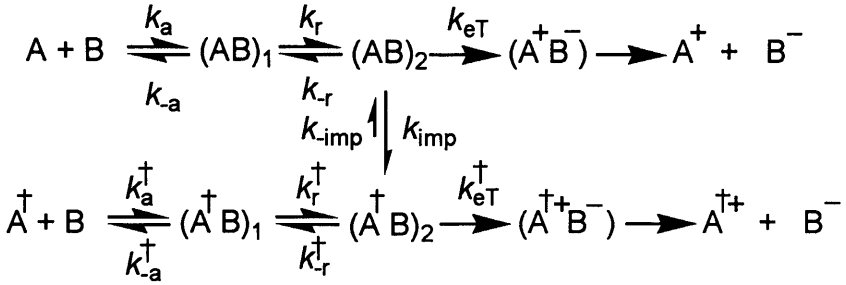

SCHEME 3

In Scheme 3, the reaction starts along the top path. However, as ETF interacts with TMADH, the ETF can undergo the imprinting reaction; once the ETF is structurally imprinted, the reaction can proceed along the bottom path, corresponding to the *in vivo* scheme. However, Scheme 3 does not suggest that formation of the productive electron transfer complex is necessarily a prerequisite for the ETF imprinting reaction. The

kinetic data presented in this chapter are consistent with a scheme for the imprinting reaction that occurs independently of the productive complex formation and electron transfer steps.

The results presented in this chapter have significant implications not only for our understanding of the mechanism of interprotein electron transfer reactions *in vivo*, but also for how we interpret experimental data from kinetic analyses of electron transfer proteins in the presence and/or absence of their various physiological redox partners. If imprinting is an influential factor in other enzyme systems, then the methods used for purification of the individual enzymes and the sources from which they are obtained (*i.e.* native or recombinant) may be significant in any kinetic study performed on such systems.

CHAPTER 6
DISCUSSION

6.1 Discussion of Results

The work described in this thesis has provided a multi-parameter characterisation of the structural and dynamic processes involved in the assembly of physiological electron transferring flavoprotein complexes. The results of this work reveal that W_3A_1 ETF undergoes a large-scale conformational change when it forms a complex with TMADH, which confirms the predictions of previous molecular modelling analyses (Chohan *et al.*, 1998). The results also reveal that W_3A_1 ETF, human ETF and *Paracoccus denitrificans* ETF are conformationally flexible in solution. Furthermore, the results show that the structure and catalytic activity of W_3A_1 ETF are altered in a stable manner by transient interaction with TMADH. Finally, the results demonstrate the importance of a specific residue of TMADH (Tyr-442) in the stabilisation and propagation of molecular interactions between TMADH and W_3A_1 ETF, which confirms the predictions of previous kinetic analyses (Basran *et al.*, 2000).

As discussed in Chapter 3, high yields of W_3A_1 ETF have been purified from a recombinant source. The results of the spectroscopic comparisons of native and recombinant W_3A_1 ETF, together with the data obtained on the kinetic behaviour of W_3A_1 ETF in its reaction with TMADH, have indicated that the native and recombinant forms of W_3A_1 ETF are structurally and functionally identical.

Analysis of W_3A_1 ETF using small angle X-ray solution scattering (SAXS) has confirmed that both the oxidised and the anionic semiquinone forms of W_3A_1 ETF have an essentially identical molecular conformation in solution. SAXS analyses have also revealed that W_3A_1 ETF samples a range of conformations in free solution, corresponding to a large-scale rotation of domain II with respect to domains I and III. These data, together with the proposed molecular model for the TMADH-ETF complex (Chohan *et al.*, 1998), have suggested an "induced fit" mechanism for the assembly of the active electron transfer complex.

SAXS analyses of human and *P. denitrificans* ETF have revealed that, like W_3A_1 ETF, both proteins sample a range of conformations in free solution. Molecular

modeling of the human ETF-MCAD complex has indicated that a rotation of domain II of ETF by 30° to 50° towards domain I [relative to its position in the crystal structure of human ETF (Roberts *et al.*, 1996)] is required to optimize electron transfer within the complex.

The difference spectroscopy analyses of the interaction between W_3A_1 ETF and TMADH have revealed that conformational changes occur during the assembly of the TMADH-ETF complex. Furthermore, difference spectroscopy and kinetic analyses using mutant TMADH have indicated that the presence of Tyr-442 in the interaction surface of TMADH plays an important role in the formation of the active electron transfer complex. These results have also revealed, in conjunction with previously determined data for electron transfer within mutant complexes (Basran *et al.*, 2000), that electron transfer between ETF and mutant TMADH does not take place in the most thermodynamically stable state. Electron transfer in these complexes takes place in one or more metastable states, which are formed more rapidly than the most stable state.

The fluorescence spectroscopy studies of the TMADH-ETF complex have indicated that W_3A_1 ETF undergoes a stable structural change, termed structural imprinting, when it interacts transiently with TMADH. The rate of the imprinting reaction is severely compromised in the mutant complex, indicating that structural imprinting is dependent on native interactions that occur between ETF and the interaction surface of TMADH.

Imprinted W_3A_1 ETF exhibits an enhanced rate of electron transfer to the artificial electron acceptor ferricenium relative to non-imprinted ETF. Fluorescence spectroscopic analyses of imprinted and non-imprinted ETF have revealed that the rotation correlation times for the FAD cofactor are reduced in imprinted ETF. However, SAXS analyses have revealed that the overall molecular conformation of imprinted ETF is indistinguishable from that of non-imprinted ETF. Hence, these results suggest that changes that occur in the structure of ETF during the imprinting reaction are likely to involve small-scale structural rearrangements in the locus of the FAD moiety.

6.2 General Discussion

The results presented in this thesis are of general significance for several reasons. Firstly, they provide information on the mechanism of complex assembly for a class of proteins (*i.e.* ETFs) that form a vital component of many electron transfer pathways in nature (Whitfield & Mayhew, 1974; Sato *et al.*, 1993; Duplessis *et al.*, 1994; Roberts *et al.*, 1996; Roberts *et al.*, 1999; *for a review, see* Thorpe, 1991). Given that the ETFs from different organisms possess a high degree of sequence identity (Chen & Swenson, 1996), it is highly likely that the structural information obtained for W_3A_1 ETF, human ETF and *Paracoccus denitrificans* ETF can be extrapolated to ETFs from other sources. The assumption that electron transferring flavoproteins have a propensity towards conformational flexibility may have implications in the study of the molecular interactions of these proteins with their physiological redox partners. The implications of conformational flexibility in human ETF with respect to its interaction with one of its physiological redox partners, MCAD, have been investigated using molecular modeling and are discussed in this thesis. In contrast to W_3A_1 ETF, most forms of ETF are capable of accepting electrons from more than one electron donor *in vivo*. For example, human ETF acts as an electron acceptor for nine different physiological redox partners (Ikeda & Tanaka, 1983). Hence, the results presented in this thesis are potentially relevant to a wide range of physiological electron transfer reactions, both in prokaryotes and eukaryotes.

Secondly, these results demonstrate clearly the importance of conformational flexibility in the assembly of electron transfer complexes. Previous crystallographic studies have indicated that large-scale conformational changes may occur during the assembly of active electron transfer complexes in the cytochrome bc_1 complex (Zhang *et al.*, 1998) and sulfite reductase (Gruez *et al.*, 2000). Also, kinetic analyses have revealed that small-scale conformational changes are associated with the electron transfer reaction between cytochrome *c* and ferricytochrome (Qin & Kostic, 1994), and between methanol dehydrogenase and cytochrome c_{551i} (Harris *et al.*, 1994). The spectroscopic, kinetic and solution structural analyses described in this thesis demonstrate that W_3A_1 ETF undergoes a large-scale conformational change on formation of the physiological electron transfer complex with TMADH. Furthermore, these analyses have demonstrated that

W_3A_1 ETF samples a range of conformations in free solution, and that the spectroscopic, kinetic and thermodynamic properties of W_3A_1 ETF can be altered by transient interaction with TMADH. These results illustrate the important role of molecular dynamics in propagating interprotein electron transfer reactions and suggest a combined spectroscopic, kinetic and structural approach to the characterisation of protein complex assembly.

Thirdly, this thesis describes *the first time* that small angle X-ray solution scattering has been used to draw inferences on the large-scale conformational flexibility of proteins in solution. Small angle X-ray solution scattering has been used previously to characterise large-scale alterations in the domain structure of proteins, *e.g.* conformational changes in transferrin caused by ligand binding (Grossmann *et al.*, 1998) and conformational changes in methane monooxygenase caused by the formation of the multi-enzyme complex (Gallagher *et al.*, 1999). In these previous analyses, SAXS was used to obtain low-resolution structural information for proteins *before* and *after* the induction of a discrete conformational change, *e.g.* by incubation with an appropriate ligand. However, this thesis describes the use of SAXS to obtain information on the *large-scale conformational flexibility* of a single, homogeneous population of W_3A_1 ETF. Not only did these analyses allow the identification of the mobile domain in W_3A_1 ETF, but they also enabled the determination of the boundaries of domain motion and the plane through which the domain rotates. The ability to determine such parameters represents a distinct advantage of this technique over other structural techniques, such as NMR, CD and X-ray crystallography. The work presented in this thesis represents a further demonstration of the utility of SAXS, and suggests a novel approach to the structural characterisation of highly flexible proteins in solution.

Finally, as discussed in Chapter 5, these results indicate that the properties of electron transfer proteins can be altered lastingly by transient interaction with their physiological redox partners. This finding might have significant implications for our understanding of biological electron transfer reactions *in vivo*, because the organisation of living cells is such that soluble proteins are in frequent contact with one another in the cellular matrix (Srere, 1982; Goodsell, 1991). The results presented in this thesis suggest

that caution needs to be exercised when extrapolating the properties of *in vitro* electron transfer reactions to those occurring *in vivo*.

6.3 Future Work

In the future, it might be desirable to examine the kinetics of electron transfer between TMADH and imprinted ETF. Previous kinetic analyses of interprotein electron transfer within the TMADH-ETF complex have been performed using non-imprinted ETF (*e.g.* Basran *et al.*, 2000). Repetition of these analyses using imprinted ETF would demonstrate whether or not the structural imprinting of ETF has any measurable effect on the kinetics of the electron transfer reaction.

A mutant of W_3A_1 ETF, modified in the putative hinge region, has been isolated by Dr François Talfournier at Leicester University (Nigel Scrutton, personal communication). The poly-glycine sequence (^{193}GGG^{195}) in the α-subunit of ETF has been substituted for the corresponding sequence in *Paracoccus denitrificans* ETF (Ala-Glu-Ser). Preliminary findings are that mutation of the "hinge" region of W_3A_1 ETF severely compromises the kinetics of the TMADH-ETF binding reaction. Furthermore, the kinetics of electron transfer between TMADH and ETF are compromised in the mutant complex. Small angle X-ray scattering analysis of the ETF mutant have revealed small differences between the scattering profiles of mutant and wild type ETF. These results support the hypothesis that mobility of domain II of ETF is required for assembly of the active complex. However, the results of the SAXS analysis indicate that motion of domain II is not completely inhibited in the mutant enzyme. In the future, an extension of these analyses might include cross-linking of residues in, for example, domains I and II of ETF, in order to "lock" ETF into the proposed "active" conformation.

Recently, the crystal structures for W_3A_1 ETF and the 2ETF-TMADH complex have been determined at 1.8 Å and 2.0 Å, respectively, by Dr David Leys at the University of Leicester (Nigel Scrutton, personal communication). Crystallization of W_3A_1 ETF was achieved by limited proteolysis of the ETF molecule. Although there are small differences between the crystal structures of W_3A_1 ETF and human ETF, the overall polypeptide conformation for both proteins is almost identical. The most notable difference between the two structures is that the FAD moiety of W_3A_1 ETF is more

tightly embedded in the protein structure than that of human protein. This observation might provide a further explanation for the stability of the semiquinone form of W_3A_1 ETF.

The crystal structure for the 2ETF-TMADH complex is shown in Figure 6.1. Due to the conformational flexibility of the ETF molecule, the structure of domain II of ETF could not be determined from crystallographic data. Domain II of ETF was positioned in the structure by molecular modeling. These results confirm that domain II of W_3A_1 ETF is highly mobile within the electron transfer complex. The crystal structure shows the extensive interaction between an exposed α–helix from domain III of ETF and TMADH. Significantly, the distance between the redox centres of TMADH and ETF, as shown in the crystal structure, is far greater than was predicted in the molecular model of the TMADH-ETF complex (Chohan *et al.*, 1998). This suggests that the orientation and/or conformation of ETF in the crystal structure does not accurately represent the structure of the active electron transfer complex.

As a complete molecular structure for the 2ETF-TMADH complex is not yet available, and as the optimum conformation of W_3A_1 ETF for efficient electron transfer within the complex is not known, it might be desirable to carry out molecular modeling analyses of the ETF-TMADH complex similar to those performed on the human ETF-MCAD complex. Such analyses would involve computational modeling of W_3A_1 ETF bound to TMADH in different orientations and/or conformations, based upon a rotation of domain II of ETF. Calculation of intrinsic electron transfer rates for each model of the complex will allow a more accurate determination of the active conformation of ETF in the electron transfer complex, and might possibly establish a "robust engineering" principle for electron transfer between TMADH and ETF.

In the future, cross-linking of residues within the interacting surfaces of TMADH and ETF may allow crystallization of a TMADH-ETF complex in which ETF is present in the "active" conformation, and hence may allow determination of the structure of domain II of ETF in the complex with TMADH. The residues Tyr-442 and Arg-237 on the interacting surfaces of TMADH and ETF, respectively, are possible candidates for mutation to cysteine. Formation of a disulphide bridge between the interacting surfaces

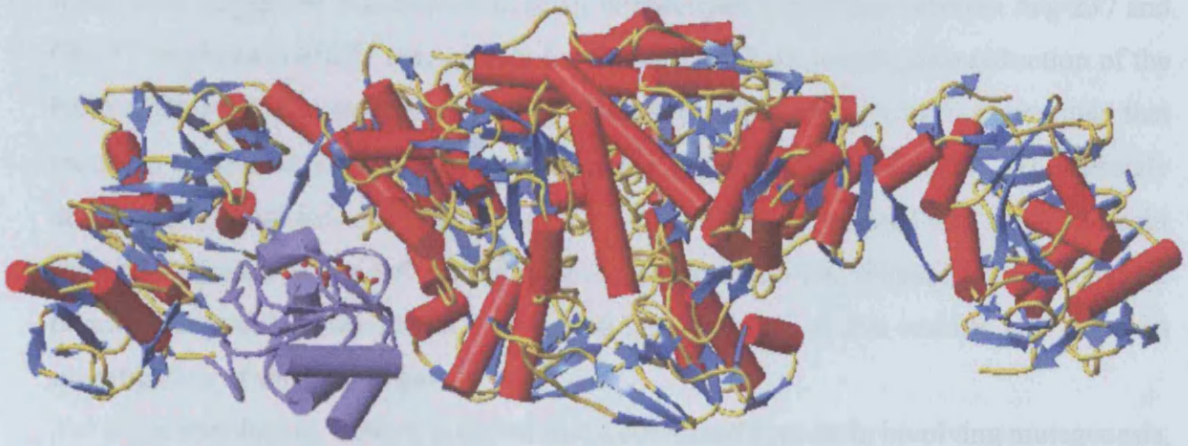

Figure 6.1
Crystal structure of the 2ETF-TMADH complex at 2.0 Å. This structure was determined by Dr David at the University of Leicester. This structure shows two molecules of ETF (left and right) bound to one TMADH homodimer (center). Due to the conformational flexibility of the ETF molecule, the structure of domain II of ETF could not be determined from crystallographic data. Domain II of the right-hand molecule of ETF (shown in purple), together with the FAD cofactor of ETF, was positioned in the structure by molecular modeling. The crystal structure shows the extensive interaction between an exposed α–helix from domain III of ETF and TMADH.

of TMADH and ETF may lock ETF into the active conformation within the electron transfer complex.

Finally, members of the Scrutton lab have generated a further mutant of W_3A_1 ETF in which Glu-37 is substituted with Gln (Nigel Scrutton, personal communication). It has been suggested that formation of an interdomain salt bridge between Arg-237 and Glu-37 might be partially responsible for the kinetic block to complete reduction of the FAD cofactor (Talfournier *et al.*, 2001). However, it has recently been determined that mutation of Glu-37 has no effect on the redox properties of W_3A_1 ETF. The recently determined crystal structure for W_3A_1 ETF has, however, suggested that Arg-237 might form a salt bridge with a different residue in domain I, Glu-163 (Nigel Scrutton, personal communication). In the future, it is hoped that mutation of this residue will allow an investigation of this hypothesis.

In conclusion, then, it is hoped that a combined approach, involving mutagenesis, spectroscopic analysis, kinetic analysis, protein engineering and structural techniques, will provide further information on the characteristics of this important family of proteins and increase our understanding of the mechanisms of biological electron transfer.

REFERENCES

Affleck, R., Haynes, C.A., & Clark, D.S. (1992) Solvent Dielectric Effects on Protein Dynamics. *Proc. Natl. Acad. Sci. USA 89*, 5167-5170

Andersson, L.I., Müller, R., Vlatakis, G., & Mosbach, K. (1995) Mimics of the binding sites of opioid receptors obtained by molecular imprinting of enkephalin and morphine. *Proc. Natl. Acad. Sci. USA 92*, 4788-4792

Ansell, R.J., Kriz, D., Mosbach, K. (1996) Molecularly imprinted polymers for bioanalysis: Chromatography, binding assays and biomimetic sensors. *Curr. Opin. Struct. Biol. 7*, 89-94

Arai, M., Ikura, T., Semisotnov, G.V., Kihara, H., Amemiya, Y., & Kuwajima, K. (1998) Kinetic refolding of beta-lactoglobulin. Studies by synchrotron X-ray scattering, and circular dichroism, absorption and fluorescence spectroscopy. *J. Mol. Biol. 275*, 149-162

Avilan, L., Gontero, B., Lebreton, S., & Ricard, J (1997) Memory and imprinting effects in multienzyme complexes .1. Isolation, dissociation, and reassociation of a phosphoribulokinase-glyceraldehyde-3-phosphate dehydrogenase complex from Chlamydomonas reinhardtii chloroplasts. *Eur. J. Biochem. 250*, 296-302

Basran, J., Chohan, K.K., Sutcliffe, M.J., & Scrutton, N.S. (2000) Differential Coupling through Val-344 and Tyr-442 of Trimethylamine Dehydrogenase in Electron Transfer Reactions with Ferricenium Ions and Electron Transferring Flavoprotein. *Biochemistry 39*, 9188-9200

Basran, J., Mewies, M., Mathews, F.S., & Scrutton, N.S. (1997) Selective Modification of Alkylammonium Ion Specificity in Trimethylamine Dehydrogenase by the Rational Engineering of Cation-π Bonding. *Biochemistry 36*, 1989-1998

Bedzyk, L.A., Escudero, K.W., Gill, R.E., Griffin, K.J., & Frerman, F.E. (1993) Cloning, Sequencing, and Expression of the Genes Encoding Subunits of *Paracoccus denitrificans* Electron Transfer Flavoprotein. *J. Biol. Chem. 268*, 20211-20217

Bishop, G.R., & Davidson, V.L. (1995) Intermolecular Electron Transfer from Substrate-Reduced Methylamine Dehydrogenase to Amicyanin is Linked to Proton Transfer. *Biochemistry 34*, 12082-12086

Bishop, G.R., & Davidson, V.L. (1997) Catalytic Role of Monovalent Cations in the Mechanism of Proton Transfer Which Gates an Interprotein Electron Transfer Reaction. *Biochemistry 36*, 13586-13592

Bosshard, H.R., Anni, H., & Yonetani, T. (1991) Peroxidases in Chemistry and Biology. (editors: Everse, I., Everse, K., & Grisham, M.B.) *CRC, Boca Raton, FL, Vol. 2*

Boyd, G., Matthews, F.S., Packman, L.C., & Scrutton, N.S. (1992) Trimethylamine Dehydrogenase of Bacterium W_3A_1; Molecular Cloning, Sequence Determination and Over-Expression of the Gene. *FEBS 308*, 271-276

Byron, C.M., Stankovich, M.T., Husain, M., & Davidson, V.L. (1989) Unusual Redox Properties of Electron Transfer Flavoprotein from *Methylophilus methylotrophus*. *Biochemistry 28*, 8582-8587

Cao, Y., Musah, R.A., Wilcox, S.K., Goodin, D.B., & McRee, D.E. (1998) Protein conformer selection by ligand binding observed with crystallography. *Protein Science 7*, 72-78

Chamberlain, D., O'Hara, B.P., Wilson, S.A., Pearl, L.H., & Perkins, S.J. (1997) Oligomerisation of the Amide Sensor Protein AmiC by X-Ray and Neutron Scattering and Molecular Modeling. *Biochemistry 36*, 8020-8029

Chamberlain, D., Ullman, C.G., & Perkins, S.J. (1998) Possible arrangement of the five domains in human complement factor I as determined by a combination of X-ray and neutron scattering and homology modeling. *Biochemistry 37*, 13918-13929

Chen, L.Y., Durley, R., Polikis, B.J., Hamada, K., Chen, Z.W., Mathews, F.S., Davidson, V.L., Satow, Y., Huizinga, E., Vellieux, F.M.D., & Hol, W.G.J (1992) Crystal Structure of an Electron Transfer Complex: Methylamine Dehydrogenase and Amicyanin. *Biochemistry 31*, 4959-4964

Chen, D.W., & Swenson, R.P. (1994) Cloning, Sequence Analysis, and Expression of the Genes Encoding the Two Subunits of the Methylotrophic Bacterium W_3A_1 Electron Transfer Flavoprotein. *J. Biol. Chem. 269*, 32120-32128

Chen, L., Durley, R.C.E., Mathews, F.S., & Davidson, V.L. (1994) Structure of an Electron Transfer Complex: Methylamine Dehydrogenase, Amicyanin and Cytochrome c_{55ii}. *Science 264*, 86-90

Chohan, K.K., Scrutton, N.S., & Sutcliffe, M.J. (1998) Major Structural Reorganization Most Likely Accompanies the Transient Formation of a Physiological Electron Transfer Complex. *Protein & Peptide Letters Vol. 5 No. 4*, 231-236

Colby, H., & Zatman, L.J. (1973) Trimethylamine Metabolism in Obligate and Facultative Methylotrophs. *Biochemical J. 132*, 101-112

Coon, M.J., Ding, X., Pernecky, S.J., & Vaz, A.D.N. (1992) Cytochrome P450: Progress and Predictions. *FASEB J. 6*, 686-694

Craig, D.H., Moody, P.C.E., Bruce, N.C., & Scrutton, N.S. (1998) Reductive and Oxidative Half-Reactions of Morphinone Reductase from *Pseudomonas pudita* M10: A Kinetic and Thermodynamic Analysis. *Biochemistry 37*, 7598-7607

Dabulis, K., & Klibanov, A.M. (1993) Dramatic Enhancement of Enzymatic Activity in Organic Solvents by Lyoprotectants. *Biotechnol. Bioeng. 41*, 566-571

Davidson, V.L. (1993) Principles and Applications of Quinoproteins. (editor: Davidson, V.L.) Marcel Decker, NY

Davidson, V.L., Husain, M., & Neher, J.W. (1986) Electron Transfer Flavoprotein from *Methylophilus methylotrophus*: Properties, Comparison with Other Electron Transfer Flavoproteins, and Regulation of Expression by Carbon Source. *J. Bacteriology 166*, 812-817

Davidson, V.L. (1996) Unraveling the Kinetic Complexity of Interprotein Electron Transfer Reactions. *Biochemistry 35*, 14035-14039

Davidson, V.L., & Jones, L.H. (1995) Complex Formation with Methylamine Dehydrogenase Affects the Pathway of Electron Transfer from Amicyanin to Cytochrome c_{551i}. *J. Biol. Chem. 270*, 23941-23943

Davidson, V.L., & Jones, L.H. (1996) Electron Transfer from Copper to Heme within the Methylamine Dehydrogenase-Amicyanin-Cytochrome c_{551i} Complex. *Biochemistry 35*, 8120-8125

Davidson, V.L., Jones, L.H., Graichen, M.E., Mathews, F.S., & Hosler, J.P. (1997) Factors Which Stabilize the Methylamine Dehydrogenase-Amicyanin Electron Transfer Protein Complex Revealed by Site-Directed Mutagenesis. *Biochemistry 36*, 12733-12738

Davidson, V.L., Jones, L.H., Graichen, M.E., & Zhu, Z.Y. (2000) Tyr(30) of amicyanin is not critical for electron transfer to cytochrome c-551i: implications for predicting electron transfer pathways. *BBA-Bioenergetics 1457*, 27-35

Dennison, C., Kohzuma, T., McFarlane, W., Suzuki, S., & Sykes, A.G. (1994) Reactivity of Pseudoazurin from *Achromobacter cycloclastes* with Inorganic Redox Partners and Related NMR and Electrochemical Studies. *Inorg. Chem. 33*, 3299-3305

Deisenhofer, J., & Michel, H. (1989) The Photosynthetic Reaction Center from The Purple Bacterium Rhodopseudomonas viridis. *Science 245*, 1463-1473

Dewey, T.G. (1991) Biophysical and Biochemical Aspects of Fluorescence Spectroscopy. *Plenum publishing corporation, NY*

Dordick, J.S. (1992) Designing Enzymes for Use in Organic Media. *Biotechnol. Prog. 8*, 259-267

Duplessis, E.R., Rohlfs, R.J., Hille, R., & Thorpe, C. (1994) Electron Transferring Flavoprotein from Pig and the Methylotrophic Bacterium W_3A_1 Contains AMP as well as FAD. *Biochem. Mol. Biol. Int. 32*, 195-199

Falzon, L., & Davidson, V.L. (1996a) Intramolecular Electron Transfer in Trimethylamine Dehydrogenase: A Thermodynamic Analysis. *Biochemistry 35*, 12111-12118

Falzon, L., & Davidson, V.L. (1996b) Kinetic Model for the Regulation by Substrate of Intramolecular Electron Transfer in Trimethylamine Dehydrogenase. *Biochemistry 35*, 2445-2452

Feigin, L.A., & Svergun, D.I., (1987) Structure Analysis by Small angle X-ray and Neutron Scattering. *Plenum publishing corporation, NY*

Finocchiaro, G., Ito, M., Ikeda, Y., & Tanaka, K. (1988) Molecular Cloning and Nucleotide Sequence of cDNAs Encoding the α-Subunit of Human Electron Transfer Flavoprotein. *J. Biol. Chem. 263*, 15773-15780

Finzel, B.C., Poulos, T.L., & Kraut, J. (1984) Crystal Structure of Yeast Cytochrome *c* Peroxidase Refined at 1.7 Å Resolution. *J. Biol. Chem. 259*, 3027-3036

Gabdoulline, R.R., & Wade, R.C. (2001) Protein-Protein Association: Investigation of Factors Influencing Association Rates by Brownian Dynamics Simulations. *J. Mol. Biol. 306*, 1139-1155

Gallagher, S.C., Callaghan, A.J., Zhao, J., Dalton, H., & Trewhella, J. (1999) Global Conformational Changes Control the Reactivity of Methane Monooxygenase. *Biochemistry 38*, 6752-6760

Glatter, O., & Kratky, O. (1982) Small Angle X-Ray Scattering. *Academic Press, NY, pp 167-196*

Goodsell, D.S. (1991) Inside a living cell. *TIBS 16*, 203-206

Gorren, A.C.F., de Vries, S., & Duine, J.A. (1995) Binding of Monovalent Cations to Methylamine Dehydrogenase in the Semiquinone State and its Effect on Electron Transfer. *Biochemistry 34*, 9748-9754

Gray, K.A., Knaff, D.B., Husain, M., & Davidson, V.L. (1986) Measurement of the Oxidation-Reduction Potentials of Amicyanin and *c*-Type Cytochromes from *Paracoccus denitrificans*. *FEBS Lett. 207*, 239-242

Gray, K.A., Davidson, V.L., & Knaff, D.B. (1988) Complex Formation between Methylamine Dehydrogenase and Amicyanin from *Paracoccus denitrificans*. *J. Biol. Chem. 263*, 13987-13990

Gray, H.B. & Winkler, J.R. (1996) Electron Transfer in Proteins. *Annu. Rev. Biochem. 65*, 537-561

Griebenow, K., & Klibanov, A.M. (1995) Lyophilization-Induced Reversible Changes in the Secondary Structure of Proteins. *Proc. Natl. Acad. Sci. USA 92*, 10969-10976

Griffin, K.J., Dwyer, T.M., Manning, S.G., Meyer, J.D., Carpenter, J.F., & Frerman, F.E. (1997) α-T244M mutation affects the redox, kinetic, and in vitro folding properties of *Paracoccus denitrificans* electron transfer flavoprotein. *Biochemistry 36*, 4194-4202

Grossmann, J.G., Mason, A.B., Woodworth, R.C., Neu, M., Lindley, P.F., & Hasnain, S.S. (1993) Asp-Ligand Provides the Trigger for Closure of Transferrin Molecules: Direct Evidence from X-Ray Scattering Studies of Site-Specific Mutants of the N-Terminal Half-Molecule of Human Transferrin. *J. Mol. Biol. 231*, 554-558

Grossmann, J.G., Crawley, J.B., Strange, R.W., Patel, K.J., Murphy, L.M., Neu, M., Evans, R.W., & Hasnain, S.S. (1998) The Nature of Ligand-induced Conformational Change in Transferrin in Solution. An Investigation using X-ray Scattering, XAFS and Site-directed Mutants. *J. Mol. Biol. 279*, 461-472

Grossmann, J.G., & Hasnain, S.S. (1997) X-Ray Scattering Studies of Metalloproteins in Solution: A Quantitative Approach for Studying Molecular Conformations. *J. Appl. Crystallog. 30*, 770-775

Gruez, A., Pignol, D., Zeghouf, M., Coves, J., Fontecave, M., Ferrer, J.L., & Fontecilla-Camps, J.C. (2000) Four crystal structures of the 60 kDa flavoprotein monomer of the sulfite reductase indicate a disordered flavodoxin-like module. *J. Mol. Biol. 299*, 199-212

Guinier, A. (1939) La diffraction des rayons X aux très petits angles; application à l'étude de phénomènes ultramicroscopiques. *Ann. Phys. 12*, 161-237

Guinier, A., & Fournet, G. (1955) Small Angle Scattering of X-Rays. *Wiley, NY*

Hahm, S., Durham, B., & Millett, F. (1992) Photoinduced Electron Transfer between Cytochrome *c* Peroxidase and Horse Cytochrome *c* Labeled at Specific Lysines with (Dicarboxypyridine)(Bispyridine)Ruthenum(II). *Biochemistry 30*, 3472-3477

Hahm, S., Durham, B., & Millett, F. (1993) Reaction of Cytochrome *c* with the Radical in Cytochrome *c* Peroxidase Compound I. *J. Am Chem. Soc. 115*, 3372-3373

Hahm, S., Miller, M.A., Geren, L., Kraut, J., Durham, B., & Millett, F. (1994) Reaction of Horse Cytochrome *c* with the Radical and the Oxyferryl Heme in Cytochrome *c* Peroxidase Compound I. *Biochemistry 33*, 1473-1480

Harris, T.K., Davidson, V.L., Chen, L., Mathews, F.S., & Xia, Z. (1994) Ionic Strength Dependence of the Reaction between Methanol Dehydrogenase and Cytochrome c_{551i}: Evidence of Conformationally Coupled Electron Transfer. *Biochemistry 33*, 12600-12608

Hartsough, D.S., & Merz, K.M. Jr (1992) Protein Flexibility in Aqueous and Nonaqueous Solutions. *J. Am. Chem. Soc. 114*, 10113-10116

Hazzard, J.T., Cusanovich, M.A., Tainer, J.A., Getzoff, E.D., & Tollin, G. (1986) Kinetic Studies of Reduction of a Cytochrome *c*-Flavodoxin Complex by Free Flavin Semiquinones and Rubredoxin. *Biochemistry 25*, 3318-3328

Hazzard, J.T., Govindaraj, S., Poulos, T.L., & Tollin, G. (1997) Electron Transfer between the FMN and Heme Domains of Cytochrome P450BM-3. *J. Biol. Chem.272*, 7922-7926

Hazzard, J.T., McIntire, W.S., & Tollin, G. (1991) Laser Flash Photolysis Study of Intermolecular and Intramolecular Electron Transfer in Trimethylamine Dehydrogenase. *Biochemistry 30*, 4559-4564

Herrick, K.R., Salazar, D., Goodman, S.I., Finocchiaro, G., Bedzyk, L.A., & Frerman, F.E. (1994) Expression and Characterization of Human and Chimeric Human-*Paracoccus denitrificans*. Electron Transfer Flavoproteins *J. Biol. Chem 269*, 32239-32245

Huang, L., Rohlfs, R.J., & Hille, R. (1995) The Reaction of Trimethylamine Dehydrogenase with Electron Transferring Flavoprotein. *J. Biol. Chem. 270*, 23958-23965

Huang, L., Scrutton, N.S., & Hille, R. (1996) Reaction of the C30A Mutant of Trimethylamine Dehydrogenase with Dimethylamine. *J. Biol. Chem. 271*, 13401-13406

Husain, M., & Davidson, V.L. (1985) An inducible Periplasmic Blue Copper Protein from *Paracoccus denitrificans*: Purification, Properties and Physiological Role. *J. Biol. Chem. 260*, 4626-4629

Husain, M. & Davidson, V.L. (1986) Characterization of Two Inducible Periplasmic *c* Type Cytochromes from *Paracoccus denitrificans*. *J. Biol. Chem. 261*, 8577-8580

Huyett, J.E., Doan, P.E., Gurbiel, R., Houseman, A.L.P., Sivaraja, M., Goodin, D.B., & Hoffman, B.M. (1995) Compound ES of Cytochrome *c* Peroxidase Contains a Trp π-

Cation Radical: Characterisation by CW and Pulsed Q-Band Endor Spectroscopy. *J. Am. Chem. Soc. 117*, 9033-9041

Iffland, A., Tafelmeyer, P., Saudan, C., & Johnsson, K. (2000) Directed Molecular Evolution of Cytochrome *c* Peroxidase. *Biochemistry 39*, 10790-10798

Ikeda, Y., & Tanaka, K. (1983) Purification and characterization of 2-methyl-branched chain acyl coenzyme A dehydrogenase, an enzyme involved in the isoleucine and valine metabolism, from rat liver mitochondria. *J. Biol. Chem. 258*, 9477-9487

Jang, M-H., Basran, J., Scrutton, N.S., & Hille, R. (1999) The reaction of trimethylamine dehydrogenase with trimethylamine. *J. Biol. Chem. 274*, 13147-13154

Jang, M-H., Scrutton, N.S., & Hille, R. (2000) Formation of W_3A_1 Electron-transferring Flavoprotein (ETF) Hydroquinone in the Trimethylamine Dehydrogenase-ETF Protein Complex. *J. Biol. Chem. 275*, 12540-12552

Kasprzak, A.A., Papas, E.J., & Steenkamp, D.J. (1983) Identity of the Subunits and the Stoichiometry of Prosthetic Groups in Trimethylamine Dehydrogenase and Dimethylamine Dehydrogenase. *Biochem. J. 211*, 535-541

Khmelnitsky, Y.L., & Rich, J.O. (1999) Biocatalysis in Nonaqueous Solvents. *Curr. Opin. Chem. Biol. 3*, 47.52

Klibanov, A.M. (1995) What is Remembered and Why? *Nature 374*, 596

Kojima, M., Tanokura, M., Maeda, M., Kimura, K., Amemiya, Y., Kihara, H., & Takahashi, K. (2000) pH-Dependent Unfolding of Aspergillopepsin II Studied by Small-Angle X-ray Scattering. *Biochemistry 39*, 1364-1372

Kornblatt, J.A., & English, A.M. (1986) The Binding of Porphyrin Cytochrome *c* to Yeast Cytochrome *c* Peroxidase: A Fluorescence Study of the Number of Sites and their Sensitivity to Salt. *Eur. J. Biochem. 155*, 505-511

Kriz, D., & Mosbach, K. (1995) Competitive Amperometric Morphine Sensor Based on an Agarose Immobilized Molecularly Imprinted Polymer. *Anal. Chim. Acta 300*, 71-75

Kumar, M.A., & Davidson, V.L. (1990) Chemical Cross-Linking Study of Complex Formation between Methylamine dehydrogenase and Amicyanin from *Paracoccus denitrificans*. *Biochemistry 29*, 5299-5304

Kyritsis, P., Dennison, C., Kalverda, A.P., Canters, G.W., & Sykes, A.G. (1994) Redox Reactivity of the Type 1 (Blue) Copper Protein Amicyanin from *Thiobacillus versutus* with Inorganic Complexes. *J. Chem. Soc. Dalton Trans. 20*, 3017-3023

Kyritsis, P., Lundberg, L.G., Nordling, M., Vanngard, T., Young, S., Tomkinson, N.P., & Sykes, A.G. (1991) The Reactivity of Spinach Plastocyanin Mutants with Inorganic Oxidants $[Fe(CN)_6]^{3-}$ and $[Co(phen)_3]^{3+}$. *J. Chem. Soc. Chem. Commun. 20*, 1441-1442

Labesse, I., Ferrari, D., Chen, Z.W., Rossi, G.L., Kuusk, V., McIntire, W.S., & Mathews, F.S. (1998) Crystallographic and spectroscopic studies of native, aminoquinol, and monovalent cation-bound forms of methylamine dehydrogenase from *Methylobacterium extorquens* AM1. *J. Biol. Chem. 273*, 25703-25712

Lakowicz, J.R. (1999) Principles of Fluorescence Spectroscopy (2^{nd} Edition). *Plenum publishing corporation, NY*

Laemmli, U.K. (1970) Cleavage of Structural Proteins during the Assembly of the Head of Bacteriophage T4. *Nature 227*, 680-685

Lebreton, S., Gontero, B., Avilan, L., & Ricard, J. (1997a) Memory and imprinting effects in multienzyme complexes .2. Kinetics of the bienzyme complex from Chlamydomonas reinhardtii and hysteretic activation of chloroplast oxidized phosphoribulokinase. *Eur. J. Biochem. 246*, 85-91

Lebreton, S., Gontero, B., Avilan, L., & Ricard, J (1997b) Information transfer in multienzyme complexes .1. Thermodynamics of conformational constraints and memory effects in the bienzyme glyceraldehyde-3-phosphate-dehydrogenase-phosphoribulokinase complex of Chlamydomonas reinhardtii chloroplasts. *Eur. J. Biochem. 250*, 286-295

Lebreton, S., & Gontero, B. (1999) Memory and Imprinting in Multienzyme Complexes. *J. Biol. Chem. 274*, 20879-20884

Lee, H.J., Basran, J., & Scrutton, N.S. (1998) Electron Transfer from Flavin to Iron in the *Pseudomonas oleovorans* Rubredoxin Reductase-Rubredoxin Electron Transfer Complex. *Biochemistry 37*, 15513-15522

Leesch, V.W., Bujons, J., Mauk, A.G., & Hoffman, B.M. (2000) Cytochrome *c* Peroxidase-Cytochrome *c* Complex: Locating the Second Binding Domain on Cytochrome *c* Peroxidase with Site-Directed Mutagenesis. *Biochemistry 39*, 10132-10139

Lehman, T.C., Hale, D.E., Bhala, A., & Thorpe, C. (1990) An Acyl-Coenzyme A Dehydrogenase Assay Utilising the Ferricenium Ion. *Analytical Biochemistry 186*, 280-284

Lewis, R.R. (1994) Multiwire Gas Proportional Counters – Decrepit Antiques or Classic Performers. *J. Synchotron Rad. 1*, 43-53

Lim, L.W., Shamala, N., Mathews, F.S., Steenkamp, D.J., Hamlin, R., & Xuong, N.H. (1986) 3-Dimansional Structure of the Iron-Sulfur Flavoprotein Trimethylamine Dehydrogenase at 2.4 Å Resolution. *J. Biol. Chem. 261*, 15140-15146

Lindsey, J.S. (1991) Self-Assembly in Synthetic Routes to Molecular Devices – Biological Routes and Chemical Perspectives – A Review. *New J. Chem. 15*, 153-180

Liu, X-C., & Dordick, J.S. (1999) Sugar Acrylate-based Polymers as Chiral Molecularly Imprintable Hydrogels. *J. Polym. Sci. Part A: Polym. Chem. 37*, 1665-1671

Louie, G.V., & Brayer, G.D. (1990) High-Resolution Refinement of Yeast Iso-1-Cytochrome *c* and Comparisons with Other Eukaryotic Cytochromes *c*. *J. Mol. Biol. 214*, 527-555

Marcus, R.A., & Sutin, N. (1985) Electron Transfers in Chemistry and Biology. *Biochim. Biophys. Acta 881*, 265-322

Mauk, M.R., Ferrer, J.C., & Mauk, A.G. (1994) Proton Linkage in Formation of the Cytochrome *c*-Cytochrome *c* Peroxidase Complex – Electrostatic Properties of the High-Affinity and Low-Affinity Cytochrome Binding-Sites on the Peroxidase. *Biochemistry 33*, 12609-12614

McIntire, W.S., Wemmer, D.E., Chistoserdov, A., & Lidstrom, M. (1991) A New Cofactor in a Prokaryotic Enzyme – Tryptophan Tryptophylquinone as the Redox Prosthetic Group in Methylamine Dehydrogenase. *Science 252*, 817-824

Mei, H., Wang, K., Peffer, N., Weatherly, G., Cohen, D.S., Miller, M., Pielak, G., Durham, B., & Millett, F. (1999) Role of Configurational Gating in Intracomplex Electron Transfer from Cytochrome *c* to the Radical Cation in Cytochrome *c* Peroxidase. *Biochemistry 38*, 6846-6854

Merli, A., Brodersen, D.E., Morini, B., Chen, Z., Durley, R.C.E., Mathews, F.S., Davidson, V.L., & Rossi, G.L. (1996) Enzymatic and Electron Transfer Activities in Crystalline Protein Complexes. *J. Biol. Chem. 271*, 9177-9180

Mewies, M., Packman, F.S., Mathews, F.S., & Scrutton, N.S. (1996) Flavinylation in Wild-Type Trimethylamine Dehydrogenase and Differentially Charged Mutant Enzymes: A study of the Protein Environment Around the N1 of the Flavin Isoalloxazine. *Biochemical J. 317*, 267-272

Miller, M.A. (1996) A Complex Mechanisn for Steady-State Oxidation of Yeast Cytochrome *c* by Yeast Cytochrome *c* Peroxidase. *Biochemistry 35*, 15791-15799

Miller, M.A., Geren, L., Han, G.W., Saunders, A., Beasley, J., Pielak, G.J., Durham, B., Millett, F., & Kraut, J. (1996) Identifying the Physiological Electron Transfer Site of Cytochrome *c* Peroxidase by Structure-Based Engineering. *Biochemistry 35*, 667-673

Mosbach, K. (1994) Molecular Imprinting. *Trends Biochem. Sci 19*, 9-14

Mosbach, K., & Ramström, O (1996) The Emerging Technique of Molecular Imprinting and its Future Impact on Biotechnology. *Bio/Technology 14*, 163-170

Moser, C.C., Keske, J.M., Warncke, K., Farid, R.S., & Dutton, P.L. (1992) Nature of biological electron transfer. *Nature 355*, 796-802

Nagy, J., Kenney, W.C., & Singer, T.P. (1979) The reaction of phenylhydrazine with trimethylamine dehydrogenase and with free flavins. *Journal of Biological Chemistry. 254*, 2684-2688

Northrup, S.H., Boles, J.O., & Reynolds, J.C.L.(1988) Brownian Dynamics of Cytochrome *c* and Cytochrome *c* Peroxidase Association. *Science 261*, 67-70

Ochi, H., Hata, Y., Tanaka, N., Kakudo, M., Sakurai, T., Aihara, S., & Morita, Y. (1983) Structure of Rice Ferricytochrome *c* at 2.0 Å Resolution. *J. Mol. Biol. 166*, 407-418

Orii, Y. (1993) Immediate Reduction of Cytochrome *c* by Photoexcited NADH: Reaction Mechanism s Revealed by Flow-Flash and Rapid-Scan Studies. *Biochemistry 32*, 11910-11914

Pace, C.P., & Stankovich, M.T. (1991) Oxidation-reduction properties of trimethylamine dehydrogenase: effect of inhibitor binding. *Archives of Biochemistry & Biophysics. 287*, 97-104

Packman, L.C., Mewies, M., & Scrutton, N.S. (1995) The Flavinylation Reaction of Trimethylamine Dehydrogenase. *J. Biol. Chem. 270*, 13186-13191

Page, C.C., Moser, C.C., Chen, X. & Dutton, P.L. (1999) Natural engineering principles of electron tunneling in biological oxidation-reduction. *Nature 402*, 47-52

Pappa, H.S., Tajbaksh, S., Saunders, A., Pielak, G.J., & Poulos, T.L. (1996) Probing the Cytochrome *c* Peroxidase - Cytochrome *c* Electron Transfer Reaction using Site-Specific Cross-Linking. *Biochemistry 35*, 4837-4845

Pauling, L. (1942) The Manufacture of Antibodies *in vitro*. *J. Expl. Med. 76*, 211-220

Pelletier, H., & Kraut, J. (1992) Crystal Structure of a Complex Between Electron Transfer Partners, Cytochrome *c* Peroxidase and Cytochrome *c*. *Science 258*, 1748-1755

Perkins, S.J. (1988) Structural Studies of Proteins by High-Flux X-Ray and Neutron Solution Scattering. *Biochem. J. 254*, 313-327

Porod, G. (1951) Die Röntgenkleinwinkelstreuung von dichtgepackten kolloiden Systemen I. *Kolloid Zeitschrift 124*, 83-144

Poulos, T.L., & Kraut, J. (1980) A Hypothetical Model of the Cytochrome *c* Peroxidase-Cytochrome *c* Electron Transfer Complex. *J. Biol. Chem. 255*, 10322-10330

Qin, L., & Kostic, N.M. (1994) Photoinduced Electron Transfer from the Triplet State of Zinc Cytochrome *c* to Ferricytochrome b_5 is Gated by Configurational Fluctuations of the Diprotein Complex. *Biochemistry 33*, 12592-12599

Rich, J.O., & Dordick, J.S. (1997) Controlling Subtilisin Activity and Selectivity in Organic Media by Imprinting with Nucleophilic Substrates. *J. Am. Chem. Soc. 119*, 3245-3252

Roberts, D.L., Frerman, F.E., Kim, J-J.P. (1996) Three-dimensional structure of human electron transfer flavoprotein to 2.1-Å resolution. *Proc. Natl. Acad. Sci. USA 93*, 14355-14360

Roberts, D.L., Salazar, D., Fulmer, J.P., Frerman, F.E., & Kim, J-J.P. (1999) Crystal Structure of *Paracoccus denitrificans* Electron Transfer Flavoprotein: Structural and Electrostatic Analysis of a Conserved Flavin Binding Domain. *Biochemistry 38*, 1977-1989

Roberts, P.T., Basran, J., Wilson, E.K., Hille, R., & Scrutton, N.S. (1999) Redox Cycles in Trimethylamine Dehydrogenase and Mechanism of Substrate Inhibition. *Biochemistry 38*, 14927-14940

Rohlfs, R.J., & Hille, R. (1991) Intramolecular Electron Transfer in Trimethylamine Dehydrogenase from Bacterium W_3A_1. *J. Biol. Chem. 266*, 15244-15252

Rohlfs, R.J., & Hille, R. (1994) The Reaction of Trimethylamine Dehydrogenase with Dimethylamine. *J. Biol. Chem. 269*, 30869-30879

Rohlfs, R.J., Huang, L., & Hille, R. (1995) Prototropic Control of Intramolecular Electron Transfer in Trimethylamine Dehydrogenase. *J. Biol. Chem. 270*, 22196-22207

Russell, A.J., & Klibanov, A.M. (1988) Inhibitor-Induced Enzyme Activation in Organic Solvents. *J. Biol. Chem. 263*, 11624-11626

Ruzicka, F.J., & Beinert, H. (1977) A new iron-sulfur flavoprotein of the respiratory chain. A component of the fatty acid beta oxidation pathway. *J. Biol. Chem. 252*, 8440-8445

Sato, K., Nishina, Y., & Shiha, K. (1993) Electron Transferring Flavoprotein has an AMP Binding Site in Addition to the FAD Binding Site. *J. Biol. Chem. 114*, 215-222

Savenkova, M.I., Satterlee, J.D., Erman, J.E., Siems, W.F., & Helms, G.L. (2001) Expression, Purification, Characterization and NMR Studies of a Highly Deuterated Recombinant Cytochrome *c* Peroxidase. *Biochemistry 40*, 12123-12131

Scrutton, N.S., Packman, L.C., Mathews, F.S., Rohlfs, R.J., & Hille, R. (1994) Assembly of Redox Centres in the Trimethylamine Dehydrogenase of Bacterium W_3A_1: Properties of the Wild-Type Enzyme and a C30A Mutant Expressed from a Cloned Gene. *J. Biol. Chem. 269*, 13942-13950

Scrutton, N.S., Basran, J., Wilson, E.K., Chohan, K.K., Jang, M.-H., Sutcliffe, M.J., & Hille, R. (1999) Electron transfer in trimethylamine dehydrogenase and electron transferring flavoprotein. *Bioch. Soc. Trans. Vol. 27, No.2*, 196-201

Semenyuk, A.V., & Svergun, D.I. (1991) GNOM – A Program Package for Small-Angle Scattering Data Processing. *J. Appl. Crystallog. 24*, 537-540

Semisotnov, G.V., Kihara, H., Kotova, N.V., Kimura, H., Amamiya, Y., Wakabayashi, K., Serdyuk, I.N., Timchenko, A.A., Chiba, K., Nikaido, K., Ikura, T., & Kuwajima, K. (1996) Protein globularization during folding. A study by synchrotron small-angle X-ray scattering. *J. Mol. Biol. 262*, 559-574

Shinzawa, K., Inagaki, T., Ohishi, N., Ichihara, C., Tsukagoshi, N., Udaka, S., & Yagi, K. (1988) Molecular Cloning of a cDNA for the α-Subunit of Rat Liver Electron Transfer Flavoprotein. *Biochem. Biophys. Res. Comm. 155*, 300-304

Sigman, J.A., Pond, A.E., Dawson, J.H., & Lu, Y. (1999) Engineering Cytochrome *c* Peroxidase into Cytochrome P450: A Proximal Effect on Heme-Thiolate Ligation. *Biochemistry 38*, 11122-11129

Sivaraja, M., Goodin, D.B., Smith, M., & Hoffman, B.M. (1989) Identification by ENDOR of Trp191 as the free-radical site in cytochrome *c* peroxidase compound ES. *Science 245*, 738-740

Srere, P.A. (1982) The Structure of the Mitochondrial Inner Membrane Matrix Compartment. *Trends Biochem. Sci. 7*, 375-378

Stahl, M., Mansson, M-O., & Mosbach, K. (1990) The Synthesis of a D-Amino Acid Ester in an Organic Media with α-Chymotrypsin Modified by a Bio-Imprinting Procedure. *Biotechnol. Lett. 12*, 161-166

Stahl, M., Jeppsson-Wistrand, U., Mansson, M-O., & Mosbach, K. (1991) Induced Stereoselectivity and Substrate Selectivity of Bio-Imprinted α-Chymotrypsin in Anhydrous Organic Media. *J. Am. Chem. Soc. 113*, 9366-9368

Steenkamp, D.J., & Beinert, H. (1982a) Mechanistic Studies of the Dehydrogenases of Methylotrophic Bacteria. 1. The Influence of Substrate Binding to Reduced

Trimethylamine Dehydrogenase on the Intramolecular Electron Transfer between its Prosthetic Groups. *Biochem. J. 207*, 233-239

Steenkamp, D.J., & Beinert, H. (1982b) Mechanistic Studies of the Dehydrogenases of Methylotrophic Bacteria. 2. Kinetic Studies on the Intramolecular Electron Transfer in Trimethylamine and Dimethylamine Dehydrogenase. *Biochem. J. 207*, 241-252

Steenkamp, D.J., & Mallinson, J. (1976) Trimethylamine Dehydrogenase from a Methylotrophic Bacterium. I. Isolation and Steady-State Kinetics. *Biochim. Biophys. Acta 429*, 705-719

Steenkamp, D.J., & Gallup, M. (1978) The Natural Flavoprotein Electron Acceptor of Trimethylamine Dehydrogenase. *J. Biol. Chem. 253*, 4086-4089

Stryer, L. (1995) Biochemistry (4^{th} Edition). *W.H. Freeman & Company, NY*

Stuhrmann, H.B. (1970) Interpretation of Small-Angle Scattering Functions of Dilute Solutions and Gases. A Representation of the Structures Related to a One-Particle-Scattering Function. *Acta Crystallogr. Sect.A, 26*, 297-306

Sun, D.P., & Davidson, V.L. (2001) Re-engineering monovalent cation binding sites of methylamine dehydrogenase: Effects on spectral properties and gated electron transfer. *Biochemistry 40*, 12285-12291

Svergun, D.J., Semenyuk, D.I., & Feigin, F.A. (1988) Small-Angle Scattering – Data Treatment by the Regularization Method. *Acta Crystallog. Sect. A. 44*, 244-250

Svergun, D.I., Barberato, C., & Koch, M.H.J. (1995) CRYSOL - A Program to Evaluate X-Ray Solution Scattering of Biological Macromolecules from Atomic Coordinates. *J. Appl. Cryst. 28*, 768-773

Svergun, D.I., Volkov, V.V., Kozin, M.B., & Stuhrmann, H.B. (1996) New Developments in Direct Shape determination from Small-Angle Scattering. 2. Uniqueness. *Acta Crystallog. Sect. A, 52*, 419-426

Svergun, D.I., Volkov, V.V., Kozin, M.B., Stuhrmann, H.B., Barberato, C., & Koch, M.H.J. (1997) Shape Determination from Solution Scattering of Biopolymers. *J. Appl. Cryst. 30*, 798-802

Svergun, D.I., & Stuhrmann, H.B. (1991) New Developments in Direct Shape determination from Small-Angle Scattering. 1. Theory and Model Calculations. *Acta Crystallog. Sect. A, 47*, 736-744

Swenson, R.P., & Chen, D. (1996) Nucleotide Binding Properties of Recombinant W_3A_1 Electron Transferring Flavoprotein. *Flavins and Flavoproteins, University of Calgary Press*

Takano, T., & Dickerson, R.E. (1981) Conformation change of cytochrome *c*. 1. Ferrocytochrome *c* structure refined at 1.5 Å resolution. *J. Mol. Biol. 153*, 79-94

Talfournier, F., Munro, A.W., Basran, J., Sutcliffe, M.J., Daff, S., Chapman, S.K., & Scrutton, N.S. (2001) αArg-237 in *Methylophilus methylotrophus* (sp. W_3A_1) Electron-transferring Flavoprotein Affords ~200-Millivolt Stabilization of the FAD Anionic Semiquinone and a Kinetic Block on Full Reduction to the Dihydroquinone. *J. Biol. Chem. 276*, 20190-20196

Thorpe, C. (1991) Chemistry and Biochemistry of Flavoenzymes. (editor: Muller, F.) *CRC, Boca Raton, FL, Vol. 2*

Towns-Andrews, E., Berry, A., Bordas, J., Mant, P.K., Murray, K., Roberts, K., Sumner, I., Morgan, J.S., Lewis, R., & Gabriel, A. (1989) Time-resolved X-ray diffraction station: X-ray optics, detectors, and data acquisition. *Rev. Sci. Instrum 60*, 2346-2349

Trickey, P., Basran, J., Lian, L.Y., Chen, Z., Barton, J.D., Sutcliffe, M.J., Scrutton, N.S., & Mathews, F.S. (2000) Structural and biochemical characterization of recombinant wild type and a C30A mutant of trimethylamine dehydrogenase from *Methylophilus methylotrophus* (sp. W_3A_1). *Biochemistry 39*, 7678-88

van Gelder, R., Roberts, K.J., & Rossi, A. (1995) Using Synchotron Radiation to Examine the *in-situ* Processing of Long-Chain Hydrocarbons. *The CCP13 Newsletter 4*, 28

Wang, J.M., Mauro, J.M., Edwards, S.L., Oatley, S.J., Fishel, L.A., Ashford, V.A., Xuong, N.H., & Kraut, J. (1990) X-Ray Structures of Recombinant Yeast Cytochrome *c* Peroxidase and Three Heme-Cleft Mutants Prepared by Site-Directed Mutagenesis. *Biochemistry 29*, 7160

Welinder, K.G., Mauro, J.M., & Norskovlauritsen, L. (1992) Structure of Plant and Fungal Peroxidases. *Biochem. Soc. Trans. 20*, 337-40

White, S.A., Mathews, F.S., Rohlfs, R.J., & Hille, R. (1994) Crystallization and Preliminary Crystallographic Investigation of Electron Transfer Flavoprotein from the Bacterium Methylophilus W_3A_1. *J. Mol. Biol. 240*, 265-266

Whitfield, C.D., & Mayhew, S.G. (1974) Purification and properties of electron-transferring flavoprotein from *Peptostreptococcus elsdenii*. *J. Biol. Chem. 249*, 2808-2810

Wilson, E.K., Mathews, F.S., Packman, L.C., & Scrutton, N.S. (1995) Electron Tunneling in Substrate-Reduced Trimethylamine Dehydrogenase: Kinetics of Electron Transfer and Analysis of the Tunneling Pathway. *Biochemistry 34*, 2584-2591

Wilson, E.K., Scrutton, N.S., Huang, L., Hille, R., & Mathews, F.S. (1996) Electron Transfer Complex Assembly: The Association of Trimethylamine Dehydrogenase with Electron Transferring Flavoprotein. *Flavins and Flavoproteins, University of Calgary press*, 957-960

Wilson, E.K., Scrutton, N.S., Colfen, H., Harding, S.E., & Winzor, D.J. (1997a) An ultracentrifugal approach to quantitative characterization of the molecular assembly of a physiological electron-transfer complex. *Eur. J. Biochem. 243*, 393-399

Wilson, E.K., Huang, L., Sutcliffe, M.J., Mathews, F.S., Hille, R., & Scrutton, N.S. (1997b) An Exposed Tyrosine on the Surface of Trimethylamine Dehydrogenase Facilitates Electron Transfer to Electron Transferring Flavoprotein: Kinetics of Transfer in Wild-Type and Mutant Complexes. *Biochemistry 36*, 41-48

Yi, Q., Erman, J.E., & Satterlee, J.D. (1994) Studies of ProteinProtein Association Between Yeast Cytochrome *c* Peroxidase and Yeast Iso-1 Ferricytochrome *c* by Hydrogen Deuterium Exchange Labeling and Proton NMR-Spectroscopy. *Biochemistry 33*, 12032-12041

Yonetani, T. (1976) The Enzymes (Vol. 13). (editor: Boyer, P.D.) *Academic Press, Orlando, FL*, pp 345-361

Zhang, H-Y., Faridoon, K.Y., & Sykes, A.G. (1992) Kinetic studies on the dithionite reduction of beef-heart aconitase in the $[3Fe\text{-}4S]^{+}$ inactive form. *Inorg. Chim. Acta 201*, 239-242

Zhang, Z., Huang, L., Shulmeister, V.M., Chi, Y.I., Kim, K.K., Hung, L.W., Crofts, A.R., Berry, E.A., & Kin, S.H. (1998) Electron transfer by domain movement in cytochrome *bc*1. *Nature 392*, 677-684

Zhou, J.S., & Hoffman, B.M. (1993) Cytochrome *c* Peroxidase Simultaneously Binds Cytochrome *c* at Two Different Sites with Strikingly Different Reactivities: Titrating a Substrate with an Enzyme. *J. Am. Chem. Soc. 115*, 11008-11009

Zhou, J.S., & Hoffman, B.M. (1994) Stern-Volmer in Reverse – 2/1 Stoichiometry of the Cytochrome *c*- Cytochrome *c* Peroxidase Electron Transfer Complex. *Science 265*, 1693-1696

Zhou, J.S., Nocek, J.M., Devan, M.L., & Hoffman, B.M. (1995) Inhibitor Enhanced Electron Transfer: Copper Cytochrome *c* as a Redox-Inert Probe of Ternary Complexes. *Science 269*, 204-207

Zhou, J.S., & Kostic, N.M. (1992) Photoinduced Electron Transfer from Zinc Cytochrome *c* to Plastocyanin is Gated by Surface Diffusion within the Metalloprotein Complex. *J. Am. Chem. Soc. 114*, 3562-3563

Zhou, J.S., & Kostic, N.M. (1993) Gating of Photoinduced Electron Transfer from Zinc Cytochrome *c* and Tin Cytochrome *c* to Plastocyanin: Effects of Solution Viscosity on Rearrangement of the Metalloprotein Complex. *J. Am. Chem. Soc. 115*, 10796-10804

Zhu, Z., Cunane, L.M., Chen, Z., Durley, R.C.E., Mathews, F.S., & Davidson, V.L. (1998) Molecular Basis for Interprotein Complex-Dependent Effects on the Redox Properties of Amicyanin. *Biochemistry 37*, 17128-17136

Zhu, Z., Jones, L.H., Graichen, M.E., & Davidson, V.L. (2000) Molecular Basis for Complex Formation between Methylamine Dehydrogenase and Amicyanin Revealed by Inverse Mutagenesis of an Interprotein Salt Bridge. *Biochemistry 39*, 8830-8836

Ziegler, G.A., Vonrhein, C., Hanukoglu, I., & Schulz, G.E. (1999) The structure of adrenodoxin reductase of mitochondrial P450 systems: electron transfer for steroid biosynthesis. *J. Mol. Biol. 289*, 981-990

PUBLICATIONS

Publications arising from work described in this thesis

Jones, M., Basran, J., Sutcliffe, M.J., Grossmann, J.G., & Scrutton, N.S. (2000) X-ray Scattering Studies of *Methylophilus methylotrophus* (sp. W_3A_1) Electron Transferring Flavoprotein: Evidence for Multiple Conformational States and an Induced Fit Mechanism for Assembly with Trimethylamine Dehydrogenase. *Journal of Biological Chemistry 275*, 21349-21354

Chohan, K.K., **Jones, M.**, Grossmann, J.G., Frerman, F.E., Scrutton, N.S., & Sutcliffe, M.J. (2001) Molecular Dynamics Enhance Electronic Coupling in Electron Transfer Complexes. *Journal of Biological Chemistry 276*, 34142- 34147

Jones, M., Talfournier, F., Bobrov, A., Grossmann, J.G., Vekshin, N., Sutcliffe, M.J., & Scrutton, N.S. (2002) Electron Transfer and Conformational Change in Complexes of Trimethylamine Dehydrogenase and Electron Transferring Flavoprotein. *Journal of Biological Chemistry 277*, 8457- 8465